

# Stacked Modulation Formats Enabling Highest-Sensitivity Optical Free-Space Communications

Zur Erlangung des akademischen Grades eines

DOKTOR-INGENIEURS

der Fakultät für Elektrotechnik und Informationstechnik  
des Karlsruher Instituts für Technologie

genehmigte

DISSERTATION

VON

Dipl.-Ing. Alexandra Ludwig

geboren in

München

Tag der mündlichen Prüfung:

25. April 2016

Hauptreferent:

Prof. Dr. sc. nat. Juerg Leuthold

Korreferenten:

Prof. Dr.-Ing. Dr. h. c. Wolfgang Freude







## Abstract (German)

Die vorliegende Arbeit befasst sich mit hochempfindlichen optischen Kommunikationssystemen, wie sie z.B. bei Intersatellitenlinks verwendet werden. Theoretische Überlegungen zur Steigerung der Empfängerempfindlichkeit werden mit Simulations- und Messergebnissen ergänzt und verifiziert.

Auf Grund der steigenden Nachfrage nach optischen Links zwischen Satelliten stellt sich die Frage, was sind geeignete Eckparameter, um ein solches System zu beschreiben. Die gigantischen Datenmengen, die von diversen Messgeräten, wie z.B. hochauflösende Kameras auf einem Satelliten generiert werden, bringen die Kapazitäten klassischer HF-Datenlinks an ihre Grenzen. Hier können optische Kommunikationssysteme auf Grund ihrer hohen Trägerfrequenz im Infrarotbereich sehr hohe Datenraten im Terabit/s Bereich ermöglichen. Systeme mit Radiowellen im GHz Bereich als Trägerfrequenz sind hier deutlich limitierter. [7]

Linkdistanz, verfügbare Leistung, Pointinggenauigkeit und verfügbare Antennengröße sind einige Parameter, die einen wichtigen Einfluss auf die Leistungsfähigkeit des Systems haben. Je größer die Distanz und desto kleiner die verfügbare Antennengröße sowohl am Sender als auch am Empfänger sind, desto weniger Signalleistung wird den Detektor erreichen. Nimmt man dann noch ungenaues Pointing hinzu, d.h. Sender und Empfänger sind nicht exakt aufeinander ausgerichtet, treten zusätzliche Verluste auf. [7]

Ziel dieser Arbeit ist es, ein vereinfachtes System zu implementieren und zu testen, das mit möglichst wenigen Photonen pro Bit bei einer gegebenen Bitfehlerwahrscheinlichkeit bei einer möglichst hohen Datenrate arbeiten kann. Hierfür werden alle Freiheitsgrade einer optischen Welle zur Modulation verwendet, um mit sog. „Stapeln“ von Modulationsformaten eine Empfindlichkeitssteigerung zu erreichen. Die Amplitude des Signals wird durch Pulspositionsmodulation (PPM) moduliert, wobei das zeitlich variable Vorhandensein eines Pulses innerhalb des Symbols die Information enthält. Dieses Modulationsformat weist bis dato die höchste Empfindlichkeit in Literatur und Experimenten auf [4]. Je mehr Möglichkeiten es gibt, einen Puls in einem Symbol zu platzieren, desto höher ist die zu erwartende Empfindlichkeit des Systems. Mit anderen Worten: Steigert man die zeitliche Dauer eines PPM-Symbols, so wächst ebenfalls die Empfängerempfindlichkeit. Da bei diesem Ansatz die Datenrate sinkt, wird in dieser Arbeit eine andere Methode vorgestellt, die

Empfindlichkeit eines Übertragungssystems zu steigern, ohne die Symbollänge unnötig in die Länge zu ziehen.

Diese Arbeit befasst sich mit dem Stapeln (sog. „Stacking“) von Modulationsformaten, in dem neben der Amplitudenmodulation weitere Freiheitsgrade, wie die Frequenz, Phase und Polarisation geschickt genutzt werden. Bei der Frequenzumtastung (FSK) wird die optische Frequenz je nach Symbol um ein gewisses Maß  $\Delta f$  verschoben. Bei der polarisationsgeschalteten Quadratur-Phasenumtastung (PS-QPSK) werden sowohl die Phase, als auch die Polarisation der optischen Welle moduliert [12]. Als Endergebnis erhält man PPM-FSK-PS-QPSK als Modulationsformat mit hoher Empfindlichkeit. Gegenüber dem reinen PPM wird eine theoretische Empfindlichkeitssteigerung von mehr als 1 dB erreicht. Sowohl Simulations- als auch Messergebnisse bestätigen den Empfindlichkeitsgewinn.

## Abstract (English)

The present work discusses highly sensitive optical communication systems as they are used for example in inter-satellite links. Theoretical analysis about receiver sensitivity improvements are complemented and verified with simulation and measurement results.

There is an ever increasing demand for bandwidth and accordingly an increased demand for satellite links. The gigantic amount of data that is generated by measurement devices such as high-resolution cameras brings classical RF data links to their limits. Here, optical communication systems can enable very high data rates in the Terabit/s thanks to a high carrier frequency in the infra-red range. Systems using radio frequency in the GHz regime are much more limited. A key question then is what parameters will be needed to describe satellite links well. [7]

Link distance, available power, pointing accuracy and available antenna sizes are a few parameters that have an important influence onto the performance of the system. The larger the distance and the smaller the available antenna diameter at transmitter side as well as receiver side, the lesser signal power reaches the detector. Adding in addition inaccurate pointing, i.e. a system where transmitter and receiver are not aligned correctly, will lead to additional losses. [7]

It is the goal of this work to implement and test a simplified system that works with as few photons per bit at a given bit error ratio with the highest possible data rate. In this thesis we pursue an approach where all degrees of freedom of an optical wave are used for modulation to achieve an increase in the highest spectral sensitivity by “stacking” modulation formats. A key aspect of this approach is the modulation of the amplitude of the signal by pulse-position modulation (PPM), where the time variable presence of a pulse within the symbol contains the information. This modulation format has shown the highest sensitivity in literature and experiments, so far [4]. The more possibilities exist to position a pulse within a symbol, the higher the system sensitivity is to be expected. In other words: Increasing the duration of a PPM symbol leads to an increase of the receiver sensitivity. However, since this leads to very low data rates a different method is presented in this work to improve the sensitivity of a transmission system without lengthening the symbol unnecessarily.

This work addresses stacking modulation formats by using besides amplitude modulation additional degrees of freedom, like frequency, phase and polarization in a clever way. With frequency-shift keying (FSK), the

optical frequency is shifted depending on the symbol by a certain amount  $\Delta f$ . For polarization-switched quadrature-phase-shift keying (PS-QPSK) the phase as well as the polarization of an optical wave are modulated [12]. As a result, one gets PPM-FSK-PS-QPSK as a modulation format with high receiver sensitivity. Compared to pure PPM a theoretical sensitivity improvement of more than 1 dB is achieved. Simulation results as well as measurement results prove this gain of sensitivity.

## Introduction

The ever increasing demand for data from planetary probes pushes the frequency of telecommunications from radio frequency (RF) bands to the optical and near-infrared regime, since higher carrier frequencies allow higher bandwidths for data transmission. Early NASA spacecraft telecom systems relied on the S-band with carrier frequencies in the range of 2.025-2.290 GHz [7, 10, 13, 14].

Today, X-band carrier frequencies in the range of 8.025-8.400 GHz are state of the art with data rates of 10-400 Mbit/s per channel. The commonly used modulation format is QPSK, which is often combined with polarization multiplexing to further increase the data rate. For example the TerraSAR-X earth observation LEO satellite uses QPSK on single polarization with 200 Mbit/s, whereas WorldView-2 reaches 800 Mbit/s with the help of polarization multiplexing. Some notable deep space probe programs that employed X-band communications include the Viking Mars landers, the Voyager missions to Jupiter and Saturn, and the Curiosity rover. Twenty-five years later, the K<sub>a</sub>-band systems with frequency ranging between 17-31 GHz become the new standard in satellite communications with data rates of 0.6-1.2 Gbit/s per carrier and polarization.

After a number of successful and convincing technology validation demonstrations, the optical band is expected to be tested soon, i.e., it is coming into the “operational readiness” phase. So-called laser communication terminals were developed and delivered for optical broadband communications in space. In 2014, the inter-satellite link between the two low earth orbit (LEO) satellites NFIRE (U.S.) and TerraSAR-X (Germany) has been tested, operating at 5.6 Gbit/s and over a distance up to 5 000 km. However, only dummy data was transmitted for system-in-space validation.

In November 2014 Sentinel-1A (low-earth orbit; LEO) and Alphasat (geostationary satellite; GEO) have been connected by laser communication terminals over a distance of approximately 36 000 km to deliver earth observation data just moments after they were captured. This scenario is interesting, since the GEO is used as relay-satellite, which will forward the data down to earth in the K<sub>a</sub> band (RF frequency) with a data rate of 600 Mbit/s. The earth observation satellite Sentinel-2A is also equipped with a laser communication terminal for LEO-to-GEO intersatellite links. The commissioning of the laser communication is currently ongoing.

In the future, it is planned to have a constellation of three of these relay-satellites to form the European Data Relay Satellite System, where the first satellite is foreseen to be launched in 2016. Relay satellites are equipped with laser communication terminals to provide laser communications in space with data rates of up to 1.8 Gbit/s as well as with  $K_a$  band transmitters. This shows that optical space-communication systems are currently moving forward to become a promising new data transmission technology. However, for the downlink to earth, RF systems are still used and require multi-carrier solutions to provide the necessary capacity.

All optical inter-satellite communication systems named previously have the usage of complex modulation of the carrier in combination with a coherent receiver in common. The reason for this can be found in two key aspects: Receiver sensitivity and spectral efficiency. A high receiver sensitivity is desired, meaning that the signal can be demodulated error-free even if only very little signal energy is received. On the other hand, one wants to transmit as much data as possible within this little signal energy leading to a high spectral efficiency. The trade-off between these two aspects will be discussed in more detail later in Chapter 1. Optical inter-satellite links are commonly quadrature phase-shift keying (QPSK) based that is demodulated by a coherent receiver.

On the contrary, in the case of optical downlinks to earth, on-off keying (OOK) systems with direct detection are under investigation, although their receiver sensitivity is commonly quite poor. Atmospheric distortions make the implementation of phase-sensitive modulation formats rather challenging [8, 15].

However, optical free-space transmission systems, like optical inter-satellite communication systems, suffer from tremendous link losses, i.e. free-space losses, because intermediate in-line amplification like in terrestrial long-haul systems is not possible [16]. As feasible antenna sizes and the size of optical receiver telescope systems cannot be made arbitrarily large, the possibilities to boost the signal are restricted. Therefore, the receivers of such systems must be able to demodulate the signal correctly, even if only little signal energy per bit is available [10, 13, 14].

Besides the optical free-space communication systems that are under operation in space right now, there is research going on to push the limits of maximum possible link lengths and maximum data-rates even further. As an alternative to the commonly implemented QPSK modulation format, it has been proposed that stacking of multiple modulation formats is the best

option to enhance the receiver sensitivity for optical free-space links [11, 17, 18].

Besides stacking multiple modulation formats, another way of increasing the energy efficiency of a modulation format has been proposed: Polarization-switched quadrature phase-shift keying (PS-QPSK) is the most power-efficient type of modulation format among the common PSK signals [3]. By combining this scheme with pulse-position modulation (PPM), the sensitivity can be enhanced even further [10]. In the past, PPM has mostly been used in direct detection schemes, where it shows unbeaten sensitivity if used with a large number of time slots [4, 8]. Yet, to achieve high data rates at high sensitivity using PPM, a large bandwidth is required.

Thus, there still is room for improvement by additionally stacking frequency-shift keying (FSK) and polarization-switched QPSK (PS-QPSK). So far, FSK is rather rarely found in optical transmission schemes. This is due to the fact that, similar to PPM, a high number of symbols, i.e. frequencies are required for achieving a better sensitivity. This is the reason, why this work thoroughly investigates the stacking of the following modulation formats: PPM, FSK and PS-QPSK.

The thesis is structured as follows: Chapter 1 presents a general approach to receiver sensitivity. Second, several promising modulation formats, like quadrature phase-shift keying (QPSK), polarization-switched QPSK (PS-QPSK), pulse-position modulation (PPM) and frequency shift keying (FSK) are discussed together with implementation challenges, see Chapter 2. In Chapter 3 the receiver sensitivity of each modulation format is derived in an analytical approach. This chapter concludes with analytical formulas describing the theoretical receiver sensitivity for stacked modulation formats combining from two or three different modulation formats.

In Chapter 4, multipulse PPM is introduced as a modulation format that is interesting for systems, where not only the sensitivity is of importance, but also the spectral efficiency (SE). In multipulse PPM the sensitivity slightly decreases, if more than one pulse per symbol is transmitted. However, the transmitted amount of data can be increased since the position of the additional pulse carries data as well.

In Chapter 5, measurement results of stacking 64PPM with PS-QPSK are discussed and presented. It is shown that only 2.6 photons per bit are required to demodulate such a modulated signal with a bit-error ratio (BER) of  $10^{-3}$ .

In Chapter 6, the previous measurement results are improved by adding an additional degree of freedom to the modulation: Frequency shift keying. This results in 64PPM-4FSK-PS-QPSK transmitting eleven bit per symbol. It results in only 2.3 photons per bit as a sensitivity measure for a BER of  $10^{-3}$ .

Chapter 7 concludes this work and summarizes the achieved results.

# Table of Contents

<b>Abstract (German)</b> .....	<b>i</b>
<b>Abstract (English)</b> .....	<b>iii</b>
<b>Introduction</b> .....	<b>v</b>
<b>Table of Contents</b> .....	<b>ix</b>
<b>Table of Figures</b> .....	<b>xii</b>
<b>1 The Shannon Limit</b> .....	<b>1</b>
1.1 Introduction .....	1
1.2 Digital Communications.....	2
1.3 Stacking Modulation Formats .....	5
1.4 Conclusion .....	7
<b>2 Modulation of Optical Signals</b> .....	<b>8</b>
2.1 The Optical Dual-Polarization IQ Modulator .....	8
2.2 Discussion About Selected Modulation Formats .....	10
2.2.1 Phase-Shift-Keying (PSK).....	10
2.2.2 Polarization-Shift Keying (PolSK) .....	13
2.2.3 Polarization Switched Quadrature-Phase-Shift Keying (PS-QPSK) .....	14
2.2.4 Pulse-Position Modulation (PPM).....	18
2.2.5 Frequency Shift Keying (FSK).....	19
<b>3 Theoretical Background about Receiver Sensitivity</b> .....	<b>25</b>
3.1 The Coherent Receiver .....	26
3.2 Measurement of the Receiver Sensitivity.....	28
3.3 Receiver Sensitivity of Selected Modulation Formats.....	30
3.3.1 Theoretical Sensitivity of Binary and Quadrature Phase Shift Keying (BPSK and QPSK) .....	32
3.3.2 Theoretical Sensitivity of Polarization Switched QPSK (PS-QPSK).....	34
3.3.3 Theoretical Sensitivity of Pulse-Position Modulation (PPM) and Orthogonal Frequency Shift Keying (FSK) .....	36
3.4 Receiver Sensitivity of Multiplexed Signals .....	47
3.5 Theoretical Sensitivity of Stacked Modulation Formats.....	48
3.5.1 <i>Mary</i> PPM-PS-QPSK.....	49

3.5.2	Theoretical Receiver Sensitivity of Stacked MPPM-NFSK-PS-QPSK .....	49
3.5.3	Theoretical Receiver Sensitivity of Stacked MPPM-KOFDM-PS-QPSK .....	51
3.6	Conclusion .....	53
<b>4</b>	<b>Multi-Pulse PPM and Multi-Frequency FSK.....</b>	<b>54</b>
4.1	Receiver Sensitivity of Multi-Pulse PPM and Multi-Frequency FSK..	54
4.1.1	One Dimensional Multi-Pulse PPM .....	55
4.1.2	Two Dimensional Multi-Pulse PPM.....	57
4.2	FSK versus 2ASK-OSDM.....	58
4.3	Conclusion .....	59
<b>5</b>	<b>Sensitivity Measurements of 64PPM-PS-QPSK .....</b>	<b>60</b>
5.1	Introduction .....	60
5.2	Measurement Principle.....	61
5.3	Analytical Analysis of Sensitivity .....	63
5.4	Results .....	64
5.5	Conclusion .....	65
<b>6</b>	<b>Sensitivity Measurements of 64PPM-4FSK–PS-QPSK.....</b>	<b>66</b>
6.1	Introduction .....	67
6.2	Stacking Modulation Formats .....	68
6.3	Operation Principle and Measurement Setup.....	70
6.3.1	Measurement Setup.....	70
6.3.2	Signal Generation.....	71
6.3.3	Signal Demodulation .....	74
6.4	Theoretical Sensitivity Analysis of Stacked Modulation Formats.....	76
6.5	Experiment and Simulation .....	78
6.6	Conclusion .....	82
6.7	Appendix 1: Number of Photons per Bit.....	82
6.8	Appendix 2: Sensitivity of PPM, FSK and PS-QPSK formats .....	83
6.9	Acknowledgements .....	89
6.10	Addendum: Discussion of Results .....	89
<b>7</b>	<b>Conclusion.....</b>	<b>93</b>
	<b>Appendix A: Methods.....</b>	<b>94</b>

A.1	Energy Considerations.....	94
A.2	Synchronization Preambles for PPM .....	96
A.2.1	Principal-Secondary Maximum Relation (PSMR) and Merit Factor (MF) .....	96
A.2.2	Sequences with Good Auto-Correlation Function Properties .....	97
A.2.3	Conclusion .....	99
A.3	Phase- and Polarization Estimation: Kalman Filter .....	100
<b>Appendix B:</b>	<b>References.....</b>	<b>104</b>
<b>Appendix C:</b>	<b>Glossary .....</b>	<b>111</b>
C.1	List of Abbreviations.....	111
C.2	List of Symbols.....	112
C.2.1	Calligraphic Symbols.....	112
C.2.2	Greek Symbols.....	112
C.2.3	Latin Symbols .....	113
<b>Appendix D:</b>	<b>Acknowledgements (German) .....</b>	<b>115</b>
<b>Appendix E:</b>	<b>List of Publications .....</b>	<b>118</b>
E.1	Journal Publications.....	118
E.2	Conference Proceedings .....	119

# Table of Figures

Fig. 1.1 Theoretical limit of signal to noise ratio per bit  $\mathcal{E}_b/N_0$  and spectral efficiency (SE) per polarization according to Shannon [8, 9]. In addition some common modulation formats as well as some stacked modulation formats as will be discussed below are plotted. All results correspond to the best achievable theoretical sensitivities and spectral efficiencies at a BER =  $10^{-3}$ . Results in this plot have been taken from [2, 3, 8, 10, 11]. The stacked modulation formats shown here, are a combination of PS-QPSK (PSQ), Pol-Mux QPSK (PMQ), and PPM. .... 4

Fig. 2.1 Schematic diagram of a dual polarization (DP) IQ-Mach-Zehnder modulator commonly used for PM-QPSK or QAM modulation. It consists of two IQ-modulators, where the output signal of one of them is rotated in its polarization by a half wave plate ( $\lambda/2$ ). The bias voltages are omitted for simplification. In yellow, the signal-electrode of the ground-signal-ground (GSG) configuration is depicted. The ground electrodes are omitted as well. .... 9

Fig. 2.2 PSK representation in (a) time domain for NRZ-BPSK, (b) complex plane for BPSK and QPSK and (c) frequency domain. .... 11

Fig. 2.3 QPSK constellation diagrams: (a) in 4QAM representation, (b) IQ imbalance (c) Quadrature error. .... 12

Fig. 2.4 One possible way of implementing 2PolSK, comprising only linear states of polarization for  $\theta = \frac{\pi}{4}$ . This can be achieved by modulating the phases  $\varphi_x$  and  $\varphi_y$  as depicted leading to relative phases of  $\varphi_r(t) = 0$  and  $\varphi_r(t) = \pi/2$  or  $\varphi_r(t) = -\pi/2$  [3]. .... 14

Fig. 2.5 Phase values of the PM-QPSK symbols in blue circles (o) depending either on the phases of the two polarizations  $\varphi_{x,y}$  or on the absolute and relative phases  $\varphi_{a,r}$  with  $\theta = \frac{\pi}{4}$ . In red filled circles the PS-QPSK symbols are depicted [3]. .... 15

Fig. 2.6 Generation and representation of PS-QPSK symbols. (a) Dual-polarization IQ modulator for generating an optical PS-QPSK signal assuming the three bits encoded in one symbol B1-3 represent voltages with amplitudes smaller than the  $\pi$  voltage of the modulator and signs according to their logical value, i.e. a positive voltage for a logical one and a negative voltage for the logical zero, see [3]. (b) Constellation diagram of the PS-QPSK symbols according to [3], the logical dependence of  $Q_y$  from the  $I_x$ ,  $Q_x$  and  $I_y$  cannot be seen from this representation of symbols. If the reference plane of the polarization is rotated by  $45^\circ$ , and replaced by the  $x'$ ,  $y'$  coordinate system (c), then the constellation diagrams of the two polarization bits can be seen (d). .... 17

- Fig. 2.7 4PPM symbols depicted in time-domain (—). It can be seen that the average signal power (avg.  $P_{\text{sig}}$ ) is much smaller than the peak power. The symbol can still be detected correctly, as long as the peak power is higher than the noise power  $P_{\text{noise}}$  (---). [4] ..... 18
- Fig. 2.8 Possible 2FSK sequence in time domain..... 19
- Fig. 2.9 Generation of a frequency shift  $f_{\text{shift}}$ . The phasor of the IQ-diagram is rotating in a circle. This is achieved by modulating the real part of the signal by a cosine and the imaginary part with a sine wave with frequency equal to  $f_{\text{shift}}$ . ..... 21
- Fig. 2.10 Implementation challenges of FSK, solid line: the ideal signal, (a) amplitude imbalance, (b) phase offset between  $I$  and  $Q$  (c) Spectrum of the shifted laser frequency  $f_c$  in positive direction by  $f_{\text{shift}}$  (c) ideal shift (d) distorted shift either due to amplitude imbalance or phase offset. Both effects lead to non-perfect suppression of the mirror frequency at  $f_c - f_{\text{shift}}$ . ..... 23
- Fig. 2.11 Optical spectrum of the 4FSK modulated signal with orthogonal frequencies and NRZ pulse shape. The center tone, i.e. the laser frequency  $f_c$  is not used. The vertical axis is plotted linearly. .... 23
- Fig. 3.1 Scheme of a polarization diverse and phase diverse coherent receiver. The signal at the input carries information in both polarizations,  $x$  and  $y$ . It is split into its two components by a polarization beam splitter (PBS), and each is fed into a phase-diversity coherent receiver. Due to implementation advantages, the local oscillator (LO) carries only light in  $x$ -polarization. Thus, its power is split, whereas one half is fed to the phase-diversity coherent receiver demodulating the  $x$ -part of the signal, while the polarization of the other half is rotated by a half-wave plate ( $\lambda/2$ ) to achieve a local oscillator that interferes with the  $y$ -part of the signal. .... 27
- Fig. 3.2 Symbol decision for BPSK (a) The two symbols sent:  $s_1$  in blue, and  $s_2$  in red (b) shows the imaginary part of the analytical received signal in the presence of AWGN (c) shows the real part of the analytical received signal in the presence of AWGN. For BPSK, the optimum threshold  $\rho_{\text{th}}$  that is applied for symbol decision is zero. .... 33
- Fig. 3.3 PS-QPSK: (a) bit mapping of PS-QPSK symbols (red) in the phase state diagram, while all PM-QPSK symbols are shown as well (dark blue) (b) bit error ratio (BER) versus  $\mathcal{E}_b/N_0$  characteristics for PS-QPSK and (PM-). The sensitivity advantage of PS-QPSK is clearly visible..... 35
- Fig. 3.4 Analytical results of  $M$ -PPM or  $M$ -FSK for different ways of demodulation. It can be seen that the higher the number of slots per symbol, the higher the sensitivity. (a) homodyne reception in one polarization (b) single polarization envelope detection (c) envelope detection with polarization diverse reception. .... 43

- Fig. 3.5 Sensitivity of 64PPM when detected with different power splitting ratios  $\alpha_p$  on the two polarizations if the sum of the absolute values is used for demodulation. It becomes clear that here the result strongly depends on  $\alpha_p$ . For comparison the result using the  $\chi^2$ -distribution is used is shown as well, which is  $\alpha_p$ -independent..... 47
- Fig. 4.1 The difference of “conventional” PPM and multi-pulse PPM is depicted in time domain (a) two exemplarily PPM symbols of 4PPM are depicted with the pulse either in the first or second slot. (b) four possible symbols of 1-dimensional multi-pulse PPM with two pulses per symbol are depicted. 54
- Fig. 4.2 Receiver sensitivities for 1dimensional multipulse PPM for different values of  $M$  and  $M_p$ . The ratio of signal to noise ratio per bit over signal to noise ratio per symbol of “conventional” PPM is depicted as a function of number of slots per symbol  $M$  for different number of pulses  $M_p$  encoded in one symbol..... 55
- Fig. 4.3 Channel capacity as a function of number of slots per symbol  $M$  for different number of pulses  $M_p$  encoded in one symbol. It is assumed that in one time slot only one pulse can be found. .... 56
- Fig. 4.4 “Conventional” PPM versus 2D-Multipulse PPM (a) “Conventional” 2PPM (Manchester coding) alphabet. There is the pulse either in the first or second half of the symbol. (b) New alphabet, called 2amplitude shift keying orthogonal slot-division multiplexing (2ASK-OSDM), with four symbols.58
- Fig. 5.1(a) Setup scheme with transmitter and preamplified coherent receiver to mimick a free space communication system. The transmitter consists of an external cavity laser (ECL) providing 0 dBm output power at 1549 nm. The laser provides both the cw signal to be encoded with information as well as the local oscillator for reception. The signal is modulated by a dual-polarization IQ-modulator driven by an Arbitrary Waveform Generator (AWG) with four output ports and 12 GHz sampling rate. The effect of the free-space optical channel is reduced to a variable optical attenuator followed by an optical splitter that allows monitoring the optical input power into the preamplified receiver that is used to receive the signal. The signal is detected by a dual polarization  $90^\circ$  hybrid followed by four balanced detectors. Two synchronized real-time oscilloscopes with a sampling rate of 80 GSamples/s store the signals for later offline processing. (b,c) the IQ diagram with color-coded histogram of the first 10000 PS-QPSK-64PPM encoded slots are depicted for x and y polarization. The plots have been taken for a receiver input power of 8.7 photons per bit. .... 62
- Fig. 5.2 Here the results are shown: BER vs. Photons per Bit in dB for measured, simulated and analytical results. It can be seen that the simulations match very well with the measurement, and there is a slight offset of 0.75 dB to the analytical theory. This offset can be explained by non-ideal noise figure of the preamplifying EDFA and the non-ideal equalization of phase noise. ... 64

- Fig. 6.1 Setup with transmitter and pre-amplified coherent receiver. The signal is modulated by a dual-polarization (DP) IQ-modulator driven by an arbitrary waveform generator (AWG). The free-space optical channel is emulated by a variable optical attenuator (VOA), followed by a coupler that taps the optical input and monitors the power entering the pre-amplified receiver with a power meter (PM). An optical spectrum analyzer (OSA) is used to monitor the OSNR and the polarization controlled (PC) signal is detected by a coherent polarization-diversity receiver. Two real-time oscilloscopes store the signals for offline processing. The laser acts both as a continuous-wave source for the transmitter and as a local oscillator (LO) for the receiver..... 71
- Fig. 6.2 Schematic display of stacking PPM with FSK and PS-QPSK symbols represented in time domain (top row), in constellation space (middle row), and in frequency domain (bottom row). The columns show typical (a) PPM, (b) FSK and (c) PS-QPSK symbols. The PS-QPSK symbols are depicted as a subset of the PM-QPSK symbols. The right-most column (d) displays the PPM-FSK-PS-QPSK stack. Each PPM pulse comprises optical sine and cosine-shaped optical fields that contain the information on the frequencies, phases and polarization. .... 72
- Fig. 6.3 Calculated bit error ratios (BER) for different modulation/multiplexing stacks. (a) BER as a function of the number of photons per bit (b) BER as a function of the number of *photons per symbol*. .... 78
- Fig. 6.4 Measured 64PPM-4FSK-PS-QPSK receiver signal. (a) In-phase (blue) and quadrature (red) components of a baseband signal as a function of time. The plots show the x-polarization components of 4 random symbols with symbol duration  $T_{sym}$ . (b) Zoom into the non-zero slot of the 4th symbol. (c) Optical spectrum. Four peaks at  $\pm 750$  MHz and  $\pm 1.5$  GHz are to be seen. The carrier  $f_c$  in the center of the spectrum is (not perfectly) suppressed.... 79
- Fig. 6.5 Bit error ratio (BER) as a function of the number of photons per bit for different modulation formats. PSQ abbreviates the format PS-QPSK. (a) Individual modulation formats 4FSK, PS-QPSK, and 64PPM with sensitivities per bit of 9 dB, 7 dB, and 5 dB, respectively, at a target  $BER = 10^{-3}$ . (b) Stacked modulation formats 4FSK-PS-QPSK, 64PPM-4FSK-PS-QPSK, and 64PPM-2OFDM-PS-QPSK. The limiting number of photons per bit reduces when stacking more modulation formats. The stacked format 64PPM-4FSK-PS-QPSK shows a limiting photon number per bit of 3.7 dB, slightly better than 64PPM-2OFDM-PS-QPSK. Theoretically calculated BER for various modulation format stacks comprising 64PPM, 4FSK, PS-QPSK and including 2OFDM are shown for comparison. .... 80
- Fig. 6.6 Comparison of the results derived from the power meter (PM) and the optical spectrum analyzer (OSA) for 64PPM-4FSK-PS-QPSK. .... 83

Fig. 6.7 Bit error ratio vs. photons per symbol for (a) 64PPM-4FSK-PS-QPSK and (b) 64PPM-2OFDM-PS-QPSK and its respective BER contributions of 64PPM (green), 4FSK (black), PS-QPSK (red) or 2OFDM-PS-QPSK (magenta). The abbreviation PSQ stands for PS-QPSK. The contributing BER of each modulation format, i.e. each step in the demodulation chain is depicted for clarity. In (a) all modulation formats show the same performance. This leads to the conclusion that 64PPM as the first to be demodulated limits the performance of the consecutive modulation formats. In (b) a different situation is shown: 2OFDM-PS-QPSK shows worse performance than 64PPM. Here, 64PPM does not limit the performance. However, 64PPM shows slightly worse performance, since a higher bandwidth for symbol decision is needed, since now two OFDM subcarriers are looked at with their respective bandwidth. Total BER of the 64PPM-2OFDM-PS-QPSK can be found in the middle of both curves, since it represents an average BER of the 64PPM BER and 2OFDM-PS-QPSK BER. .... 91

# 1 The Shannon Limit

In this chapter, the ultimate sensitivity limit, i.e. the so-called Shannon limit is introduced and discussed.

## 1.1 Introduction

The aim of highly sensitive transmission links is to minimize the amount of energy per bit required for an error-free data reception. However, there are several limiting factors that must be taken into consideration. On the one hand, there is only limited bandwidth available. In free-space transmission, the electrical bandwidth of the devices at transmitter and receiver are limiting. In contrast to their bandwidth, the channel in inter-satellite-link itself can be considered to have infinite bandwidth. However, opto-electronic devices with large bandwidth are costly and latest state of the art devices show approximately a hundred gigahertz electro-optic bandwidth.

This bandwidth limit sets an upper bound of the amount of data that can be transmitted via such a communication system. However, there is also an advantage of limited bandwidth: in the presence of a white noise source, the bandwidth helps to limit the noise power in the system, and thus gives us a finite signal-to-noise-ratio (SNR). This shows that there is a link between SNR, i.e., sensitivity, and maximum data rate that can be transmitted via a communication system. This link is also known in information theory as the Shannon–Hartley theorem. It tells the maximum rate at which information can be transmitted in the presence of noise.

The theorem establishes Shannon's channel capacity for a specific communication link, a bound on the maximum amount of information that can be transmitted and received error-free with a certain bandwidth in the presence of noise. The assumptions Shannon has made are several: First, he assumes that the signal power is restricted, which is usually the case. Every transmitter is only capable of sending out a finite signal power and every channel at least attenuates the signal.

The second assumption Shannon is making concerns the noise. He assumes a linear communication channel, which just adds additive Gaussian noise to the signal. This process is characterized by its known power spectral density. This is a general assumption that is valid in many cases, and can also often be applied to the free-space transmission channel of inter-satellite links. For further details, please refer to Chapter 6.

In addition, Shannon also makes a third assumption now regarding the signal: He assumes the signal's field to be also randomly Gaussian distributed, i.e. all symbols of the communication alphabet are not discrete, but behave and look like noise. It should be noted that this assumption however is not valid in real communication systems, where usually discrete symbols are common practice. This will be discussed in the following in more detail.

However, to summarize, Shannon stated a simple formula concerning the maximum amount of random data that can be transmitted error-free over an additive white Gaussian noise (AWGN) channel at a given signal power, noise power and available bandwidth. This chapter follows [2] and [19], chapter 1.4.

## 1.2 Digital Communications

One of the earliest forms of a digital communication system was the telegraph that was developed by Samuel F.B. Morse in 1837 including the famous Morse code. However, it was Nyquist who investigated in 1924 the problem of determining the maximum signaling rate that can be used over a telegraph channel with a given bandwidth without inter-symbol interference.

He defined the transmitted signal  $s(t)$  carrying the binary data sequence  $a_n \in \{\pm 1\}$  and having a pulse shape  $g(t)$

$$s(t) = \sum_n a_n g(t - nT) \quad (1.1)$$

with a data rate of  $1/T$  bit/s. Nyquist also figured out that if the system is bandwidth-limited to a bandwidth  $B$  the maximum bit rate is  $2B$ , assuming that we have a sampling rate of  $k/T$  with  $k$  being an integer number or zero. This maximum pulse rate can be achieved by using sinc-pulses of the form

$$g(t) = \frac{\sin(2\pi Bt)}{2\pi Bt}. \quad (1.2)$$

In 1948 Shannon cited Nyquist and agreed to his pioneer action, when he stated his famous sampling theorem that says that a signal having a bandwidth  $B$  can be reconstructed from samples taken at the Nyquist rate  $2B$  with the help of sinc-interpolation.

It was also Shannon who established the mathematical formulations describing the limits of digital communication systems. He stated that the three limiting factors of any communication system, i.e. limited signal

power  $P_{\text{Sig}}$ , restricted bandwidth  $B$ , and noise can be summarized in the measure of the so called channel capacity  $C$ . Assuming additive white Gaussian noise with spectral density  $N_0$  measured in a bandwidth  $B$  leads to the signal-to-noise power ratio  $\text{SNR} = P_{\text{Sig}} / (N_0 B)$ , which determines the channel capacity [2]

$$C = B \log_2(1 + \text{SNR}). \quad (1.3)$$

With this formula Shannon stated that if a systems is operated at a data rate smaller or equal  $C$ , it is theoretically possible to achieve error free transmission. However, if the data rate is larger than  $C$ , reliable transmission is not possible, regardless of the amount of signal processing efforts [19].

In contrary to Eq. (1.3) one often refers to the spectral efficiency (SE) as a measure of the amount of data one can transmit per symbol. It is defined as:

$$\text{SE} = \frac{C}{B} = \log_2(1 + \text{SNR}) \quad (1.4)$$

The spectral efficiency is usually given in bit/s/Hz. In many cases, not the overall SNR is of interest, but the SNR per bit  $\text{SNR}_{\text{bit}}$ . With a given number of bits per symbol  $n_{\text{bits/sym}}$  it is defined by

$$\text{SNR}_{\text{bit}} = \frac{P_{\text{Sig}}}{n_{\text{bits/sym}} N_0 B} = \frac{\mathcal{E}_{\text{Sig}} B}{n_{\text{bits/sym}} N_0 B} = \frac{\mathcal{E}_{\text{b}}}{N_0} \quad (1.5)$$

with  $\mathcal{E}_{\text{Sig}}$  being the signal energy and  $\mathcal{E}_{\text{b}}$  the energy per bit, respectively.

It is assumed that we have an analytical low-pass signal  $s_l(t) = I(t) + jQ(t)$  modulated onto an optical carrier having an amplitude  $A$  and a frequency  $f_c$ . We define the passband signal

$$\begin{aligned} s_p(t) &= \Re\{s_l A \exp(j 2\pi f_c t)\} \\ &= A [I(t) \cos(2\pi f_c t) - Q(t) \sin(2\pi f_c t)]. \end{aligned} \quad (1.6)$$

This equation can also be interpreted such that we have two real oscillators, one generating a sine and one generating cosine shaped carrier that form an orthogonal basis. Each real carrier is modulated by the real signals  $I(t)$  and  $Q(t)$ . Due to the orthogonality, no cross-talk takes place.

Shannon stated in Eq. (1.3) the best distribution of the signal which is affected by the AWGN channel would be a bidimensional Gaussian

distribution, that would lead to Gaussian distributions of  $I(t)$  and  $Q(t)$ . However, practical purposes suggest to use discrete signaling [2].

For a symbol decision, one usually sets a certain threshold and checks, if the received value is larger or smaller than the given threshold. This is how a decision is made to which constellation point in the diagram the received symbol might most probably belong. As an example a discrete-valued modulation format would be QPSK. After detection, the discrete-valued symbols are superimposed by Gaussian noise on both oscillators, the I and Q, i.e. the cosine and sine oscillations, see Eq. (1.6).

Using discrete-valued symbols instead of Gaussian distributed ones one might expect that there is a draw-back from the maximum channel capacity, and with this, also from the maximum receiver sensitivity. And indeed, assuming a binary modulation format, such as BPSK, 1 bit per symbol and Hz can be transmitted with a required SNR of 6.8 dB at  $\text{BER} = 10^{-3}$ . The Shannon limit given in Eq. (1.3) for 1 bit/s/Hz would predict an SNR of 0 dB at error-free detection.

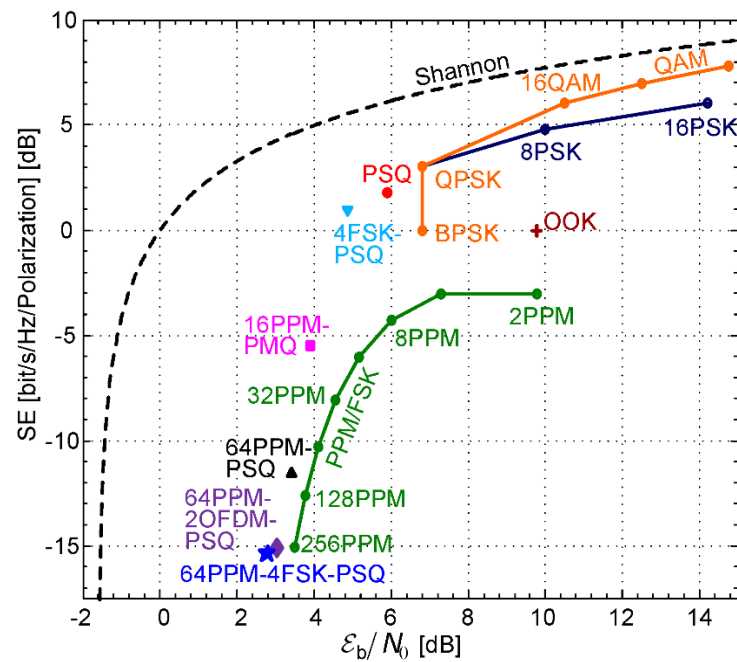


Fig. 1.1 Theoretical limit of signal to noise ratio per bit  $\mathcal{E}_b/N_0$  and spectral efficiency (SE) per polarization according to Shannon [8, 9]. In addition some common modulation formats as well as some stacked modulation formats as will be discussed below are plotted. All results correspond to the best achievable theoretical sensitivities and spectral efficiencies at a  $\text{BER} = 10^{-3}$ . Results in this plot have been taken from [2, 3, 8, 10, 11]. The stacked modulation formats shown here, are a combination of PS-QPSK (PSQ), Pol-Mux QPSK (PMQ), and PPM.

In Fig. 1.1 the Shannon limit is depicted as a dashed black line. In addition, binary phase-shift keying (BPSK), quadrature phase-shift keying (QPSK), and pulse-position modulation (PPM) are depicted as well at a BER =  $10^{-3}$ , all modulation formats that are well known for their receiver sensitivity [4]. The various results will be discussed in the following chapter in more detail. Looking at Fig. 1.1 one can see, that there is still room for improvement as none of the modulation formats can work with very low SNRs in order to come sufficiently close to the Shannon plot. The figure also shows  $N$ -ary PSK and QAM and how both modulation formats provide a large SE. Amongst the non-stacked modulation formats, *M*-ary PPM is the one with the highest sensitivity, especially for large  $M$ . However, this comes at a price of poor spectral efficiency. To understand this phenomenon, one must imagine a PPM symbol. It is divided into  $M$  timeslots, where one of these slot is occupied by one pulse. Thus, the average symbol power is very low, compared to the high pulse power that is  $M$  times the symbol power. Thus, as long as the pulse power is larger than the noise power, one can assume to demodulate the symbol correctly. The larger  $M$  becomes, the larger the average noise power can get before the symbol is detected wrongly. However, this comes at a price of reduced data rates/spectral efficiency. There is a better way to push modulation formats closer to the error-free reception. The best idea to do so is to stack modulation formats.

### 1.3 Stacking Modulation Formats

Before stacking modulation formats is discussed in more detail, an important measure must be introduced, the Euclidean distance  $d_{\min}$ . It is defined by the minimum distance between neighboring symbols with respect to the average signal power. The larger two neighboring symbols are separated from each other, the smaller is the probability to detect a symbol error [19].

For a transmission system where a high receiver sensitivity is to be combined with a reasonably large spectral efficiency (SE), a modulation format must be chosen where for a given average transmitter power the symbols have a large Euclidean distance while the number of encoded bits per symbol is still acceptably good.

Comparing  $N$ -ary PSK and QAM in Fig. 1.1, one can see that QAM has an advantage over PSK concerning SNR-requirements as well as spectral efficiency. This reason can be found in the larger Euclidean distance between the neighboring symbols for QAM, if the same number of

constellation points is assumed. This leads to an  $\mathcal{E}_b/N_0$  advantage over 3 dB of 16QAM over 16PSK.

“While optimizing the Euclidean distance of symbols, it has been shown in Ref. [3, 12] that polarization switched QPSK (PS-QPSK) is the modulation format with the largest possible Euclidean distance between symbols. PS-QPSK encodes 3 bits per symbol by stacking binary polarization-shift keying with QPSK [2, 11]” [14], see Fig. 1.1.

“The number of encoded bits per symbol can be increased by exploiting other degrees of freedom in the transmitted optical field strength. The previous discussion tacitly assumed that the PS-QPSK symbols occupy consecutive time intervals, the width of which determines the symbol duration (the symbol period). However, if each symbol period is subdivided in  $M$  time slots, and the PS-QPSK symbol is assigned to 1 out of these  $M$  possible time slots, we form a modulation stack of pulse position modulation (PPM) and PS-QPSK. The information content of this new symbol increases by  $\log_2 M$ . Assuming the same symbol duration and the same average power as before, the peak power in the occupied time slot is increased by  $M$ . This fact together with the increased information content per symbol allows one to reduce the required number of photons per bit at the receiver and thus to increase the sensitivity. The spectral efficiency is decreased though. Yet, if it is sensitivity that is most important, this could be worth the price [10]. In addition, the modulation stack can be extended by  $N$ -ary FSK. This increases the information content of the symbol by another factor  $\log_2 N$  and therefore reduces the required number of photons per bit once more – at the price of another reduction of spectral efficiency” [14], see Fig. 1.1. The reason for this can be found by thinking about an FSK-signal in frequency domain. For a given symbol rate, there must be a minimum frequency spacing according to Nyquist. Thus, by adding more frequencies to the symbol alphabet at a given symbol rate, the required bandwidth increases linearly and thus reduces the spectral efficiency.

“In the quest for the ultimate sensitivity one should also weigh in the options provided by multiplexing techniques. Multiplexing typically comes at the price of increased transmitter power. As an example: In the transition from PS-QPSK to PM-QPSK one wins 1 bit of information per symbol at the price of doubling the average signal power [3, 12]. Another option for multiplexing is applying wavelength division multiplexing (WDM) [8] or orthogonal frequency division multiplexing (OFDM) [20]. While an increase of the OFDM subcarrier number  $N$  increases the spectral efficiency,

the SNR per bit remains the same: Compared to one channel, two channels need double the power and transmit double the number of bits. However, channel crosstalk, quantization errors and nonlinearities might further decrease the overall sensitivity of the system. Since our goal is to reach an ultimately low number of received photons per bit, multiplexing as such is not the proper strategy. However, if multiplexing is part of a stacked modulation format, then stacking PM-QPSK and PPM might be a good compromise between increasing the number of bits per symbol and optimizing the Euclidean distance [5]” [14].

In Fig. 1.1 the theoretical spectral efficiency as well as the sensitivity requirements of 64PPM-4FSK-PS-QPSK and 64PPM-2OFDM-PS-QPSK are depicted both showing an improvement in sensitivity and spectral efficiency over the non-stacked modulation formats. For comparison, 64PPM-PS-QPSK and 16PPM-PM-QPSK (PM stands for polarization multiplexed) and 4FSK-PS-QPSK are depicted as well. Here, already the trend of improvement is visible as well, however, if highest sensitivity is the goal, one should implement 64PPM-4FSK-PS-QPSK or 64PPM-2OFDM-PS-QPSK.

## 1.4 Conclusion

In view of the prior art discussed in this section, we can conclude that stacking the proper modulation formats reduces the required number of received photons per bit considerably as it can be seen from Fig. 1.1. In this respect a PPM-FSK-PS-QPSK format appears to be the optimum modulation stack regarding modulation complexity and sensitivity. However, a combined modulation/multiplexing stack like PPM-OFDM-PS-QPSK with more bits per symbol but a larger limiting number of received photons per bit seems to be an interesting candidate as well [14].

In the following this statement will be verified by showing in Chapter 5 results of an experimental implementation of 64PPM-PS-QPSK as well as 64PPM-4FSK-PS-QPSK modulation stack with a sensitivity of 2.3 photons per bit compared to a 64PPM-2OFDM-PS-QPSK modulation/multiplexing stack with 2.4 photons per bit in Chapter 6. First, the modulation schemes and the required hardware components are introduced in Chapter 2 and 3.

## 2 Modulation of Optical Signals

In this chapter, modulation formats are introduced that are known for their high receiver sensitivity. In addition, the most versatile optical modulator is introduced first.

### 2.1 The Optical Dual-Polarization IQ Modulator

In this section, the dual-polarization IQ modulator (DP-IQ) is introduced. It is the most versatile modulator and can be used to modulate any degree of freedom: amplitude, phase, polarization and frequency. It consists of two IQ modulators, one of which has the polarization of its output signal rotated by a half wave plate. Thus, there are four RF input signals for the single-drive configuration:  $I$  and  $Q$  for each polarization  $x$  and  $y$  ( $V_{Ix}, V_{Qx}, V_{Iy}, V_{Qy}$ ). Its schematic is shown in Fig. 2.1. With such a device, any point in the complex plane as well as any state of polarization can be addressed [12]. It is commonly used for polarization multiplexed PM-QPSK or PM-QAM signal generation.

We start the discussion following [19] with an optical input signal that is fed into the modulator with the amplitude  $A$  and the frequency  $f_c$

$$E_{\text{in}} = \Re\{A \exp(j 2\pi f_c t)\} \quad (2.1)$$

with  $\Re\{\dots\}$  denoting the real part. The input signal is split into two waves which are fed into the upper and lower IQ Mach-Zehnder modulators (IQ-MZMs). Each of the IQ-MZM consists again of two MZMs that are often called ‘‘child-MZMs’’.

Each child-MZM shows a so-called single-drive Mach-Zehnder transfer function for push-pull operation, that depends on the drive-voltages  $V_{I,Q,x,y}(t)$ :

$$E_{\text{out},I,Q,x,y}(t) = E_{\text{in}} \cos\left(\frac{V_{I,Q,x,y}(t)}{2V_\pi} \pi - \frac{V_{\text{bias}}}{2V_\pi} \pi\right) \exp\left(j \left(\frac{V_{\text{bias}}}{2V_\pi} \pi + \frac{\pi}{2}\right)\right) \quad (2.2)$$

with  $V_{\text{bias}}$  being the constant voltage applied, to achieve the desired operation point. A characteristic parameter of the modulator is the so-called  $\pi$ -voltage  $V_\pi$ . In this work, the definition common for Mach-Zehnder modulators following Ref. [21] is used. Thus,  $V_\pi$  is defined as the voltage needed to achieve a relative phase shift of  $\pi$  between the upper and lower arms of the MZM. Therefore, as an example, drive voltages with peak values of  $\pm V_\pi$  in the MZM transfer function are required for BPSK modulation.

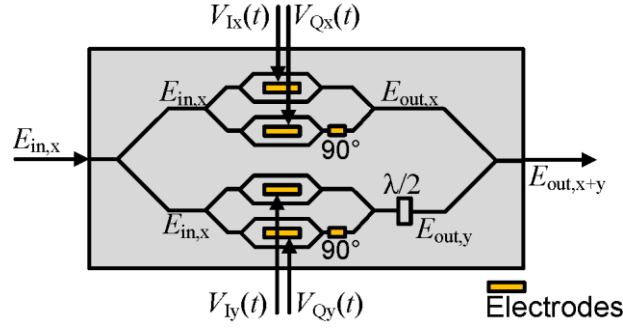


Fig. 2.1 Schematic diagram of a dual polarization (DP) IQ-Mach-Zehnder modulator commonly used for PM-QPSK or QAM modulation. It consists of two IQ-modulators, where the output signal of one of them is rotated in its polarization by a half wave plate ( $\lambda/2$ ). The bias voltages are omitted for simplification. In yellow, the signal-electrode of the ground-signal-ground (GSG) configuration is depicted. The ground electrodes are omitted as well.

However, it is also possible to reduce the voltage swing that drives the modulator. This works well, if the modulator is biased at its null point, this just leads to an additional modulation loss (ML). It is thus also possible to achieve BPSK modulation with driving signals that show amplitudes smaller than  $\pm V_\pi$ .

Assuming arbitrary driver signals of the four child-MZMs named here  $V_{I_{x,y}}(t)$  and  $V_{Q_{x,y}}(t)$ , respectively, any analytical low-pass signal in  $x$  or  $y$ -polarization, respectively  $s_{lx,y} = I_{x,y} + jQ_{x,y}$  can be modulated onto the optical carrier by using

$$\begin{aligned} V_{I_{x,y}} &= \frac{2V_\pi}{\pi} \arccos(I_{x,y}) \\ V_{Q_{x,y}} &= \frac{2V_\pi}{\pi} \arccos(Q_{x,y}). \end{aligned} \quad (2.3)$$

The transfer function of the dual-polarization IQ modulator using the orthogonal unit vectors  $\vec{e}_{x,y}$  equals

$$E_{\text{out,DP-IQ}} = E_{\text{out},x} \vec{e}_x + E_{\text{out},y} \vec{e}_y. \quad (2.4)$$

with:

$$\begin{aligned}
E_{\text{out},x,y}(t) &= \Re \left\{ s_{Ix,y} A \exp(j 2\pi f_c t) \right\} \\
&= \Re \left\{ (I + jQ) A \exp(j 2\pi f_c t) \right\} \\
&= A_{x,y} \cos \left( \frac{V_{Ix,y}(t)}{2V_\pi} \pi \right) \cos(2\pi f_c t) \\
&\quad - A_{x,y} \cos \left( \frac{V_{Qx,y}(t)}{2V_\pi} \pi \right) \sin(2\pi f_c t).
\end{aligned} \tag{2.5}$$

This modulator will be applied in the experiments presented and discussed in this work to modulate any degree of freedom of the optical field in order to achieve a higher receiver sensitivity in terms of required photons per bit for a given BER of  $10^{-3}$ .

## 2.2 Discussion About Selected Modulation Formats

In this section, common modulation formats used for optical communications are introduced. We use the orthogonal unit vectors  $\vec{e}_x$  and  $\vec{e}_y$ , representing two orthogonal states of linear polarization. Thus, our optical signal in two polarizations is described by  $\mathbf{E}_{\text{sig}} = E_{\text{sig},x} \vec{e}_x + E_{\text{sig},y} \vec{e}_y$ . With  $A_{x,y}$  being the real amplitudes of the signal in the two polarizations,  $f_c$  being the laser frequency and  $\varphi_{x,y}$  being its phases, respectively. Here, the laser frequency  $f_c$  does not depend on the polarization, and thus does the indices  $x$  and  $y$  are dropped for the following equations and thus we get [3]:

$$\mathbf{E}_{\text{sig}}(t) = \begin{pmatrix} \Re \left\{ A_x(t) \exp(j(2\pi f_c(t)t + \varphi_x(t))) \right\} \\ \Re \left\{ A_y(t) \exp(j(2\pi f_c(t)t + \varphi_y(t))) \right\} \end{pmatrix} \tag{2.6}$$

Looking at Eq. (2.6) it becomes obvious that four degrees of freedom are available for modulation [8]: Polarization, amplitude, frequency and phase. By varying these, with the help of the previously discussed modulator, the optical carrier can be modulated to transmit data.

### 2.2.1 Phase-Shift-Keying (PSK)

When searching literature for systems with a high receiver sensitivity, binary or quadrature phase-shift keying (BPSK, QPSK) is often named first [22]. As the name already indicates, the information is encoded in the phase of the signal. Depending on the number of phase states that the alphabet

contains, we speak of binary phase-shift-keying (BPSK), quadrature phase-shift keying (QPSK), 8PSK and so on. For the sake of simplicity, we discuss this modulation format in only one polarization and NRZ pulse shape. Taking Eq. (2.6) we set  $A_y = 0$ , drop the  $x$ -indices for simplicity and encode the information in the phase  $\varphi(t)$  one gets:

$$E_{\text{sig,PSK}}(t) = \Re\{A \exp(j2\pi f_c t + \varphi(t))\} \quad (2.7)$$

with  $\varphi(t) = 0, \pi$  for BPSK modulation and  $\varphi(t) = 0, \pm\pi/2, \pi$  for QPSK. Fig. 2.2 shows (a) the time domain representation of a NRZ-BPSK signal, as well as (b) the constellation diagrams of BPSK and QPSK and their NRZ-spectra. Every point in the constellation diagram placed on the unit circle represents one symbol. So, for BPSK, the alphabet consists of two symbols, for QPSK, there are four. Assuming same symbol rates for BPSK and QPSK, the spectra are the same, see Fig. 2.2(c). The QPSK constellation diagram is further more often depicted with a rotation by  $45^\circ$ , see Fig. 2.3(a). This is just a different representation but does not change the content of information. Sometimes, this  $45^\circ$  phase shift is used to differentiate between 4PSK and 4QAM, however, this does not change anything to the signal itself.

There are several ways to encode QPSK information onto an optical carrier. Recently, the optical IQ-modulator has become most popular, since the amount of chirp induced to the signal is minimized compared to a common phase-modulator. For QPSK modulation, the child Mach-Zehnder modulators are biased at the null point shifting the transfer-function in Eq. (2.2) such, that the cosine transfer-function becomes a sine. The driving signals are usually AC-coupled and have amplitudes smaller or equal  $V_\pi$ .

$$\cos\left(\frac{V_I(t)}{2V_\pi} \pi + \frac{V_{\text{bias}}}{2V_\pi} \pi\right) = \sin\left(\pm \frac{\pi}{2}\right) \quad \text{for } \frac{V_{\text{bias}}}{V_\pi} = -1 \quad \text{and} \quad \frac{V_{I,Q}(t)}{V_\pi} = \pm 1 \quad (2.8)$$

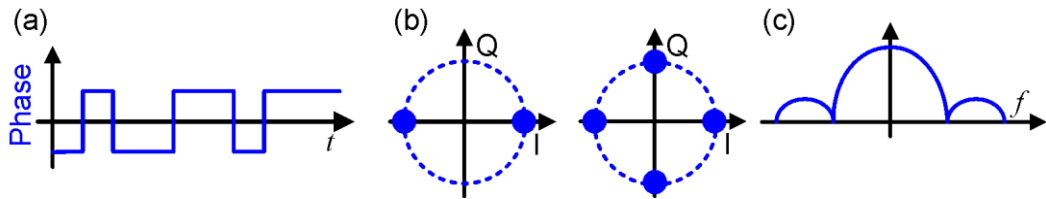


Fig. 2.2 PSK representation in (a) time domain for NRZ-BPSK, (b) complex plane for BPSK and QPSK and (c) frequency domain.

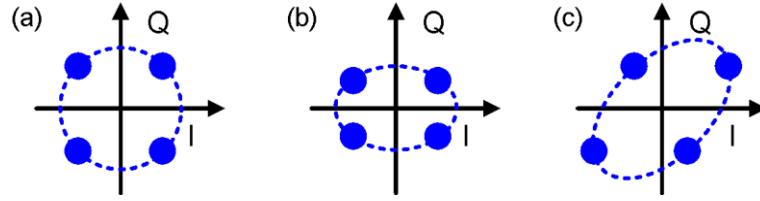


Fig. 2.3 QPSK constellation diagrams: (a) in 4QAM representation, (b) IQ imbalance (c) Quadrature error.

Thus rearranging Eq. (2.7), the QPSK signal modulated onto an optical carrier with the frequency  $f_c$  can be written as

$$E_{\text{QPSK}}(t) = A \cos(2\pi f_c t) \cdot \sin\left(\pm \frac{\pi}{2}\right) - A \sin(2\pi f_c t) \cdot \sin\left(\pm \frac{\pi}{2}\right). \quad (2.9)$$

This leads to 4 possible combinations of the  $\pm$  signs representing the four symbols of the QPSK alphabet. All symbols have the same amplitude  $A$  [23].

Implementation challenges of QSPK are manifold. The next paragraphs follow Refs. [24-28]. First, good care must be taken that both signals,  $I(t)$  and  $Q(t)$ , are well synchronized, otherwise there is a skew between the signals that leads to crosstalk between  $I$  and  $Q$ .

Another issue might be an imbalance between the amplitudes of the real and imaginary parts of the output signals. Different electrical amplitudes of the driving signals, or different  $\pi$ -voltages of the two nested Mach-Zehnder modulators can be a reason for this. This leads to a rectangular-shaped constellation diagram, see Fig. 2.3(b). This might become a limiting aspect when detecting the signal at low signal-to-noise ratios: For the same average signal power, some constellation points show a smaller distance from their neighboring constellation points than others.

A third issue is the so-called quadrature error (quad-error). Looking at Fig. 2.1 one sees the  $90^\circ$  phase shifter that rotates the signal of the lower child-MZM. This  $90^\circ$  phase shift enables the two carriers, i.e. sine and cosine in Eq. (2.9). Assuming an issue with the bias voltage applied that is responsible for this  $90^\circ$  phase-shift, the orthogonality of the two carriers is destroyed and crosstalk takes place, see Fig. 2.3(c). This can be compensated at the receiver at good signal to noise ratios [24, 26-28], but might be a limiting factor when the system works close to its sensitivity limit. It is hard to distinguish whether such a constellation diagram as shown in Fig. 2.3(c) is caused by a quadrature error or by a skew.

### 2.2.2 Polarization–Shift Keying (PolSK)

Polarization-shift keying (PolSK) is a rather seldom implemented modulation format in optical fiber communications [29]. However, it was suggested several times to be applied in free-space systems, to overcome phase-locking issues [30, 31]. It has become more common to use polarization as a degree of freedom for multiplexing rather than modulation [8, 29]. Binary PolSK (2PolSK) can be represented in two different ways [32]. On the one hand, it is interpreted as bipolar amplitude-shift keying of the two polarizations, respectively.

In this case, we get according to Eq. (2.6):

$$\mathbf{E}_{\text{sig,PolSK}}(t) = \begin{pmatrix} A_x(t) \exp(j(\omega_c t + \varphi_x)) \\ A_y(t) \exp(j(\omega_c t + \varphi_y)) \end{pmatrix} \quad (2.10)$$

$$\text{with } A_x(t) = \begin{cases} 0 & \text{for } A_y(t) = 1 \\ 1 & \text{for } A_y(t) = 0 \end{cases}$$

On the other hand, 2PolSK can also be generated by using the phase relation between  $\varphi_x$  and  $\varphi_y$ . Therefore we follow [3] and, for the sake of simplicity, set the angular frequency of the carrier to zero, i.e.  $\omega_c = 0$ . With the help of the normalized Jones vector  $\mathbf{J} = J_x \vec{e}_x + J_y \vec{e}_y$  and by introducing a new variable of the “absolute” phase of the signals field  $\varphi_a(t) = 1/2 \times (\varphi_x(t) + \varphi_y(t))$ , the electric field amplitude of the optical signal can be written as

$$\begin{aligned} \mathbf{E}_{\text{sig,PolSK}}(t) &= \begin{pmatrix} A_x \exp(j\varphi_x(t)) \\ A_y \exp(j\varphi_y(t)) \end{pmatrix} \\ &= \sqrt{|A_x|^2 + |A_y|^2} \exp(j\varphi_a(t)) \mathbf{J} \\ &= \sqrt{|A_x|^2 + |A_y|^2} \exp(j\varphi_a(t)) \begin{pmatrix} \cos \theta \exp(j\varphi_r(t)) \\ \sin \theta \exp(-j\varphi_r(t)) \end{pmatrix} \end{aligned} \quad (2.11)$$

$\varphi_r(t) = \frac{1}{2}(\varphi_x(t) - \varphi_y(t))$  describes the relative phase between the two polarizations. It is also called a measure for the ellipticity of the polarization state. The angle  $\theta$  with  $0 \leq \theta \leq \pi/2$  is called the azimuth and describes the orientation of the linear polarization states in the  $xy$ -plane. If  $\varphi_r(t) = 0, \pm\pi/2, \pi$  the light is linearly polarized, in the case of  $\varphi_r(t) = \pm\pi/4, \pm3\pi/4$  the light is circular polarized.

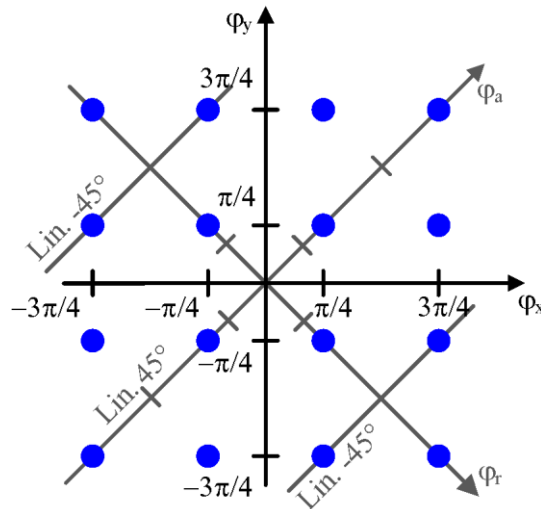


Fig. 2.4 One possible way of implementing 2PolSK, comprising only linear states of polarization for  $\theta = \frac{\pi}{4}$ . This can be achieved by modulating the phases  $\varphi_x$  and  $\varphi_y$  as depicted leading to relative phases of  $\varphi_r(t) = 0$  and  $\varphi_r(t) = \pi/2$  or  $\varphi_r(t) = -\pi/2$  [3].

Thus, if 2PolSK is implemented,  $\varphi_x$  and  $\varphi_y$  can be modulated with  $\theta = \pi/4$  such, that  $\varphi_r$  switches between  $\varphi_r(t) = 0$  and  $\varphi_r(t) = \pi/2$  or  $\varphi_r(t) = -\pi/2$ , see Fig. 2.4. This will be further discussed in more detail in the following section, when the relation between phase and polarization modulation will be investigated in the form of polarization switched QPSK (PS-QPSK).

It should be mentioned that after propagation through a fiber, the alignment of the polarization is random, due to imperfections in the circularity of the fiber core caused by manufacturing or bending. However, digital processing may be used to re-rotate the signal [32-36].

### 2.2.3 Polarization Switched Quadrature-Phase-Shift Keying (PS-QPSK)

Polarization-switched quadrature-phase-shift keying (PS-QPSK) has been introduced by Karlsson and Agrell in [3, 12]. Thus, this chapter follows these two references closely. It should be mentioned that this modulation format is also sometimes called “Hexa” [37].

PS-QPSK consists of two modulation formats: As the name already implies, it stacks 2PolSK and QPSK. Its symbols represent a subset of the symbol alphabet of polarization-multiplexed QPSK (PM-QPSK), which is briefly discussed first.

The description of the optical field of the signal has been introduced in the previous section in Eq. (2.11). For QPSK modulation the phase states of both polarizations are  $\varphi_x(t) = m\pi/4$  and  $\varphi_y(t) = n\pi/4$  where  $n$  and  $m$  are independent from each other and  $m, n \in \{-3, -1, +1, +3\}$ . This leads to  $\varphi_a(t)$  and  $\varphi_r(t)$  to be an integer multiple of  $\pi/4$ . This results in 16 possible phase combinations for PM-QPSK and they are depicted in Fig. 2.5 as blue filled circles.

Karlsson and Agrell found that, by taking the alphabet of PM-QPSK and leaving out half of the constellation points, the power efficiency per bit of the new modulation format can be increased as compared to PM-QPSK. The result is also depicted in Fig. 2.5 in red and represents the phase values of PS-QPSK. It becomes obvious that the minimum Euclidean distance (see Section 1.3 and [19]) of PS-QPSK versus PM-QPSK has increased by a factor of  $\sqrt{2}$ . The number of bits encoded in one symbol has decreased by a factor of  $\log_2(8)/\log_2(16) = 3/4$ . Therefore, we can conclude that when assuming constant signal power for both modulation formats, the power efficiency per bit of PS-QPSK is slightly increased compared to PM-QPSK.

Looking at Fig. 2.5 all red constellation points show linear polarization, since linear polarization is found for  $\varphi_r(t) = 0, \pm\pi/2$ . Thus it can be concluded that all those points switch between the two linear polarized states of  $\pm 45^\circ$ , as in the case of 2PolSK. The values of  $\varphi_a(t) = -3\pi/4, -\pi/4, +\pi/4, +3\pi/4$  for the red points in Fig. 2.5 represent QPSK.

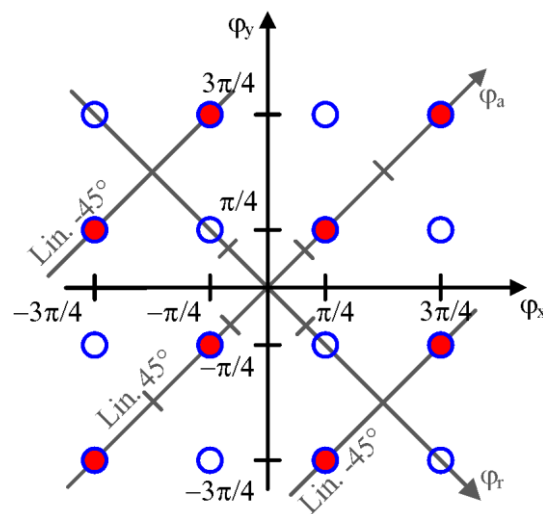


Fig. 2.5 Phase values of the PM-QPSK symbols in blue circles (○) depending either on the phases of the two polarizations  $\varphi_{x,y}$  or on the absolute and relative phases  $\varphi_{a,r}$  with  $\theta = \frac{\pi}{4}$ . In red filled circles the PS-QPSK symbols are depicted [3].

In the following, the mathematical expression that leads from the 16 phase states of PM-QPSK to the eight phase states of PS-QPSK is discussed. For this purpose Eq. (2.11) is rewritten as

$$\mathbf{E}_{\text{sig,PM-QPSK}} = \begin{pmatrix} I_x + jQ_x \\ I_y + jQ_y \end{pmatrix}. \quad (2.12)$$

The values of the real  $I_{x,y}$  and the imaginary  $Q_{x,y}$  parts of all 16 PM-QPSK symbols are given in Table 2.1. Moreover, the PS-QPSK symbols of Fig. 2.5 are translated into the new notation and highlighted in red. It becomes evident that PS-QPSK has even parity, with respect to the “+” and “-“ signs in Table 2.1. Here, even parity means that the number of 1s as well as the number of -1s is even (or zero).

The information content of a PS-QPSK symbol is 3 bits. The three bits, now called  $B_{1-3}$ , can be encoded onto  $I_x$ ,  $Q_x$  and  $I_y$  respectively. This then means that the value of  $Q_y$  is determined. Following this train of thoughts that  $Q_y$  represents a parity bit, it leads to the conclusion that PS-QPSK must be more sensitive, since the parity bit allows to correct errors. The logical operations needed to receive even parity are two XOR operations, as displayed in Fig. 2.6(a).

The close relation between PM-QPSK and PS-QPSK allows one to generate the signal by means of a dual-polarization (DP) IQ-modulator. Other

Table 2.1 Table with all possible values for the real  $I_{x,y}$  and imaginary  $Q_{x,y}$  parts of PM-QPSK, in red, the PS-QPSK symbols are highlighted.

$I_x$	$Q_x$	$I_y$	$Q_y$												
1	1	1	1	1	-1	1	1	-1	1	1	1	-1	-1	1	1
1	1	1	-1	1	-1	1	-1	-1	1	1	-1	-1	-1	1	-1
1	1	-1	1	1	-1	-1	1	-1	1	-1	1	-1	-1	-1	1
1	1	-1	-1	1	-1	-1	-1	-1	1	-1	-1	-1	-1	-1	-1

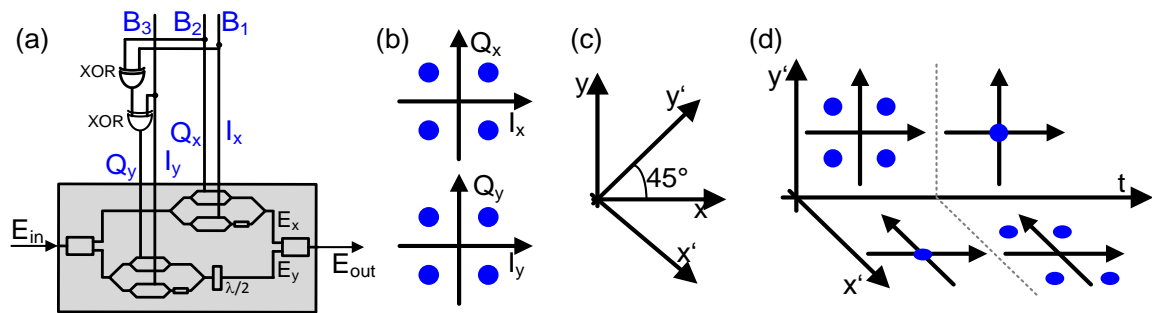


Fig. 2.6 Generation and representation of PS-QPSK symbols. (a) Dual-polarization IQ modulator for generating an optical PS-QPSK signal assuming the three bits encoded in one symbol B1-3 represent voltages with amplitudes smaller than the  $\pi$  voltage of the modulator and signs according to their logical value, i.e. a positive voltage for a logical one and a negative voltage for the logical zero, see [3]. (b) Constellation diagram of the PS-QPSK symbols according to [3], the logical dependence of  $Q_y$  from the  $I_x$ ,  $Q_x$  and  $I_y$  cannot be seen from this representation of symbols. If the reference plane of the polarization is rotated by  $45^\circ$ , and replaced by the  $x'$ ,  $y'$  coordinate system (c), then the constellation diagrams of the two polarization bits can be seen (d).

modulator configurations are also possible, but are not of interest in view of stacking other modulation formats in the future. A DP-IQ modulator consists of two IQ modulators, where one output signal is rotated in its polarization by a half wave plate. A polarization beam combiner just before the output of the device leads to dual polarization signal, see Fig. 2.6(a). Under the assumption B<sub>1-3</sub> represent voltages with amplitudes according to their logical value one uses a positive voltage for a logical one and a negative voltage for the logical zero.

Depending on the polarization reference plane chosen, the output signals displayed as constellation diagrams can look differently. In Fig. 2.6(b) we depicted the red constellation diagrams according to Table 2.1. The constellation looks like a PM-QPSK constellation since the dependence of  $Q_y$  on the values of the other bits following the XOR-role displayed in Fig. 2.6(a) is not visible, and thus PS-QPSK symbols cannot be distinguished from a polarization-multiplexed QPSK signal. When rotating the reference plane by  $45^\circ$ , as shown in Fig. 2.6(c), the “true” polarization switching becomes visible, i.e. the QPSK symbols can be found either on the linear polarization  $-45^\circ$  or the linear polarization  $+45^\circ$  depending on the “polarization-switching” bit B<sub>3</sub>, see Fig. 2.6(d).

### 2.2.4 Pulse–Position Modulation (PPM)

In pulse-position modulation (PPM) the information is encoded in the position of a pulse within a symbol. This section follows Refs. [4, 17].

The symbol duration is divided into  $M$  time slots. One of these slots is occupied by a pulse, all others are left empty. Pulse-position modulation is usually used in combination with direct detection. Depending on the number of slots  $M$  chosen, we speak about  $M$ -ary-PPM that encodes  $\log_2(M)$  bit per symbol.

All possible symbols for  $M = 4$  are depicted in the time-domain in Fig. 2.7. It can be seen that the average signal power (avg.  $P_{\text{sig}}$ ) is much smaller than the peak power. This leads to the conclusion that the symbol can still be detected correctly, as long as the peak power is higher than the average noise power  $P_{\text{noise}}$ . The average signal power is related to the peak power divided by  $M$ . Neither the phase, nor the polarization, nor the frequency information of the signal is of relevance, which leaves room for stacking modulation formats.

When increasing the number of PPM slots, like going from 4PPM to 8PPM, either the symbol duration  $T_{\text{Sym}}$  must be doubled or the slot width  $T_{\text{slot}}$  has to be shortened by a factor of two. In both cases the average signal power reduces by a factor of two, assuming that the peak power remains constant.

The first option has the advantage that the bandwidth occupied by the signal does not change, but at the price of a lower symbol rate. If a high data rate should be achieved, this is not the best option. If the symbol rate remains the same, 8PPM would require double the bandwidth as 4PPM, but encodes only one additional bit. Thus, PPM is quite bandwidth demanding when used at a high number of slots per symbol [4, 8, 16].

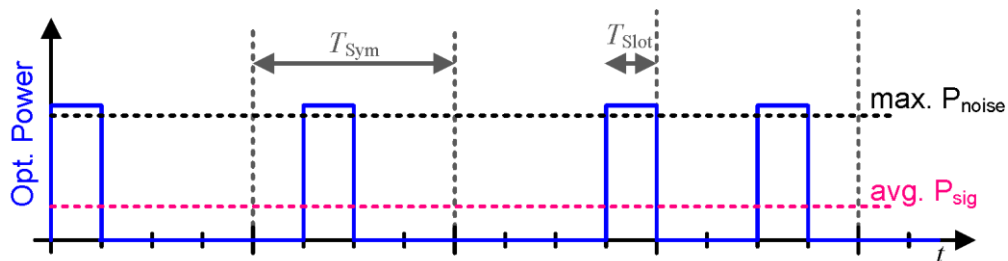


Fig. 2.7 4PPM symbols depicted in time-domain (—). It can be seen that the average signal power (avg.  $P_{\text{sig}}$ ) is much smaller than the peak power. The symbol can still be detected correctly, as long as the peak power is higher than the noise power  $P_{\text{noise}}$  (—). [4]

It must be mentioned that for the correct demodulation of PPM symbols, a proper synchronization is crucial. On the one hand, the beginning of the first transmitted PPM symbol must be known with high accuracy, and on the other hand timing jitter within the symbols should be avoided. Especially for low symbol rates a stable clock is essential, since unlike in other modulation formats a PPM pulse occurs rather seldom and clock recovery from empty slots is not possible.

Another aspect has to be considered when implementing PPM: As depicted in Fig. 2.7, the sensitivity advantage of PPM lies in its high peak pulses with respect to the low average signal power. Assuming that PPM is implemented using a Mach-Zehnder modulator, the extinction ratio of the device must be as high as possible. Thus, a modulator with suitable specification has to be chosen [4]. Another aspect are stable bias points, allowing no optical power leaking into an empty PPM slot. If the bias point drifts slightly, there is power in the empty PPM slots which reduces the ratio between the power in a pulse and the power of an empty slot. In an ideal case, the latter is zero.

### 2.2.5 Frequency Shift Keying (FSK)

In frequency-shift keying (FSK) the information is encoded to the frequency of a symbol. It is rather used in RF applications than in optical communications, since dispersive media such as fibers lead to signal distortion. However, as an additional degree of freedom it offers a possibility to add further information to a symbol by stacking modulation formats for free-space optical applications. As like polarization, frequency is more commonly used for multiplexing techniques than for modulation. Commonly frequency multiplexing based schemes are used, like coarse wavelength division multiplexing (CWDM), dense wavelength division multiplexing (DWDM) or orthogonal frequency division multiplexing (OFDM) [8, 20, 38].

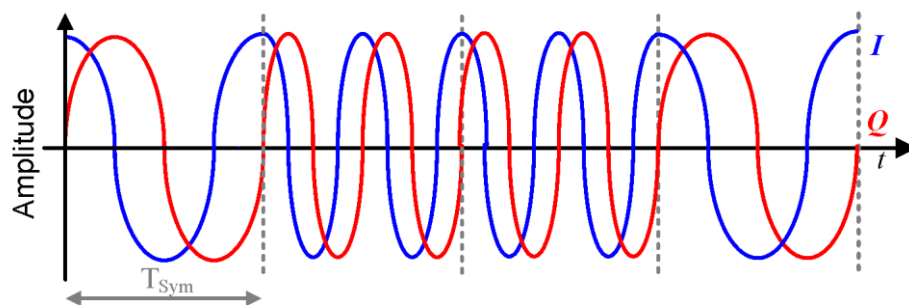


Fig. 2.8 Possible 2FSK sequence in time domain.

In this section, a possible implementation of optical FSK is introduced, following Ref. [39]. The name already implies that in  $N$ -ary FSK the information is encoded by means of  $N$  discrete frequency tones. In Fig. 2.8 a possible 2FSK sequence is shown in time-domain. The amount of bits that can be encoded in one symbol is given by  $\log_2(N)$ .

Frequency-shift keying signals can be generated in optics exploiting the fact that phase shifts and frequency shifts are linked by the derivative: To generate a frequency shift  $f_{\text{shift}}$ , phase modulation may be used according to the following relationship [40]:

$$2\pi f_{\text{shift}}(t) = \frac{d\varphi(t)}{dt} \quad (2.13)$$

If a tone at  $f_{\text{shift}} + f_c$  is generated, with  $f_c$  the center frequency of the laser, a linear phase ramp with the appropriate slope has to be applied. In optical communications, such a linear phase ramp can be generated with the help of an IQ modulator, depicted in Fig. 2.1. The modulation principle is depicted in Fig. 2.9. Sine and cosine driving signals for I and Q lead to a constant phase-ramp. This scheme is also known as single-sideband modulation, since sine and cosine driving signals are linked by the Hilbert transform [19]. Single-sideband modulation shows the big advantage that the bandwidth requirements are reduced by a factor of two over its double-sided counterpart [19]. The frequency of the sine and cosine, respectively, determine by which amount the frequency of the laser is shifted. The rotation direction, i.e. clockwise or counterclockwise, describes whether the shift is in negative or positive direction relative to the laser frequency.

The child Mach-Zehnder modulators introduced in Chapter 2.1 are biased such that an operation in the linear regime of the transfer function is possible. The cosine shaped transfer function of Eq. (2.5) is translated into a sine shape. Thus, the output of the IQ modulator, given in Eq. (2.5) becomes

$$\begin{aligned} E_{\text{out,FSK}}(t) = & A \cos(2\pi f_c t) \sin\left(\frac{V_I(t)}{2V_\pi} \pi + \frac{\pi}{2}\right) \\ & - A \sin(2\pi f_c t) \sin\left(\frac{V_Q(t)}{2V_\pi} \pi + \frac{\pi}{2}\right) \end{aligned} \quad (2.14)$$

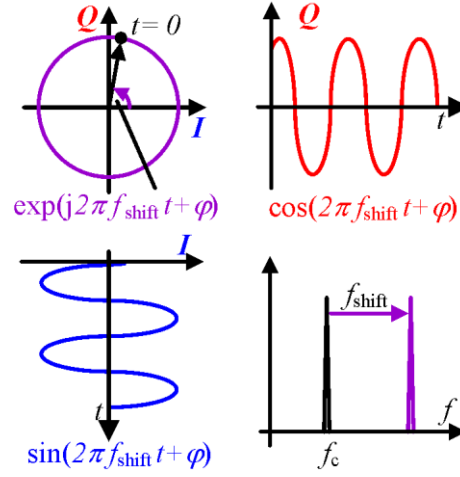


Fig. 2.9 Generation of a frequency shift  $f_{\text{shift}}$ . The phasor of the IQ-diagram is rotating in a circle. This is achieved by modulating the real part of the signal by a cosine and the imaginary part with a sine wave with frequency equal to  $f_{\text{shift}}$ .

with  $A$  being the amplitude of the electrical input field,  $f_c$  being its frequency and  $V_{I,Q}(t)$  being the driving voltages of the child MZMs respectively.

We apply modulation voltages with a constant amplitude  $a_{I,Q}$  that are much smaller than the  $\pi$ -voltage of the MZM. The driving signals are described by:

$$\begin{aligned} V_I(t) &= \frac{2V_\pi}{\pi} a_I \sin(2\pi f_{\text{shift}}(t)t) \\ V_Q(t) &= \frac{2V_\pi}{\pi} a_Q \cos(2\pi f_{\text{shift}}(t)t) \end{aligned} \quad (2.15)$$

where  $V_Q(t)$  describes the Hilbert transform of  $V_I(t)$ . Under the assumption that the transfer function of the IQ Mach-Zehnder modulators is linear for driving signals that are sufficiently small relative to the  $\pi$ -voltage of the device, i.e.  $a_{I,Q} \ll V_\pi$ , Eq. (2.14) becomes

$$\begin{aligned} E_{\text{out,FSK}}(t) &= \frac{A}{\text{ML}} \cos(2\pi f_c t) \cdot \sin(2\pi f_{\text{shift}}(t)t) \\ &\quad - \frac{A}{\text{ML}} \sin(2\pi f_c t) \cdot \cos(2\pi f_{\text{shift}}(t)t) \end{aligned} \quad (2.16)$$

with  $A$  being the amplitude of the electrical input field,  $f_c$  being its frequency. The small driving signals lead to modulation losses (ML). Thus, the amplitude  $A$  of the optical output signal is reduced. Eq. (2.16) results in the so-called lower side band, i.e. the difference frequency:

$$E_{\text{out,FSK}} = \frac{A}{2ML} \sin\left(2\pi\left(f_c - f_{\text{shift}}(t)\right)t\right) \quad (2.17)$$

By varying  $f_{\text{shift}}$  for each symbol, optical frequency shift keying is achieved. In the case of the single-sideband modulation, as described here, we have the opportunity, to shift the frequency in two directions: Relative to the center frequency a shift can be applied either in positive direction, i.e. in the direction of higher frequencies or to smaller frequencies, i.e. in the negative direction. So, if  $f_{\text{shift}}$  is negative, the sign of  $V_I(t)$  in Eq. (2.15) is flipped and as a result we get the sum frequency  $f_c + f_{\text{shift}}$  in Eq. (2.17). This is an additional possibility for modulation, which is advantageous, when it comes to electrical bandwidth limitations.

However, another FSK modulation scheme is also possible, if non-complex modulation is chosen, i.e. if a single Mach-Zehnder modulator is used for modulation instead of an IQ-MZM, and only cosine or sine driving signals are applied. Here, no longer single-sideband (SSB) modulation would be achieved and thus, double the bandwidth in the optical domain is required. However, the reduced bandwidth of the SSB modulation has a price: A costly IQ-modulator as well as a  $90^\circ$  hybrid at the receiver are required to modulate and detect the complex modulated signal.

As pointed out extensively in Refs. [29, 40], one could think of various types of frequency spacings to derive the FSK symbol alphabet from. In the following, orthogonal frequency spacings are assumed. However, there are also other spacings possible that have a large impact on the receiver sensitivity of the applied FSK scheme. We define two symbols with the frequencies  $f_1 = m/T_{\text{sym}}$  and  $f_2 = m'/T_{\text{sym}}$  with  $T_{\text{sym}}$  being the symbol duration and  $m, m'$  being random real numbers. To fulfill the criteria of orthogonality, the following equation must hold:

$$\frac{1}{T_{\text{sym}}} \int_{-\frac{T_{\text{sym}}}{2}}^{\frac{T_{\text{sym}}}{2}} \sin\left(2\pi \frac{m}{T_{\text{sym}}} t\right) \sin\left(2\pi \frac{m'}{T_{\text{sym}}} t\right) dt = \delta_{mm'} \quad (2.18)$$

with  $\delta_{mm'}$  the Kronecker delta [41].

Under the assumption of orthogonal symbols and for FSK with  $N$  given frequencies, the maximum possible symbol rate  $T_{\text{sym}}$  is thus limited: The maximum possible symbol rate  $F_s = T_{\text{sym}}^{-1}$  is given by the lowest baseband FSK frequency.

Orthogonal FSK represents a special case of OOK-OFDM. In OFDM every frequency tone carries a symbol independent from the information encoded

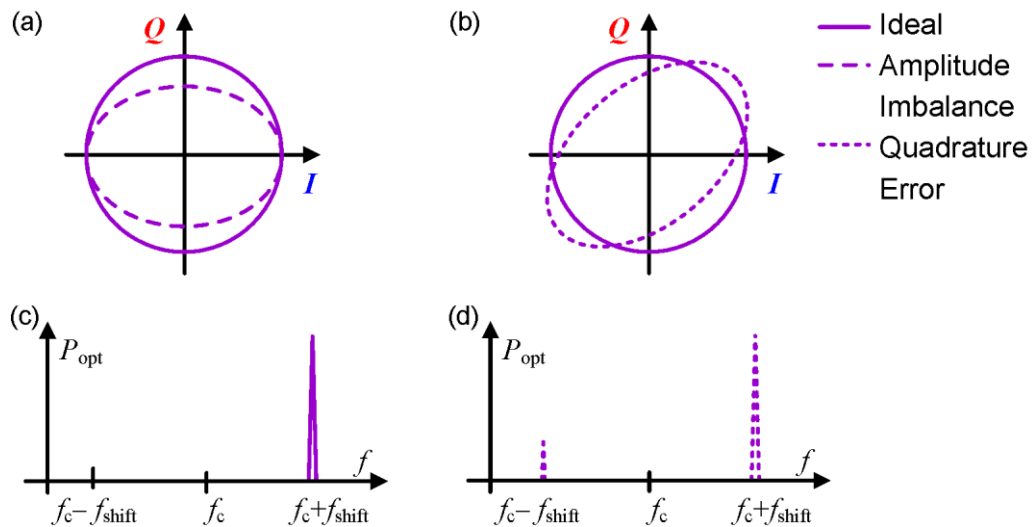


Fig. 2.10 Implementation challenges of FSK, solid line: the ideal signal, (a) amplitude imbalance, (b) phase offset between  $I$  and  $Q$  (c) Spectrum of the shifted laser frequency  $f_c$  in positive direction by  $f_{shift}$  (c) ideal shift (d) distorted shift either due to amplitude imbalance or phase offset. Both effects lead to non-perfect suppression of the mirror frequency at  $f_c - f_{shift}$ .

in neighboring subcarriers, while in FSK, only one tone at a time carries data. For FSK the frequency shift should be chosen such that in baseband  $f_{shift} \in \{\dots, f_{-2} = -2F_s, f_{-1} = -F_s, f_0 = 0, f_1 = F_s, f_2 = 2F_s, \dots\}$ . If the distance between two neighboring frequencies is smaller than  $F_s$ , the symbol rate must be reduced to distinguish the symbols from each other in the electrical domain.

For the implementation of FSK with an IQ-modulator the  $90^\circ$  phase shift between  $I$  and  $Q$  is a crucial parameter. In addition, timing skews of the RF driving signals due to different cable lengths etc. are important as well. Last, amplitude issues with respect to the  $\pi$ -voltage of the modulator can lead to signal distortions. Assuming an amplitude imbalance that can be described

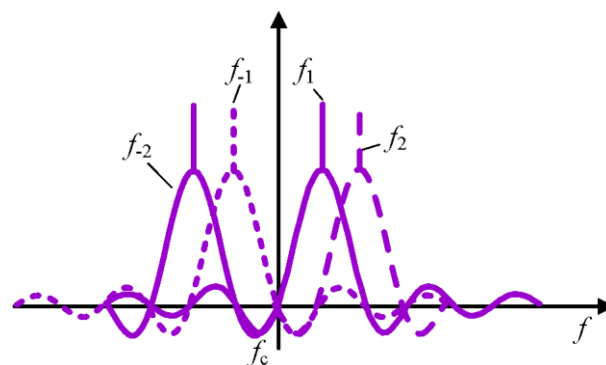


Fig. 2.11 Optical spectrum of the 4FSK modulated signal with orthogonal frequencies and NRZ pulse shape. The center tone, i.e. the laser frequency  $f_c$  is not used. The vertical axis is plotted linearly.

by  $V_I/V_\pi \neq V_Q/V_\pi$ , see Eq. (2.14) ff., the result is depicted Fig. 2.10(a) as an ellipse in the complex plane. If a timing offset between the two drive signals  $V_I$  and  $V_Q$  occurs, this results also in an elliptical shaped IQ-diagram, as shown in Fig. 2.10(b). Thus, amplitude imbalance as well as phase offsets lead to a second tone in the spectra at the so-called mirror frequency. This is disadvantageous since signal power is lost to parts of the spectrum, where the signal is not supposed to be. In Fig. 2.10(c-d) this effect is depicted.

In this thesis, a special case of 4FSK is investigated. For a given FSK-symbol rate  $F_s$ , 4 offset frequencies  $f_n \in \{f_{\pm 1} = \pm F_s, f_{\pm 2} = \pm 2F_s\}$  to the right and to the left of the optical carrier are generated by driving the  $I$  and  $Q$  inputs of the IQ modulator with the proper cosine and sine signals, see Eq. (2.15). As with orthogonal frequency division multiplexing (OFDM), the period  $1/F_s$  equals the symbol duration  $T_{\text{sym}}$ . Only one frequency out of four  $f_{\pm 1}, f_{\pm 2}$  is chosen for each symbol. The spectrum of this 4FSK scheme is depicted in Fig. 2.11 for NRZ pulse shape and linear  $y$ -axis. The tones at  $f_{\pm 1}, f_{\pm 2}$  result from the amplitude modulation of each offset frequency  $f_n$ , where the carrier is not suppressed [42]. It becomes obvious, that the center frequency, i.e. the carrier is left out. This makes the FSK symbols non-equidistant.

### 3 Theoretical Background about Receiver Sensitivity

The receiver sensitivity of a communication system is defined by the amount of received signal energy per bit or symbol that is required to achieve a certain bit-error ratio (BER). In the past, the threshold usually was set at a BER of  $10^{-9}$  for so-called error-free signal reception [22, 29]. Due to the capabilities of modern forward error correction (FEC) algorithms,  $10^{-3}$  has become the new figure of merit [43], since a pre-FEC of  $4.45 \times 10^{-3}$  allows the use of a standard FEC with only 7 % overhead for a final BER of  $10^{-15}$ .

There are numerous influences on the receiver sensitivity of an optical transmission system. One of them is the receiver itself. There are several categories, how to group the different receiver systems. On the one hand, there is *direct detection* (DD) with and without optical preamplification. This scheme works fine for intensity detection and shows a reasonable receiver sensitivity [29]: Direct detection in theory has the worst receiver sensitivity amongst all detection schemes, but its low hardware requirements of only one photo-diode can compensate for this in many cases.

On the other hand, there is the coherent receiver. Here, the signal and a reference wave, usually called local oscillator (LO), are superimposed and then detected by a so-called optical hybrid detector. Coherent reception allows phase- and polarization-sensitive detection; however, both (phase and polarization) always need stabilization mechanisms [44, 45].

Depending on the frequency offset between the local oscillator and the center frequency of the signal, there are three different reception schemes: *homodyne*, *intradyn*e and *heterodyne* [46, 47]. In homodyne receivers, the frequency offset, or so-called intermediate frequency, is zero. In intradyne systems, the intermediate frequency is larger than zero, but smaller than the signal bandwidth, and in heterodyne systems, the intermediate frequency is at least three times larger than the signal bandwidth [22, 29].

In the past few years, intradyne detection with optical preamplification has become most popular followed by digital signal processing (DSP) [5, 10, 47-50]. However, sometimes the large hardware efforts of homodyne detection are tolerated for achieving similar sensitivities [51]. In such systems, the phase and polarization of signal and LO must be locked. This requires loop-back mechanisms to tune the local oscillator accordingly [15].

Besides the distinction depending on the intermediate frequency, there are also two different demodulation processes possible: synchronous and

asynchronous [22] symbol detection, also often called coherent and non-coherent detection [19, 40].

Besides the demodulation scheme chosen, also the modulation format applied to a transmission system brings in another aspect that severely impacts the receiver sensitivity of an optical communication system [8, 22, 29, 40, 52]. In systems, where only two-level signals were applied, binary modulation schemes were commonly used for encoding the information in either binary amplitude-shift keying (2ASK), or binary phase-shift keying (BPSK), binary polarization-shift keying (2PolSK) or binary frequency-shift keying (2FSK). Until recently, just one of these degrees of freedom was commonly used to encode information [22, 29, 40].

A promising approach to improve the receiver sensitivity is exploiting more than just one degree of freedom for signal modulation and thus encode more information onto one symbol [3, 8, 11, 12, 17, 48].

Before the influence of the modulation format on the receiver sensitivity is discussed, we need a proper definition of receiver sensitivity as well as a suitable figure of merit. First, the receiver is presented and second, the impact of different modulations formats onto the receiver sensitivity is discussed. The chapter finishes with a conclusion.

### 3.1 The Coherent Receiver

Since the system discussed in this work uses, amongst others, phase and polarization to encode data, a polarization and phase diverse coherent reception scheme is set up and introduced [22, 29, 40]. This section follows Ref. [53].

The idea behind coherent reception is to use the mixing capabilities of the photo-diode to compare the signal with a reference, a so-called local oscillator (LO). Thus, constructive and destructive interference take place that is usually detected by so-called balanced photodiodes.

In the following we define the electrical field of the local oscillator  $E_{LO}$  and the signal  $E_{sig}$  in one polarization

$$E_{sig} = A_{sig}(t)e^{j(\omega_{sig}t + \varphi_{sig}(t))}, \quad E_{LO} = A_{LO}(t)e^{j(\omega_{LO}t + \varphi_{LO}(t))} \quad (3.1)$$

with  $A_{sig,LO}$  being the amplitudes of the signal and the LO,  $\omega_{sig,LO}$  being the angular frequency of the signal and the LO and  $\varphi_{sig,LO}$  the phases of signal and LO. We introduce the phase difference between signal and local

oscillator  $\Delta\varphi(t) = \varphi_{\text{sig}}(t) - \varphi_{\text{LO}}(t)$ . The (angular) frequency difference is called intermediate frequency and given by  $\omega_{\text{IF}}(t) = \omega_{\text{sig}}(t) - \omega_{\text{LO}}$ .

In the framework of this work, a polarization and phase diverse coherent receiver is applied. Its schematic is depicted in Fig. 3.1. The incoming signal is split into its  $x$ - and  $y$ -components by a polarization beam splitter (PBS) and then each respective signal portion is fed into its respective phase-diverse coherent receiver. The LO is assumed to be present in  $x$ -polarization. It is split into two equal powers, of which one is rotated in its polarization to become the LO of the  $y$ -related receiver part. This is usually done by a half-wave plate ( $\lambda/2$ ).

In each of the two phase-diverse coherent receivers (one for  $x$ - and one for  $y$ -polarization, respectively) the signal and LO are again split into two halves and one half is mixed with the local oscillator resulting in an inphase signal  $I_{x,y}$  while the other is mixed with the local oscillator with a  $\pi/2$  phase shift resulting in a quadrature phase signal  $Q_{x,y}$ .

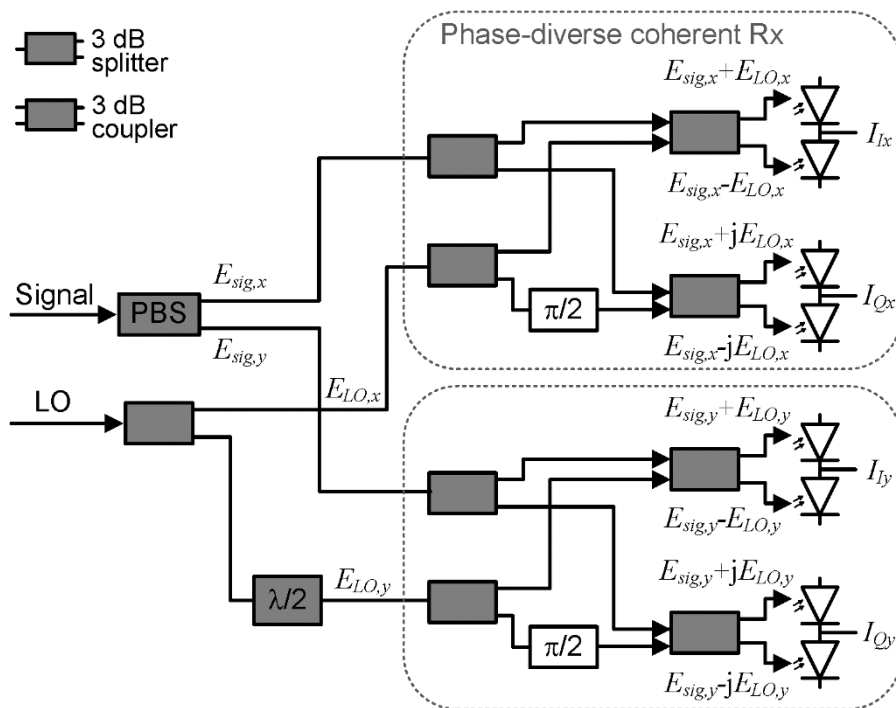


Fig. 3.1 Scheme of a polarization diverse and phase diverse coherent receiver. The signal at the input carries information in both polarizations,  $x$  and  $y$ . It is split into its two components by a polarization beam splitter (PBS), and each is fed into a phase-diversity coherent receiver. Due to implementation advantages, the local oscillator (LO) carries only light in  $x$ -polarization. Thus, its power is split, whereas one half is fed to the phase-diversity coherent receiver demodulating the  $x$ -part of the signal, while the polarization of the other half is rotated by a half-wave plate ( $\lambda/2$ ) to achieve a local oscillator that interferes with the  $y$ -part of the signal.

The currents at the balanced outputs are in the absence of noise:

$$\begin{aligned} I_{I_{x,y}}(t) &\sim A_{\text{sig } x,y}(t)A_{\text{LO}_{x,y}}(t)\cos\left(\omega_{\text{IF}}(t)t + \Delta\varphi_{x,y}(t)\right) \\ I_{Q_{x,y}}(t) &\sim A_{\text{sig } x,y}(t)A_{\text{LO}_{x,y}}(t)\sin\left(\omega_{\text{IF}}(t)t + \Delta\varphi_{x,y}(t)\right) \end{aligned} \quad (3.2)$$

In such a system, as described here, the intermediate frequency is equal in both polarizations. Any amplitude, frequency phase and state of polarization of the received signal can be extracted from the photo currents  $I_{I_{x,y}}(t)$  and  $I_{Q_{x,y}}(t)$ . We can also write them as an analytical signal (in the absence of noise)

$$\begin{aligned} \rho_{\text{NN,cohRx}}(t) &= I_{I_{x,y}}(t) + jI_{Q_{x,y}}(t) \\ &= A_{\text{sig } x,y}(t)A_{\text{LO}_{x,y}}(t)e^{j[\omega_{\text{IF}}t + \Delta\varphi_{x,y}(t)]} \\ &= A_{x,y}(t)e^{j[\omega_{\text{IF}}t + \Delta\varphi_{x,y}(t)]}. \end{aligned} \quad (3.3)$$

## 3.2 Measurement of the Receiver Sensitivity

After having briefly introduced the polarization-diverse coherent receiver, the meaning of receiver sensitivity is defined. In the framework of this thesis the receiver sensitivity is defined as the amount of photons per bit that is necessary to reach a certain bit error ratio (BER) of  $10^{-3}$  following [11].

The question is how to measure this figure of merit. For determining the BER, error counting is the most versatile method and it works for any arbitrary modulated signal. It operates on the demodulated logical bit stream and thus cannot accidentally misinterpret symbols, as it might happen when for example non-data aided error vector magnitudes (EVM) as defined in Refs. [54, 55] are measured. To calculate the bit error ratio, the received signal is demodulated and the resulting bit stream is compared to the input bit stream of the transmitter (Tx). The BER is then given by

$$\text{BER} = \frac{n_{\text{E}}}{n_{\text{Tx}}} \quad (3.4)$$

with  $n_{\text{E}}$  being the total number of erroneous bits and  $n_{\text{Tx}}$  being the overall number of received bit.

The signal energy required to reach a certain bit error probability can be derived in several ways. The most common ones in literature are the signal to noise power ratio (SNR) [2, 19], the optical signal to noise power ratio (OSNR) [2], the ratio of energy per bit over the spectral noise power density

$\mathcal{E}_b/N_0$  [8, 19]. Equivalently, the number of incident photons per bit required for a certain BER at the receiver can be given [29, 40].

The average energy per bit  $\mathcal{E}_b$  in a receiver system without optical amplifiers can be calculated from the average signal power  $P_{\text{Sig}}$  with  $\mathcal{E}_b = P_{\text{Sig}}/R_b$  with  $R_b$  being the bitrate [2]. Assuming a preamplifying system, the signal power  $P_{\text{Sig}}$  is multiplied by the power gain  $G$  of the amplifier

$$\mathcal{E}_b = \frac{G P_{\text{Sig}}}{R_b} \quad (3.5)$$

In many communication systems, the energy per bit over the noise spectral density  $\mathcal{E}_b/N_0$  is used as a figure of merit [19]. According to Refs. [2, 56] the noise spectral density of an optical preamplified system is called  $N_{\text{ASE}}$  and it is given by

$$N_{\text{ASE}} = n_{\text{sp}} (G - 1) h f_c \quad (3.6)$$

with  $h$  being the Planck's constant and  $f_c$  being the center frequency of the signal,  $n_{\text{sp}}$  being the inversion factor of the amplifier, that is set to 1 for the ideal system and  $G$  is the amplifier's power gain. Thus, we can derive the signal to noise energy ratio after an optical amplifier:

$$\frac{G P_{\text{Sig}}}{R_b n_{\text{sp}} (G - 1) h f_c} = \frac{G \text{PPB} h f_c}{n_{\text{sp}} (G - 1) h f_c} = \frac{\mathcal{E}_b}{N_0} \quad (3.7)$$

with PPB being the photons per bit and  $N_{\text{ASE}} = N_0$ . For a large amplifier gain  $G \gg 1$  and  $n_{\text{sp}} = 1$ ,  $\mathcal{E}_b/N_0$  of Eq. (3.7) equals the photons per bit (PPB) in the shot-noise limit [56].

Especially in optical communication systems, the optical signal to noise power ratio (OSNR) is commonly used as a figure of merit. Following [2] the OSNR is defined as

$$\text{OSNR} = \frac{G P_{\text{Sig}}}{2 N_{\text{ASE}} B_{\text{ref}}} = \frac{R_b}{2 B_{\text{ref}}} \frac{\mathcal{E}_b}{N_0} \quad (3.8)$$

where  $B_{\text{ref}} = c/\lambda_c^2 \times 0.1 \text{ nm}$  is commonly defined as the reference bandwidth and  $\lambda_c = c/f_c$  equals the wavelength of the carrier. Looking at Eq. (3.8) it becomes obvious that the OSNR is data rate dependent. However, a data rate dependent figure of merit to compare receiver sensitivities is not really handy, since it means that all systems must run at the same bit rate to decide (or their OSNR-values must be recalculated), what system shows the best sensitivity.

Thus, it might be more applicable to introduce the signal to noise power ratio (SNR), where the signal and the noise power is measured in the same bandwidth. This method is usually found in RF systems [19].

By rearranging Eq. (3.7) with  $P_{\text{Sig}}$  (the average signal power) and  $P_{\text{Noise}} = N_{\text{ASE}} B$  (the average noise power),  $R_{\text{Sym}}$  the symbol rate and  $n_{\text{bit/sym}}$  the number of bits encoded in one symbol,  $\text{SNR}_{\text{sym,bit}}$  denotes the signal to noise power ratio per symbol or per bit, respectively [2]:

$$\text{SNR}_{\text{bit}} = \frac{\text{SNR}_{\text{sym}}}{n_{\text{bit/sym}}} = \frac{G P_{\text{Sig}} B}{P_{\text{Noise}} B n_{\text{bit/sym}}} = \frac{\mathcal{E}_b}{N_0} \quad (3.9)$$

Eq. (3.9) is valid assuming an ideal amplifier with high gain, i.e.  $G \gg 1, n_{\text{sp}} = 1$  in the shot noise limit. Additionally, it is assumed that  $B$  is large enough.

In the shot-noise limit, the number of photons per bit (PPB) that are necessary to reach a certain BER thus is given by

$$\begin{aligned} \text{PPB} &= \frac{\mathcal{E}_b}{N_0} \\ \text{PPB} &= \frac{1}{N_0} \frac{G P_{\text{Sig}}}{R_b} = \frac{1}{hf_c} \frac{P_{\text{Sig}}}{R_{\text{Sym}} \cdot n_{\text{bit/sym}}} . \end{aligned} \quad (3.10)$$

The PPB can also be derived from measured OSNR, see Eq. (3.8). Assuming the OSNR is measured with an optical spectrum analyzer (OSA) and the measurement bandwidth equals the signal bandwidth  $B_{\text{ref}} = B$ , the PPB equals:

$$\text{PPB} = \frac{2B}{R_{\text{Sym}} n_{\text{bit/sym}}} \text{OSNR} \quad (3.11)$$

Thus, there are two measurement methods to determine the number of photons per bit: Using a power meter measuring the signal power as well as conducting an OSNR-measurement. If the experiment is well conducted, both results coincide.

### 3.3 Receiver Sensitivity of Selected Modulation Formats

As already mentioned previously, the receiver sensitivity not only depends on the receiver itself that is applied but also on the modulation format. Once the modulation format is fix, the demodulation method must be chosen. Basically one can either use asynchronous or synchronous demodulation

techniques [40]. It is also in some literature called coherent or incoherent demodulation [22].

In the following we discuss coherent reception with pre-amplification. As optical pre-amplifiers, erbium doped fiber amplifiers (EDFAs) are commonly used. These EDFAs add noise to the signal due to amplified spontaneous emission (ASE). This noise is usually present in both polarizations [2]. In the presence of an optical pre-amplifier it is valid to assume additive white Gaussian noise on both polarizations in in-phase and quadrature of the signal [2, 55]. The noise spectral density varies over frequency, as it can be exemplarily seen in Ref. [22] (Fig. 6.15). However, assuming a receiver with an electrical bandwidth  $B_e$  that is much smaller than the bandwidth of the ASE, only a small portion of the ASE noise power will be contributing to the photocurrents at the outputs of the balanced receivers shown in Fig. 3.1. Within the bandwidth  $B_e$ , the ASE induced noise spectral density can be assumed to be constant.

Assuming pre-amplified reception, the incident optical power onto the photo detectors is chosen to be high resulting in a strong photocurrent. This is why the shot noise as well as the thermal noise of the electrical amplifiers can be neglected. Thus, the ASE is the dominant noise source present in our system.

We describe the received baseband signal in  $x$  and  $y$ -polarizations by the vector  $\boldsymbol{\rho}(t) = r_x(t)\vec{e}_x + r_y(t)\vec{e}_y$  (orthogonal unit vectors  $\vec{e}_{x,y}$ ), which comprises the analytical low-pass signal vector  $\mathbf{s}(t)$  and the noise vector  $\mathbf{n}(t)$ ,

$$\boldsymbol{\rho}(t) = \mathbf{s}(t) + \mathbf{n}(t),$$

$$\mathbf{s} = \begin{pmatrix} s_x \\ s_y \end{pmatrix} = \begin{pmatrix} I_x + jQ_x \\ I_y + jQ_y \end{pmatrix}, \quad \mathbf{n} = \begin{pmatrix} n_x \\ n_y \end{pmatrix} = \begin{pmatrix} n_{I,x} + jn_{Q,x} \\ n_{I,y} + jn_{Q,y} \end{pmatrix} \quad (3.12)$$

The noise terms of in-phase and quadrature in both polarizations are  $n_{I,x,y}$  and  $n_{Q,x,y}$ , respectively. These noise terms are assumed to be independently Gaussian distributed with zero mean and variance  $\sigma_{x,y}^2 = \sigma_{I,x,y}^2 = \sigma_{Q,x,y}^2 = \sigma^2$  [2].

The question is, how correct symbol decision is affected by the noise. This question will be answered for each modulation format separately in the following sections following Refs. [29, 57].

### 3.3.1 Theoretical Sensitivity of Binary and Quadrature Phase Shift Keying (BPSK and QPSK)

In binary and quadrature phase shift keying (BPSK and QPSK) the information is encoded in the signal's phase, see section 2.2.1. For BPSK two phase states are used, i.e. 0 and  $\pi$ . For demodulation, a decision threshold is required to distinguish the symbols. If the symbol is larger than the pre-defined threshold, it is commonly considered to be a one, if it is smaller, it is a zero. In the case of BPSK that represents an antipodal signal, the threshold is zero [29, 34, 40, 58].

In the following discussion, PSK signals are demodulated coherently (or synchronously) because of the enhanced receiver sensitivity, see [22]. However differential detection like DPSK is applied in optics as well, but due to its lower sensitivity, it is not of interest for this work [29, 40, 53].

In the following, the sensitivity of BPSK is discussed. This chapter follows Ref. [29]. We assume intradyne detection with digital frequency- and phase estimation [29, 40]. We also assume perfect polarization alignment, such that all  $y$ -related terms of Eq. (3.12) can be neglected.

The symbols of a BPSK signal in passband are given in Eq. (2.7). Its analytical low-pass equivalent is hereby defined as

$$s_{\text{BPSK}}(t) = A \exp(j\varphi(t)) \quad (3.13)$$

with  $A$  the real and constant output amplitude and  $\varphi(t)$  the modulated phase of the signal having values of 0 and  $\pi$  [19]. Thus, the two BPSK symbols  $s_{1,2}$  take either one of the two values:

$$\begin{aligned} s_{1\text{BPSK}}(t) &= A \\ s_{2\text{BPSK}}(t) &= -A. \end{aligned} \quad (3.14)$$

For simplicity we assume a signal in  $x$ -polarization only with perfect polarization alignment of signal and local oscillator. Thus, the  $y$ -related noise-terms in Eq. (3.12) are zero and thus, received BPSK-symbols  $\rho_{1,2}(t)$  are

$$\begin{aligned} \rho_{1,2\text{BPSK}}(t) &= s_{1,2}(t) + n(t) \\ &= \begin{cases} A + n_1(t) + jn_Q(t) & \text{for } s_1 \\ -A + n_1(t) + jn_Q(t) & \text{for } s_2. \end{cases} \end{aligned} \quad (3.15)$$

The indices of the noise-terms indicating the  $x$ -polarization are dropped for simplicity. In Fig. 3.2(a) the BPSK-symbols of Eq. (3.14) are depicted. In

(b) and (c) the imaginary and real part of the received signal  $\rho$  according to Eq. (3.12) are shown, respectively. It can be seen that the two symbols are superimposed by AWGN. As mentioned before, in BPSK, the symbols are demodulated with the help of a decision threshold  $\rho_{th}$ , see Fig. 3.2(c). The noise in the imaginary part of the received signal can be neglected for symbol decision.

For a minimum BER the optimum decision threshold  $\rho_{th}$  must be found. In the case of a BPSK signal, where the probability density function (PDF) of both symbols differ only in their expectation value, the optimum threshold  $\rho_{th}$  for equally distributed symbols equals zero. The bit error probability can be written as

$$\text{BER}_{\text{BPSK}} = \frac{1}{2} \int_{-\infty}^{\rho_{th}} p_{2,\text{PSK}}(\rho) d\rho + \frac{1}{2} \int_{\rho_{th}}^{\infty} p_{1,\text{PSK}}(\rho) d\rho \quad (3.16)$$

with  $p_{1,2,\text{PSK}}(\rho)$  being Gaussian PDFs:

$$p_{1,2,\text{PSK}}(\rho) = \frac{1}{\sqrt{2\pi}\sigma} \exp\left(-\frac{(\rho \pm \sqrt{GA})^2}{2\sigma^2}\right) \quad (3.17)$$

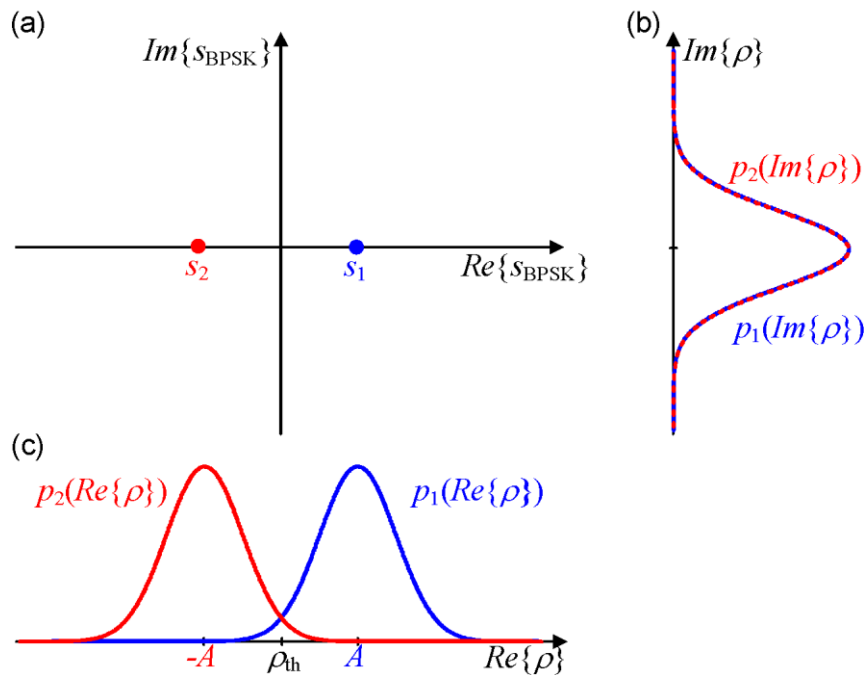


Fig. 3.2 Symbol decision for BPSK (a) The two symbols sent:  $s_1$  in blue, and  $s_2$  in red (b) shows the imaginary part of the analytical received signal in the presence of AWGN (c) shows the real part of the analytical received signal in the presence of AWGN. For BPSK, the optimum threshold  $\rho_{th}$  that is applied for symbol decision is zero.

with the variance  $\sigma^2$  and the means of  $\pm\sqrt{GA}$ , where  $G$  represents the amplifiers gain. The variance  $\sigma^2$  equals the noise power in passband. Assuming an ideal pre-amplifier the variance equals  $\sigma^2 = (G-1)hf_c B$ , with  $hf_c$  the photon energy [19, 29] and  $B$  the bandwidth. We define  $\frac{1}{2}A^2 = \mathcal{E}_{\text{sym}} T_{\text{sym}}^{-1} G^{-1}$ . By solving Eq. (3.16) with Eq. (3.17) the bit error probability (BER) of BPSK becomes

$$\begin{aligned} \text{BER}_{\text{BPSK}} &= \frac{1}{2} \text{erfc} \left( \frac{\sqrt{GA}}{\sqrt{2\sigma}} \right) \\ &= \frac{1}{2} \text{erfc} \left( \sqrt{\frac{\mathcal{E}_b}{N_0}} \right) \\ &= \frac{1}{2} \text{erfc}(\sqrt{\text{SNR}}) \end{aligned} \quad (3.18)$$

with  $T_{\text{sym}} = B^{-1}$ . For large amplifier gain  $G$  and shot noise limited reception,  $G/(G-1) \approx 1$ . For BPSK, the energy per bit equals the energy per symbol, i.e.  $\mathcal{E}_b = \mathcal{E}_{\text{sym}}$ .

### 3.3.2 Theoretical Sensitivity of Polarization Switched QPSK (PS-QPSK)

As already discussed previously, the advantage of PS-QPSK lies in an optimum constellation of symbols with respect to the Euclidian distance, i.e. all 8 symbols are separated as much as possible from their closest neighbors. Looking at Fig. 2.5 it becomes obvious that PS-QPSK belongs to the family of bi-orthogonal signals. As an example, QPSK is also bi-orthogonal, i.e. the correlation coefficient of any two QPSK-symbols  $s_i(t)$  and  $s_j(t)$  has one out of three possible values: one, minus one or zero. The correlation coefficient  $\rho_c$  is defined as follows, see [19] (Eq. 2.1-25):

$$\rho_c = \frac{1}{T_{\text{sym}} \sqrt{\mathcal{E}_{s_i} \mathcal{E}_{s_j}}} \int_{T_0 - \frac{T_{\text{sym}}}{2}}^{T_0 + \frac{T_{\text{sym}}}{2}} s_i \left( \frac{t}{T_{\text{sym}}} \right) s_j^* \left( \frac{t}{T_{\text{sym}}} \right) dt \quad (3.19)$$

with  $\mathcal{E}_{s_i, j}$  the symbols' energies,  $T_{\text{sym}}$  the symbol duration and \* denoting the conjugate complex. Eq. (3.19) becomes zero, if the symbols are orthogonal, it becomes one, if the symbol is correlated with itself, and it becomes minus one, if the symbols are antipodal [19, 34, 59].

According to [19] (p. 208) the PS-QPSK represents a bipolar orthogonal signal with eight constellation points. Assuming additive white Gaussian

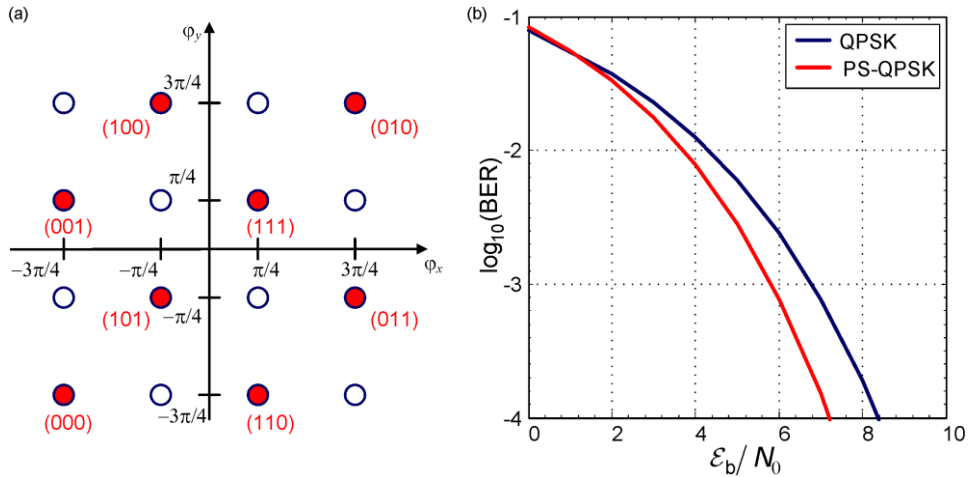


Fig. 3.3 PS-QPSK: (a) bit mapping of PS-QPSK symbols (red) in the phase state diagram, while all PM-QPSK symbols are shown as well (dark blue) (b) bit error ratio (BER) versus  $\mathcal{E}_b/N_0$  characteristics for PS-QPSK and (PM-). The sensitivity advantage of PS-QPSK is clearly visible.

noise (see previous section) we get a symbol error ratio  $\text{SER}_{\text{PSQ}}$  according to Ref. [3, 12] and [19] (pp. 207-209)

$$\text{SER}_{\text{PSQ}} = 1 - \frac{1}{\sqrt{\pi}} \int_0^{\infty} (1 - \text{erfc}(r))^3 \cdot \exp \left[ - \left( r - \sqrt{\frac{\mathcal{E}_s}{N_0}} \right)^2 \right] dr \quad (3.20)$$

with  $\mathcal{E}_s/N_0$  the ratio of energy per symbol over the noise spectral density. To determine the BER of PS-QPSK, a conversion from symbol to the bits must be performed. It is suggested in [3] to follow [59] pp 201-203. Gray coding is not possible for PS-QPSK, since each symbol has 6 nearest neighbors. Thus, optimum coding is possible by mapping the bits to the symbols such that symbols with opposite signs show the maximum Hamming distance also in their bit pattern, i.e. their bit pattern will be the inverse to each other. For example, the two symbols with opposite sign are represented by the 000 bit pattern and 111 bit pattern, see Fig. 3.3(a). In Table 3.1 the complete look-up table is shown.

In [3] Eq. (21) for such a coding the BER has been determined to be

Table 3.1 Bit mapping of PS-QPSK symbols

$I_x$	$Q_x$	$I_y$	$Q_y$	bits	$I_x$	$Q_x$	$I_y$	$Q_y$	bits
1	1	1	1	111	-1	1	1	-1	011
1	1	-1	-1	110	-1	1	-1	1	010
1	-1	1	-1	101	-1	-1	1	1	001
1	-1	-1	1	100	-1	-1	-1	-1	000

$$\text{BER}_{\text{PSQ}} =$$

$$\frac{1}{2\sqrt{\pi}} \int_{-\infty}^{\infty} \text{erfc}(r) (3 - 3 \cdot \text{erfc}(r) + \text{erfc}^2(r)) \exp\left(-\left(r + \sqrt{\frac{\mathcal{E}_s}{N_0}}\right)^2\right) dr. \quad (3.21)$$

Since three bits are encoded in each PS-QPSK symbol, the symbol energy  $\mathcal{E}_s$  equals three times the energy per bit, i.e.  $\mathcal{E}_s = 3\mathcal{E}_b$ . In Fig. 3.3(b) the BER of PS-QPSK is depicted and for comparison, the BER of QPSK is shown as well. The reader should be aware that with respect to  $\mathcal{E}_b/N_0$ , BPSK, QPSK and PM-QPSK (polarization multiplexed QPSK) show the same  $\mathcal{E}_b/N_0$  requirements, and thus receiver sensitivity [2, 11], also compare Fig. 1.1. The reason for this can be found in the fact that the required SNR increases by the same factor, as the bit per symbol increase when going from BSPK via QPSK to PM-QPSK. However, as already explained previously in Chapter 2.2.3, there is an improvement in the Euclidean distance between PM-QPSK and PS-QPSK. This sensitivity improvement is clearly visible in Fig. 3.3 and also found by measurements in Refs. [37, 60].

### 3.3.3 Theoretical Sensitivity of Pulse–Position Modulation (PPM) and Orthogonal Frequency Shift Keying (FSK)

Mary pulse position modulation (MPPM) belongs to the family of orthogonal modulation formats. If for  $N$ -ary frequency shift keying (NFSK) the frequency spacing is chosen to fulfill the orthogonality condition, it shows the same behavior as PPM concerning sensitivity [11, 19]. The definition for orthogonal signaling schemes implies that the correlation coefficient  $\rho_c$  of Eq. (3.19) must be zero for two different symbols of the alphabet [59]. In the following, PPM is discussed in more detail, however, the receiver sensitivity given is also valid for orthogonal FSK.

PPM has its information encoded in the position of a pulse with respect to the symbol duration, see Section 2.2.4, whereas an FSK symbol has the information encoded in its frequency, see Section 2.2.5. The theory in this section follows [19, 29, 40]. Excerpts are also published in [14].

In the following, the reception of PPM and FSK symbols with a coherent receiver is discussed. Since there are several ways to demodulate the PPM and FSK symbols, the differences concerning receiver sensitivities are regarded more closely in the following sections. PPM may be detected with homodyne receivers or with heterodyne receivers followed by synchronous or asynchronous demodulation schemes. All might come with or without polarization diversity schemes.

For PPM, one out of  $M$  slots contains a pulse. In the following, we start the discussion with 2PPM and will later extend the discussion to *M*ary PPM. We will write each PPM symbol as a row vector, where each column represents one slot. For 2PPM and 2FSK the two signals are defined as [29]

$$\begin{aligned} s_{1,2\text{PPM}}(t) &= (A \quad 0) \\ s_{2,2\text{PPM}}(t) &= (0 \quad A) \end{aligned} \quad (3.22)$$

with  $A$  being the signal's amplitude.

For 2FSK the symbols using the two frequencies  $f_1$  and  $f_2$  are defined as:

$$\begin{aligned} s_{1,2\text{FSK}}(t) &= (A \times \cos(2\pi f_1 t + \varphi) \quad 0 \times \cos(2\pi f_2 t + \varphi)) \\ s_{2,2\text{FSK}}(t) &= (0 \times \cos(2\pi f_1 t + \varphi) \quad A \times \cos(2\pi f_2 t + \varphi)) \end{aligned} \quad (3.23)$$

The phase information  $\varphi$  is irrelevant for FSK and is usually set to zero.

We assume a coherent receiver, as depicted in Fig. 3.1. We also assume that our signal is perfectly polarized and the polarization of the signal is aligned along the  $x$ -axis, thus all  $y$ -related output signal terms are zero. Assuming additive white Gaussian noise, each time slot can consist either of pure noise in the case of an empty slots or can consist of noise plus signal in the case of a pulse. The discussion follows Ref. [19].

The symbol alphabet for *M*PPM can be written with  $\mathbf{s}_i$  being the  $M$  symbols each containing  $M$  values, one for each slot. We now define a matrix, where each row represents one PPM symbol in pass-band. The columns of this matrix represent the slots. Since in *M*ary PPM each symbol contains only one pulse and  $M-1$  empty slots, we find in each row and column of our matrix only one non-zero element:

$$\begin{pmatrix} \mathbf{s}_1 \\ \mathbf{s}_2 \\ \vdots \\ \mathbf{s}_M \end{pmatrix} = \begin{pmatrix} A & 0 & 0 & \dots \\ 0 & A & 0 & \dots \\ \vdots & \vdots & \vdots & \vdots \\ \dots & 0 & 0 & A \end{pmatrix} \quad (3.24)$$

The received signal of Eq. (3.24) in base-band in the presence of additive noise  $\mathbf{n}$  becomes

$$\boldsymbol{\rho}_i = \mathbf{s}_i + \mathbf{n}_i \quad \text{with} \quad i = 1 \dots M \quad (3.25)$$

$$\begin{pmatrix} \boldsymbol{\rho}_1 \\ \boldsymbol{\rho}_2 \\ \vdots \\ \boldsymbol{\rho}_M \end{pmatrix} = \begin{pmatrix} \rho_{11} & \rho_{12} & \rho_{13} & \dots \\ \rho_{21} & \rho_{22} & \rho_{23} & \dots \\ \vdots & \vdots & \vdots & \vdots \\ \dots & \rho_{MM-2} & \rho_{MM-1} & \rho_{MM} \end{pmatrix} \quad (3.26)$$

$$= \begin{pmatrix} A + n_{11} & n_{12} & n_{13} & \dots \\ n_{21} & A + n_{22} & n_{23} & \dots \\ \vdots & \vdots & \vdots & \vdots \\ \dots & n_{MM-2} & n_{MM-1} & A + n_{MM} \end{pmatrix}.$$

All  $n_{ij}$  are independent, additive, complex noise values.

The value of  $\rho_{ij}$  with  $i = j$  represents the time slot containing the PPM pulse. For the sake of readability, the indices are now dropped. It should be kept in mind that the noise is independent for all values of  $\boldsymbol{\rho}_{1 \dots M}$ .

According to [19] pp. 203-205, a PPM-symbol is received and demodulated by finding the maximum value  $\rho_{ij}$  per symbol. For this case one needs to derive the probability that a PPM-symbol is demodulated correctly first. It is assumed that the symbol  $\mathbf{s}_1$  with the pulse in the first slot is sent and  $\boldsymbol{\rho}_1$  is received, see Eq. (3.26). The probability density function of  $\rho_{11}$  is  $p_1(\rho)$ . Since for orthogonal signals all symbol errors occur with the same probability, the derived equation is valid for all  $M$  PPM symbols.

Since the pulse is positioned in the first slot  $\rho_{11}$  all other slots  $\rho_{12} \dots \rho_{1M}$  are empty, i.e. contain only noise. The probability to detect a symbol correctly ( $P_{SC}$ ) thus equals [58, 61]:

$$P_{SC} = P\{\rho_{11} = \max_i \{\rho_{i1}\}\} \quad \text{for } i = 2 \dots M \quad (3.27)$$

$P\{\}$  denotes the probability that the pulse sent is detected in the slot with the highest value received.

Mathematically it is advantageous to calculate first the probability of a correct decision  $P_{SC}$ . The probability to correctly detect the pulse in slot 1 is the joint probability of the  $M - 1$  independent events that the unoccupied slots have amplitudes smaller than  $\rho_{11}$ , averaged with the PDF that actually  $\rho_{11}$  occurs, Thus, the probability that the PPM symbol is detected correctly equals:

$$\begin{aligned} P_{SC} &= \int_{-\infty}^{\infty} p_1(\rho_{th}) P\{\rho_{12} < \rho_{11}, \rho_{13} < \rho_{11}, \dots, \rho_{1M} < \rho_{11} \mid \rho_{11} = \rho_{th}\} d\rho_{th} \\ &= \int_{-\infty}^{\infty} p_1(\rho_{th}) [P\{\rho_{12} < \rho_{11} \mid \rho_{11} = \rho_{th}\}]^{M-1} d\rho_{th} \end{aligned} \quad (3.28)$$

$P\{\rho_{12} < \rho_{11}, \rho_{13} < \rho_{11}, \dots, \rho_{1M} < \rho_{11} \mid \rho_{11} = r_{th}\}$  describes the conditional probability that all values  $\rho_{1,2,\dots,M}$  are smaller than  $\rho_{11}$ , when symbol  $s_1$  is sent. The values of the samples of the slots can be assumed to be independent that allows the simplification performed in the last line of Eq. (3.28). The probability that  $\rho_{12}$  is smaller than the threshold  $\rho_{th}$ ,  $P\{\rho_{12} < \rho_{th} \mid \rho_{th}\}$  can be calculated by integrating the probability density function of the empty slots  $p_0(\rho)$ :

$$P\{\rho_{12} < \rho_{th} \mid \rho_{th}\} = \int_{-\infty}^{\rho_{th}} p_0(\rho) d\rho = 1 - \int_{\rho_{th}}^{\infty} p_0(\rho) d\rho \quad (3.29)$$

Here again we assume equal probability for all symbols, thus Eq. (3.29) is valid for all empty PPM slots.

Eq. (3.28) describes the probability that a symbol is detected correctly. However, usually the bit error ratio is of interest. Let's first rearrange Eq. (3.16) and introduce the symbol error ratio (SER). After having solved the SER, the relation between SER and BER will be derived. In the case of orthogonal signaling with an alphabet size of two, SER and BER are equal. The general form of the symbol error ratio (SER) equals

$$SER_{\text{binary}} = \int_{-\infty}^{\infty} p_0(\rho_{th}) \int_{\rho_{th}}^{\infty} p_1(\rho) d\rho d\rho_{th} \quad (3.30)$$

with  $\rho_{th}$  the optimum threshold, that has to be determined, and  $p_{1,0}$  the PDFs of the pulse and empty slots, respectively. The integral

$$\int_{\rho_{\text{th}}}^{\infty} p_1(\rho) d\rho \quad (3.31)$$

describes the probability that the PPM-pulse is detected to be above a certain threshold  $\rho_{\text{th}}$ . We assume that all symbols are sent with the same probability.

The probability that a *M*-ary-PPM symbol is detected wrongly is described by the symbol error ratio  $\text{SER}_{\text{PPM}} = 1 - P_{\text{SC}}$ :

$$\begin{aligned} \text{SER}_{\text{PPM}} &= 1 - \int_{-\infty}^{\infty} p_0(\rho_{\text{th}}) \left[ \int_{-\infty}^{\rho_{\text{th}}} p_1(\rho) d\rho \right]^{M-1} d\rho_{\text{th}} \\ &= 1 - \int_{-\infty}^{\infty} p_0(\rho_{\text{th}}) \left[ 1 - \int_{\rho_{\text{th}}}^{\infty} p_1(\rho) d\rho \right]^{M-1} d\rho_{\text{th}} \end{aligned} \quad (3.32)$$

To derive the bit error probability  $\text{BER}_{\text{PPM}}$  we know that for equiprobable orthogonal signals any wrong symbol happens with the same probability, i.e. all symbol errors happen with the same probability. Thus, since it is known that the *M*-ary PPM alphabet consists of  $M - 1$  wrong symbols, any symbol error happens with the probability  $\text{SER}_{\text{PPM}} / (M - 1)$ . Under the assumption that only one bit per symbol is wrong and the wrong bit is the first in the bit sequence, we know that half of our  $M$  symbols are wrong, since half of the symbols have the wrong bit at the beginning of their bit sequence. This leads to

$$\begin{aligned} \text{BER}_{\text{PPM}} &= \frac{M}{2} \cdot \text{SER}_{\text{PPM}} \\ &= \frac{M}{2} \frac{1}{M-1} \cdot \text{SER}_{\text{PPM}} \\ &= \frac{2^{k-1}}{2^k - 1} \cdot \text{SER}_{\text{PPM}} \end{aligned} \quad (3.33)$$

with  $k = \log_2(M)$  the number of bits per symbol. The results of *M*-PPM or *M*-FSK for homodyne detection with and without polarization diversity are depicted in Fig. 3.4(a-b).

The probability density functions that are needed for BER calculation of PPM and FSK according Eq. (3.32) and (3.33) depend on the demodulation scheme chosen. In the following, different cases will be discussed:

- 1) Coherent detection with signal and noise in one or two polarizations
- 2) Envelope detection (or asynchronous detection) with signal and noise in one or two polarizations

### 3.3.3.1 Coherent Detection of PPM and FSK Symbols with noise and signal in one and two polarizations

One way to demodulate PPM or FSK symbols is using coherent (or synchronous) detection, which is usually performed with the help of any kind of a phase-locked loop (PLL). Thus, the intermediate frequency as well as the phase difference between signal and LO equals zero. Since after such a PLL, PPM and FSK symbols look alike we will discuss in the following only PPM, which will be the same as for orthogonal FSK. It is assumed that the signal is polarized in  $x$ -direction, thus all  $y$ -related output terms can be neglected. Assuming additive white Gaussian noise, in each PPM slot either pure noise for empty slots or noise plus signal in the case of a pulse can be found.

First, 2PPM is discussed. We follow the notation already given for PSK in Section 3.3.1. In the presence of additive Gaussian noise in  $x$ -polarization and in each of the  $i=1,2$  slots with  $n_{xi}(t) = n_{Ix_i}(t) + jn_{Qx_i}(t)$ , the received signal given in Eq. (3.26) for 2PPM becomes:

$$\begin{aligned}
 \mathbf{p}_{i,\text{PPM}}(t) &= \mathbf{s}_{i,\text{PPM}}(t) + \mathbf{n}(t) \\
 \mathbf{p}_{1,2\text{PPM},1\text{p}}(t) &= \begin{pmatrix} A(t) + n_{Ix1}(t) + jn_{Qx1}(t) & n_{Ix2}(t) + jn_{Qx2}(t) \\ n_{Ix1}(t) + jn_{Qx1}(t) & A(t) + n_{Ix2}(t) + jn_{Qx2}(t) \end{pmatrix}
 \end{aligned} \tag{3.34}$$

As already discussed previously in the context of Fig. 3.2, in coherent (synchronous) detection, the imaginary parts of the noise terms do not contribute to the symbol decision and thus can be dropped. Thus, the probability density functions (PDF) of each value of Eq. (3.34) are Gaussian [29], with a mean  $A$  for the symbol slot containing a pulse, and a mean equal to zero, if the slot is empty. The PDFs in one polarization (here  $x$ -polarization) equal:

$$\begin{aligned}
p_{1,\text{PPM},1\text{p}}(\rho) &= \frac{1}{\sqrt{2\pi}\sigma} \exp\left(-\frac{(\rho - A)^2}{2\sigma^2}\right) \\
p_{0,\text{PPM},1\text{p}}(\rho) &= \frac{1}{\sqrt{2\pi}\sigma} \exp\left(-\frac{\rho^2}{2\sigma^2}\right)
\end{aligned} \tag{3.35}$$

where  $\sigma^2$  describes the noise power [29]. Thus the ratio of  $A^2 / (2\sigma^2)$  is a measure for the symbol power divided by the noise power both measured in the bandwidth  $B$  [2], see Eq. (3.18)

$$\text{SNR}_x = \frac{\mathcal{E}_s B}{N_0 B} = \frac{\mathcal{E}_s}{N_0} = \frac{G \log_2(M) \mathcal{E}_b}{N_{\text{ASE}}} = \frac{\text{GPPS } hf_c}{n_{\text{sp}}(G-1)hf_c} \tag{3.36}$$

with PPS the number of photons per symbol received and  $\mathcal{E}_b$  the energy per bit,  $hf_c$  is the photon energy,  $G$  is the preamplifier gain. For a large gain  $G/(G-1)$  equals one [2, 19, 56]. The result is depicted in Fig. 3.4 for different values of  $M$ .

However, if a polarization diverse coherent receiver is used, see Fig. 3.1, with random polarization of the signal at the input, the received signals look slightly different. We hereby introduce the polarization power splitting ratio  $\alpha_p$  [40]. The two symbols of 2PPM become now:

$$\begin{aligned}
\mathbf{p}_{i,\text{PPM}}(t) &= \mathbf{s}_{i,\text{PPM}}(t) + \mathbf{n}(t) \\
\mathbf{p}_{1,2\text{PPM},2\text{p}}(t) &= \begin{pmatrix} \sqrt{\alpha_p} A(t) + n_{\text{Ix}1}(t) + j n_{\text{Qx}1}(t) & n_{\text{Ix}2}(t) + j n_{\text{Qx}2}(t) \\ \sqrt{1-\alpha_p} A(t) + n_{\text{Iy}1}(t) + j n_{\text{Qy}1}(t) & n_{\text{Iy}2}(t) + j n_{\text{Qy}2}(t) \end{pmatrix} \\
\mathbf{p}_{2,2\text{PPM},2\text{p}}(t) &= \begin{pmatrix} n_{\text{Ix}1}(t) + j n_{\text{Qx}1}(t) & \sqrt{\alpha_p} A(t) + n_{\text{Ix}2}(t) + j n_{\text{Qx}2}(t) \\ n_{\text{Iy}1}(t) + j n_{\text{Qy}1}(t) & \sqrt{1-\alpha_p} A(t) + n_{\text{Iy}2}(t) + j n_{\text{Qy}2}(t) \end{pmatrix}
\end{aligned} \tag{3.37}$$

Again, the imaginary parts of the noise are dropped, since they do not contribute to the symbol decision. We define  $A_x(t) = \sqrt{\alpha_p} A(t)$  and  $A_y(t) = \sqrt{1-\alpha_p} A(t)$  with  $\frac{1}{2} A_x^2 + \frac{1}{2} A_y^2 = A^2$  and thus, Eq. (3.37) can be simplified to:

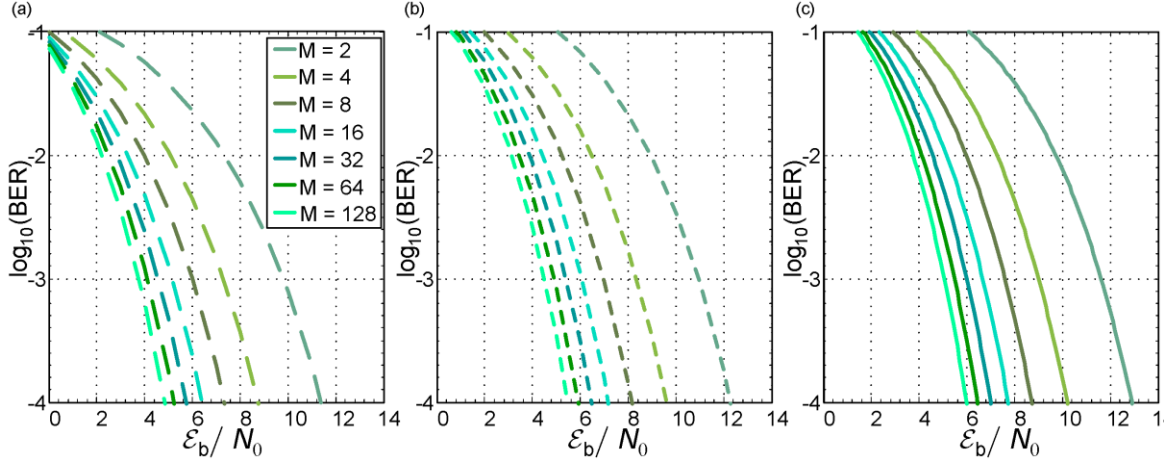


Fig. 3.4 Analytical results of  $M$ -PPM or  $M$ -FSK for different ways of demodulation. It can be seen that the higher the number of slots per symbol, the higher the sensitivity. (a) homodyne reception in one polarization (b) single polarization envelope detection (c) envelope detection with polarization diverse reception.

$$\begin{aligned}
 \mathbf{p}_{1,2\text{PPM},2\text{p}}(t) &= \begin{pmatrix} A_x(t) + n_{I_{x1}}(t) & n_{I_{x2}}(t) \\ A_x(t) + n_{I_{y1}}(t) & n_{I_{y2}}(t) \end{pmatrix} \\
 \mathbf{p}_{2,2\text{PPM},2\text{p}}(t) &= \begin{pmatrix} n_{I_{x1}}(t) & A_y(t) + n_{I_{x2}}(t) \\ n_{I_{y1}}(t) & A_y(t) + n_{I_{y2}}(t) \end{pmatrix}
 \end{aligned} \tag{3.38}$$

Now, unlike in the previous case (see Eq. (3.34)), there are two independent noise terms present in each of the received signal values, i.e.  $n_{I_{xi}}$  and  $n_{I_{yi}}$ . As thoroughly discussed in [40], Appendix A, the PDFs of  $\mathbf{p}_{i,\text{PPM}}(t)$  can be derived by a convolution of two Gaussian PDFs of  $x$  and  $y$ -polarized parts of the signals. The convolution of two Gaussian distributions results again in a Gaussian distribution with mean values and variances equal to the sum of each of the means or variances of the Gaussian distributions [40]. Thus, in the polarization-diverse case the SNR decreases by a factor of two.

### 3.3.3.2 Envelope Detection of PPM and FSK Symbols with signal and noise in one and two polarizations

There are several ways to perform envelope detection. We will discuss these in the following.

We describe the received baseband signal in  $x$  and  $y$ -polarizations by the vector  $\mathbf{p}(t) = r_x(t)\vec{e}_x + r_y(t)\vec{e}_y$  (orthogonal unit vectors  $\vec{e}_{x,y}$ ), which comprises the signal vector  $\mathbf{s}(t)$  and the noise vector  $\mathbf{n}(t)$ ,

$$\begin{aligned} \mathbf{p}(t) &= \mathbf{s}(t) + \mathbf{n}(t), \\ \mathbf{s} &= \begin{pmatrix} s_x \\ s_y \end{pmatrix} = \begin{pmatrix} I_x + jQ_x \\ I_y + jQ_y \end{pmatrix}, \quad \mathbf{n} = \begin{pmatrix} n_x \\ n_y \end{pmatrix} = \begin{pmatrix} n_{I,x} + jn_{Q,x} \\ n_{I,y} + jn_{Q,y} \end{pmatrix} \end{aligned} \quad (3.39)$$

The noise terms in both polarizations are  $n_{I,x,y}$  and  $n_{Q,x,y}$ , respectively. These noise terms are assumed to be independently Gaussian distributed with zero mean and variance  $\sigma_{x,y}^2 = \sigma_{I,x,y}^2 = \sigma_{Q,x,y}^2 = \sigma^2$ .

The received signal after heterodyne reception with random orientation of the polarization is given in Eq. (3.37). We use

$$\sqrt{\alpha_p} A = |I_x + jQ_x|, \quad \sqrt{1 - \alpha_p} A = |I_y + jQ_y|. \quad (3.40)$$

For envelope detection, first the square of the absolute value is used for demodulation. Remark: Later, a different scenario will be discussed, where only the absolute values are taken into account for symbol decision.

We define the received output signal in  $x$ - and  $y$ -polarization in the presence of noise for 2PPM by:

$$\begin{aligned} \mathbf{r}_{1,2\text{PPM}} &= \begin{pmatrix} (I_x + n_{Ix1})^2 + (Q_x + n_{Qx1})^2 + (I_y + n_{Ix1})^2 + (Q_y + n_{Qx1})^2 \\ n_{Ix2}^2 + n_{Qx2}^2 + n_{Iy2}^2 + n_{Qy2}^2 \end{pmatrix} \\ \mathbf{r}_{2,2\text{PPM}} &= \begin{pmatrix} n_{Ix1}^2 + n_{Qx1}^2 + n_{Iy1}^2 + n_{Qy1}^2 \\ (I_x + n_{Ix2})^2 + (Q_x + n_{Qx2})^2 + (I_y + n_{Ix2})^2 + (Q_y + n_{Qx2})^2 \end{pmatrix} \end{aligned} \quad (3.41)$$

Again, we assume the noise terms of the real and imaginary part of each polarization and of each slot  $n_{I,Q,x,y,1,2}$  to be independent. In addition, all show Gaussian distributions with zero mean.

Thus, we define:

$$r_{\text{sq}} = |r_x|^2 + |r_y|^2, \quad r_{x,y} = I_{x,y} + n_{I,x,y} + j(Q_{x,y} + n_{Q,x,y}). \quad (3.42)$$

The PDF of the signals in Eq. (3.41) and (3.42) are given by the  $\chi^2$ -distribution with four degrees of freedom, see [19] (pp. 46-48). It should be noted that the result is independent of the polarization power splitting ratio  $\alpha_p$ , as already pointed out in [40].

If the signal and noise are only present in one polarization, here  $x$ -polarization, all  $y$ -polarization terms in Eq. (3.41) drop, resulting in  $\chi^2$ -distribution with two degrees of freedom, see [19] (pp. 46-48).

The general non-central  $\chi^2$ -distribution with  $n$  degrees of freedom in general is given by [19] (Eq. 2.3-29):

$$p(r) = \begin{cases} \frac{1}{2\sigma^2} \left(\frac{r}{\mu^2}\right)^{\frac{n-2}{2}} e^{-\frac{\mu^2+r}{2\sigma^2}} I_{\frac{n-1}{2}}\left(\frac{\mu\sqrt{r}}{\sigma^2}\right) & r > 0 \\ 0 & \text{otherwise} \end{cases} \quad (3.43)$$

with  $\mu^2 = \sum_{i=1}^n \mu_i^2$  the sum of the mean values of the Gaussian distributions. Here for the polarization diverse case it equals  $\mu^2 = I_x^2 + Q_x^2 + I_y^2 + Q_y^2$ . The integral over Eq. (3.43) is described by Marcum Q-function that is written here in a general form:

$$Q_K(\alpha, \beta) = \int_{\beta}^{\infty} r \left(\frac{r}{\alpha}\right)^{K-1} \exp\left(-\frac{r^2 + \alpha^2}{2}\right) I_{K-1}(\alpha r) dr \quad (3.44)$$

with  $K = n - 1$ .

The result of *Mary* PPM or *Mary* FSK for envelope detection with and without polarization diversity is depicted in Fig. 3.4(b-c).

A similar but different result can be derived, if not the absolute values squared are taken into account for symbol decision, but the absolute values of our signals. Then the received symbols of 2PPM look like

$$\begin{aligned} \mathbf{r}_{1,2\text{PPM}} &= \begin{pmatrix} \sqrt{(I_x + n_{Ix1})^2 + (Q_x + n_{Qx1})^2} + \sqrt{(I_y + n_{Ix1})^2 + (Q_y + n_{Qx1})^2} \\ \sqrt{n_{Ix2}^2 + n_{Qx2}^2} + \sqrt{n_{Iy2}^2 + n_{Qy2}^2} \end{pmatrix} \\ \mathbf{r}_{2,2\text{PPM}} &= \begin{pmatrix} \sqrt{n_{Ix1}^2 + n_{Qx1}^2} + \sqrt{n_{Iy1}^2 + n_{Qy1}^2} \\ \sqrt{(I_x + n_{Ix2})^2 + (Q_x + n_{Qx2})^2} + \sqrt{(I_y + n_{Ix2})^2 + (Q_y + n_{Qx2})^2} \end{pmatrix} \end{aligned} \quad (3.45)$$

Thus, the received signal  $r_{\text{abs}}$  changes to:

$$r_{\text{abs}} = |r_x| + |r_y|, \quad r_{x,y} = I_{x,y} + n_{I,x,y} + j(Q_{x,y} + n_{Q,x,y}). \quad (3.46)$$

First, the single-polarization case is investigated first. Thus, all  $y$ -related terms of Eq. (3.45) and (3.46) become zero. The PDF of such a signal is given by the Rice distribution, if a slot containing a pulse is received and

Rayleigh distribution, if an empty slot is received [19] (pp. 48-52). The PDF is given by

$$p_{rx}(r) = \begin{cases} \frac{r}{\sigma^2} e^{-\frac{A_x^2 + r^2}{2\sigma^2}} I_0\left(\frac{A_x r}{\sigma^2}\right) & r > 0 \\ 0 & \text{otherwise} \end{cases} \quad (3.47)$$

with  $A_x^2 = I_x^2 + Q_x^2$ . The integral over Eq. (3.47) is also given by the Marcum Q-function, see Eq. (3.44). It can mathematically be shown that the integral over the  $\chi^2$ -distribution with two degrees of freedom equals the integral over the Rayleigh-distribution. Thus it is irrelevant for the receiver sensitivity performance, whether one uses the absolute values squared for symbol decision or only the absolute values [29]. This statement is valid in single-polarization case only.

However, if the polarization diverse-case is of interest, i.e.  $r_{\text{abs}}$ , one has to perform the convolution of the Rice and Rayleigh distributions of Eq. (3.47) [40].

$$\begin{aligned} p_{\text{abs}}(r_{\text{abs}}, A) &= p_r(|r_x|, A_x) * p_r(|r_y|, A_y) \\ &= (p_r * p_r)(r_{\text{abs}}, A) \end{aligned} \quad (3.48)$$

This time the result strongly depends on the polarization power splitting ratio  $\alpha_p$ :

$$A_x^2 = \alpha_p (I_x^2 + Q_x^2); \quad A_y^2 = (1 - \alpha_p) (I_y^2 + Q_y^2) \quad (3.49)$$

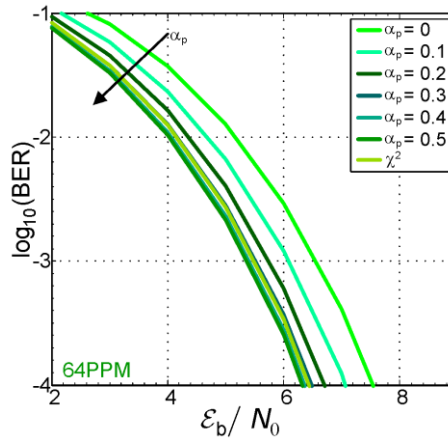


Fig. 3.5 Sensitivity of 64PPM when detected with different power splitting ratios  $\alpha_p$  on the two polarizations if the sum of the absolute values is used for demodulation. It becomes clear that here the result strongly depends on  $\alpha_p$ . For comparison the result using the  $\chi^2$ -distribution is used is shown as well, which is  $\alpha_p$ -independent.

There is the best receiver sensitivity if the symbol powers are split equally for both polarizations, resulting in  $\alpha_p = \frac{1}{2}$ , see Fig. 3.5 for 64PPM. The worst case is if  $\alpha_p = 0$ , leading to all symbol power either on  $x$  or  $y$ -polarization, and only noise on the other outputs. In Fig. 3.5 also the result is shown for  $\chi^2$ -distribution with four degrees of freedom, which is  $\alpha_p$ -independent. However, the best receiver sensitivity amongst all envelope detection schemes using a polarization diverse receiver is given by summing the absolute values of the signals in both polarizations, each having equal powers.

### 3.4 Receiver Sensitivity of Multiplexed Signals

Whenever a high amount of data has to be transmitted simultaneously, multiplexing comes into play. Multiplexing means that the overall data rate can be increased by a factor of  $K$ , if  $K$  *different* degrees of freedom are used to transmit *different* data simultaneously. These degrees of freedom are usually wavelength, frequency, polarization, space or time [8]. All have in common that - in the ideal case - the sensitivity per channel does not change. With other words, sensitivity improvements are not possible with the help of multiplexing. On the contrary, when crosstalk between neighboring channels takes place, the sensitivity performance degrades.

This will be discussed in the following using polarization multiplexed PSK. As discussed in Section 3.3.1, Eq. (3.18), the BER for binary PSK, in one ( $x$ -)polarization is can be rearranged to

$$\text{BER}_{\text{BPSK}} = \frac{1}{2} \text{erfc} \left( \sqrt{\frac{\mathcal{E}_s}{N_0}} \right) = \frac{1}{2} \text{erfc} \left( \sqrt{\frac{\mathcal{E}_b}{N_0}} \right) \quad (3.50)$$

with  $\mathcal{E}_s/N_0$  the symbol energy over the noise spectral density. As already shown in Fig. 1.1, BPSK and QPSK show the same energy per bit over noise spectral density requirements. For BPSK, we have the symbol energy equal to the bit energy, i.e.  $\mathcal{E}_b = \mathcal{E}_s$  since in BPSK one bit per symbol is encoded. For QPSK, we double the bit per symbol. However, also the noise doubles, since the influence of  $n_{Ix}$  and  $n_{Qx}$  of Eq. (3.15) has to be taken also into account. For QPSK we thus get

$$\text{BER}_{\text{QPSK}} = \frac{1}{2} \text{erfc} \left( \sqrt{\frac{\mathcal{E}_s}{2N_0}} \right) = \frac{1}{2} \text{erfc} \left( \sqrt{\frac{\mathcal{E}_b}{N_0}} \right). \quad (3.51)$$

Once, we use a polarization multiplexed (PM-) QPSK, we can encode 4 bit per symbol. However, now also the  $y$ -polarization related noise terms  $n_{Iy}$  and  $n_{Qy}$  must be taken into account, in addition to  $n_{Ix}$  and  $n_{Qx}$ . Thus, we get the BER for PM-QPSK [11]

$$\text{BER}_{\text{PM-QPSK}} = \frac{1}{2} \text{erfc} \left( \sqrt{\frac{\mathcal{E}_s}{4N_0}} \right) = \frac{1}{2} \text{erfc} \left( \sqrt{\frac{\mathcal{E}_b}{N_0}} \right). \quad (3.52)$$

Since all three equations, Eq. (3.50), Eq. (3.51) and Eq. (3.52), are equal regarding their bit energy over the noise spectral density, it can be said that this is a good example, why the BER as a function of bit energy over noise spectral density does not change, when multiplexing is applied. Thus, exemplarily for PSK signals it has been demonstrated that the receiver sensitivity does not change, when multiplexing is applied.

### 3.5 Theoretical Sensitivity of Stacked Modulation Formats

Up to now, modulation formats with only one or two modulated degrees of freedom were discussed. By “stacking” modulation formats we are discussing modulation formats where multiple degrees of freedom are modulated, see Chapter 5 and 6.

In the following the receiver sensitivities of stacked modulation formats are introduced. When stacking, it has to be taken care of the demodulation order. If, for example, a stack of two modulation formats is regarded, where the symbol of the first modulation format is detected wrongly, the second modulation format consists of only noise. Thus pure guessing takes place,

and thus, there is a 50% chance that any bit encoded in the second modulation format can be right or wrong.

### 3.5.1 *Mary* PPM–PS–QPSK

In the following the sensitivity of the stacked modulation format PS-QPSK-MPPM is discussed. In [11] the sensitivity of DP-QPSK-16PPM is introduced. The sensitivity of PS-QPSK-MPPM is similar [10]:

$$\text{BER}_{\text{PPM, PSQ}} = \frac{\text{SER}_{\text{PPM}} \left( \frac{M}{2(M-1)} \cdot \log_2(M) + \frac{n_{\text{PSQ}}}{2} \right)}{\log_2(M) + n_{\text{PSQ}}} + (1 - \text{SER}_{\text{PPM}}) \frac{\text{BER}_{\text{PSQ}} \times n_{\text{PSQ}}}{\log_2(M) + n_{\text{PSQ}}} \quad (3.53)$$

with  $n_{\text{PSQ}}$  being the bits per symbol encoded in PS-QPSK that equals 3.

The first summand of Eq. (3.53) represents the situation, that there is an error in the PPM symbol that happens with the probability of  $\text{SER}_{\text{PPM}}$ , see Eq. (3.32). The symbol error ratio is multiplied by two summands. The first describes factor of Eq. (3.33), that relates the  $\text{SER}_{\text{PPM}}$  to  $\text{BER}_{\text{PPM}}$ . It is weighted by the number of bits encoded in the PPM symbol  $\log_2(M)$ . If the PPM symbol is wrong, we can assume that half of the bits encoded in the PS-QPSK symbol  $n_{\text{PSQ}}$  are wrong, too, leading to the second summand that is multiplied by  $\text{SER}_{\text{PPM}}$ . The probability of an error is then obtained by dividing the wrongly decoded bits by the total number of bit  $n_{\text{PSQ}} + \log_2(M)$ .

The second term in Eq. (3.53) describes the case, when there is no error in the PPM symbol, but the error is found in the PS-QPSK symbol. The probability that the PPM symbol is detected correctly equals  $1 - \text{SER}_{\text{PPM}}$ . The probability that the error happens in the PS-QPSK symbol is  $\text{BER}_{\text{PSQ}}$  and can be found in Eq. (3.21). Here again, the term is weighted by the number of bits encoded in the PS-QPSK symbol  $n_{\text{PSQ}}$  and divided by the total number of bits per PPM-PS-QPSK symbol  $n_{\text{PSQ}} + \log_2(M)$ .

### 3.5.2 Theoretical Receiver Sensitivity of Stacked MPPM–NFSK–PS–QPSK

In analogy to the previous section we stack now an additional modulation format to PPM and PS-QPSK. We choose 4FSK that has been introduced previously and equals in its sensitivity PPM with  $M=N=4$ . This section follows closely Ref. [14], Section 4. The demodulation order of this

modulation format is that we first demodulate the PPM symbol, then the FSK symbol and finally the PS-QPSK symbol [11].

For PPM-FSK-PS-QPSK we distinguish three cases:

1. The *M*-ary PPM symbol was detected wrongly with a symbol error probability  $SER_{PPM}$  and an associated bit error probability  $BER_{PPM} = SER_{PPM} M / (2(M-1))$  according to Eq. (3.33). In this case the detected *N*-ary FSK and PS-QPSK information is random so that on average half of their bits are wrong, i. e., the average number of erroneous bits is  $\frac{1}{2} \log_2(N)$  and  $\frac{1}{2} \times 3$ , respectively.
2. The PPM symbol was correctly detected with a probability equal to  $1 - SER_{PPM}$ , but the *N*-ary FSK symbol was detected wrongly with a symbol error probability  $SER_{FSK}$  and an associated bit error probability  $BER_{FSK} = SER_{FSK} N / (2(N-1))$  according to Eq. (3.33). In this case the detected PS-QPSK bits are random so on average half of them are wrong leading to an average number of  $\frac{1}{2} \times 3$  erroneous bits.
3. The PPM and the FSK symbols were correctly detected with a probability  $(1 - SER_{PPM})(1 - SER_{FSK})$ , but the PS-QPSK symbol (PSQ for short) was detected wrongly with a bit error probability  $BER_{PSQ}$  according to Eq. (3.21).

Since not all these cases contribute the same amount of erroneous bits, the respective bit error probabilities have to be calculated by relating the number of erroneous bits to the total number  $\log_2(M)|_{PPM} + \log_2(N)|_{FSK} + 3|_{PS-QPSK}$  of bits which are transmitted by the stacked *M*PPM-*N*FSK-PS-QPSK modulation format. As a result we find [14]:

$$\begin{aligned}
 BER_{total}^{(FSK)} = & \frac{SER_{PPM} \left( \frac{M}{2(M-1)} \log_2(M) + \frac{1}{2} \log_2(N) + \frac{1}{2} \times 3 \right)}{\log_2(M) + \log_2(N) + 3} \\
 & + (1 - SER_{PPM}) \frac{SER_{FSK} \left( \frac{N}{2(N-1)} \log_2(N) + \frac{1}{2} \times 3 \right)}{\log_2(M) + \log_2(N) + 3} \\
 & + (1 - SER_{PPM})(1 - SER_{FSK}) \frac{BER_{PSQ} \times 3}{\log_2(M) + \log_2(N) + 3}
 \end{aligned} \tag{3.54}$$

### 3.5.3 Theoretical Receiver Sensitivity of Stacked *M*PPM–*K*OFDM–PS–QPSK

This section follows closely Ref. [14], Section 4. In analogy to the previous section we replace the FSK-PS-QPSK symbols by PS-QPSK symbols on  $K$  OFDM subcarriers. The demodulation order of this modulation format is that we first demodulate the PPM symbol, then the OFDM-PS-QPSK symbols. Thus, the bit error ratio becomes:

$$\text{BER}_{\text{total}}^{(\text{OFDM})} = \frac{\text{SER}_{\text{PPM}} \left( \frac{M}{2(M-1)} \cdot \log_2(M) + \frac{1}{2} \times K \times 3 \right)}{\log_2(M) + K \times 3} + (1 - \text{SER}_{\text{PPM}}) \frac{\text{BER}_{\text{PSQ}} \times K \times 3}{\log_2(M) + K \times 3} \quad (3.55)$$

The first summand gives us the case that there is an error in the PPM symbol that happens with the probability of  $\text{SER}_{\text{PPM}}$  that has been discussed in Eq. (3.32). The symbol error ratio is multiplied by two summands. The first describes multiplication factor of Eq. (3.33) that calculates  $\text{BER}_{\text{PPM}}$  from  $\text{SER}_{\text{PPM}}$ . It is weighted by the number of bits encoded in the PPM symbol  $\log_2(M)$ . If the PPM symbol is wrong, we can assume that half of the bits encoded in the PS-QPSK symbols in all  $K$  OFDM subcarriers are wrong i.e.  $K \times 3$ , are wrong, too.

The second term in Eq. (3.55) describes the case, when there is no error in the PPM symbol, but the error is found in the PS-QPSK symbols. The probability that the PPM symbol is detected correctly equals  $1 - \text{SER}_{\text{PPM}}$ . The sensitivity per bit of PS-QPSK does not change if ideal multiplexing is assumed.

All summands are divided by the total number of bits encoded in the symbol. For PPM symbol demodulation as applied in [14] the absolute values of the  $2K$  complex coefficients are summed up. Thus, the  $\text{SER}_{\text{PPM}}$  of Eq. (3.55) differs from the  $\text{SER}_{\text{PPM}}$  of Eq. (3.54). This will be discussed in the following more closely for *M*PPM-2OFDM where per occupied PPM slot two OFDM subcarriers are transmitted, which are subscripted with  $\alpha$  and  $\beta$ . We apply an FFT to the signal in each PPM time slot and for each polarization, and look at the  $2 \times 2$  complex Fourier coefficients  $s_{x,y,\alpha}$  and  $s_{x,y,\beta}$  which are associated with the two OFDM subcarrier signals,

$$s_\alpha = \begin{pmatrix} s_{x\alpha} \\ s_{y\alpha} \end{pmatrix} = \begin{pmatrix} I_{x\alpha} + jQ_{x\alpha} \\ I_{y\alpha} + jQ_{y\alpha} \end{pmatrix}, \quad s_\beta = \begin{pmatrix} s_{x\beta} \\ s_{y\beta} \end{pmatrix} = \begin{pmatrix} I_{x\beta} + jQ_{x\beta} \\ I_{y\beta} + jQ_{y\beta} \end{pmatrix}. \quad (3.56)$$

We form the sum of the moduli for  $x$  and  $y$ -polarizations  $r_{\text{FSK}\alpha} = |r_{x\alpha}| + |r_{y\alpha}|$  and  $r_{\text{FSK}\beta} = |r_{x\beta}| + |r_{y\beta}|$  for each subcarrier  $\alpha$  and  $\beta$ ,

$$\begin{aligned} r_{\text{OFDM}} &= r_{\text{FSK}\alpha} + r_{\text{FSK}\beta} = |r_{x\alpha}| + |r_{y\alpha}| + |r_{x\beta}| + |r_{y\beta}| \\ &= \left| I_{x\alpha} + n_{I,x\alpha} + j(Q_{x\alpha} + n_{Q,x\alpha}) \right| \\ &\quad + \left| I_{y\alpha} + n_{I,y\alpha} + j(Q_{y\alpha} + n_{Q,y\alpha}) \right| \\ &\quad + \left| I_{x\beta} + n_{I,x\beta} + j(Q_{x\beta} + n_{Q,x\beta}) \right| \\ &\quad + \left| I_{y\beta} + n_{I,y\beta} + j(Q_{y\beta} + n_{Q,y\beta}) \right| \end{aligned} \quad (3.57)$$

with

$$|s_{x\alpha}| = |s_{x\beta}| = |s_{y\alpha}| = |s_{y\beta}| \equiv A_{\text{OFDM}} \quad \text{and} \quad 2A_{\text{OFDM}}^2 \in \{0, \mathcal{E}_{\text{slot}}/T_{\text{slot}}\}. \quad (3.58)$$

Again, the sum of the pure signal powers  $\frac{1}{2}|s_{x\alpha}|^2 + \frac{1}{2}|s_{x\beta}|^2 + \frac{1}{2}|s_{y\alpha}|^2 + \frac{1}{2}|s_{y\beta}|^2 = 2A_{\text{OFDM}}^2$  in an occupied PPM slot represents the energy  $\mathcal{E}_{\text{slot}}$  per slot duration  $T_{\text{slot}}$ , and is zero elsewhere. The random variables  $|r_{x\alpha}|$ ,  $|r_{y\alpha}|$ ,  $|r_{x\beta}|$  and  $|r_{y\beta}|$  are statistically independent with respect to their noise contributions, therefore the PDF of  $r_{\text{OFDM}}$  is computed by the convolution

$$\begin{aligned} p_{\text{OFDM}}(r_{\text{OFDM}}, A_{\text{OFDM}}) &= \\ & p_{\text{FSK}}(r_{\text{FSK}\alpha}, A_{\text{OFDM}}) * p_{\text{FSK}}(r_{\text{FSK}\beta}, A_{\text{OFDM}}) \\ &= (p_{\text{FSK}} * p_{\text{FSK}})(r_{\text{OFDM}}, A_{\text{OFDM}}) \end{aligned} \quad (3.59)$$

The result of Eq. (3.59) should be used in Eq. (3.32) to derive the symbol error ratio of PPM required in Eq. (3.55).

If PPM-KOFDM-PS-QPSK should be applied this scheme has to be adapted accordingly for 2 to  $K$  subcarriers.

RSoft Optsim simulations have shown that there is an optimum receiver sensitivity for 64PPM-KOFDM-PS-QPSK for  $K=2$ . This is why it has been chosen to be applied in the experiments later presented and discussed in Chapter 6.

### 3.6 Conclusion

In this chapter, the theoretical receiver sensitivity of several modulation formats is introduced, like QPSK, PS-QPSK, PPM and FSK. Several demodulation schemes are presented for PPM and FSK detection and their sensitivity is discussed. Finally, the theoretical receiver sensitivity for stacked modulation formats is given. It will be shown in the Chapter 5 and 6 that the modulation formats and their stacks as presented here will show very good sensitivity performances.

## 4 Multi-Pulse PPM and Multi-Frequency FSK

In this section the influence of the implementation of multi-pulse PPM sequences onto the receiver sensitivity is discussed. Multi-pulse PPM is about the idea of inserting more than one pulse into a PPM symbol. In the case of FSK, the effect is investigated, what happens, if we use more than one frequency simultaneously at a time in one symbol. This will be discussed in the following.

### 4.1 Receiver Sensitivity of Multi-Pulse PPM and Multi-Frequency FSK

In the following, basic estimations are conducted exemplarily discussed with the help of PPM. However, the statements derived are also applicable to orthogonal FSK [62, 63].

Two different ways of implementing multi-pulse PPM are introduced. In the first case, the generation of a multi-pulse PPM symbol follows the rule that only one PPM pulse can be positioned within one time slot. This scheme is in the following called one dimensional multi-pulse (1D-MP) PPM, since for the symbol demodulation only one type of information, i.e. the slot number must be determined.

The second idea of implementing multi-pulse PPM symbols will be called two dimensional multi-pulse (2D-MP) PPM. Here, every PPM-slot can be occupied by as many multi-pulses as available. This will be discussed later in more detail.

However, it should be mentioned that the naming and counting of dimensions is not consistent with the counting of dimensions in multi-dimensional modulation formats, as introduced in Refs. [18] and [17].

First, 1D multi-pulse PPM is discussed.

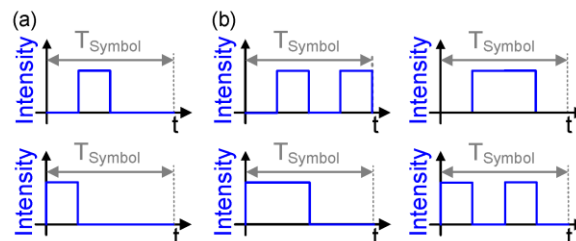


Fig. 4.1 The difference of “conventional” PPM and multi-pulse PPM is depicted in time domain (a) two exemplarily PPM symbols of 4PPM are depicted with the pulse either in the first or second slot. (b) four possible symbols of 1-dimensional multi-pulse PPM with two pulses per symbol are depicted.

### 4.1.1 One Dimensional Multi-Pulse PPM

Each PPM-symbol consists of  $M$  timeslots. Assuming the noise power  $P_{\text{Noise}}$  in each time slot and defining  $g$  the PPM signal power to be  $P_{\text{sig}}$ , the signal to noise power (SNR) ratio equals to  $P_{\text{sig}}/P_{\text{Noise}}$ . The pulse power  $P_{\text{pulse}}$  equals the symbol power, since there is no power in the empty PPM slots. Since the sensitivity performance per bit is of interest, the signal power  $P_{\text{sig}}$  is divided by the number of bits per symbol encoded in this symbol  $n_{\text{bits}}$ . The signal to noise power ratio per bit is thus also divided by the number of bits per symbol and equals  $1/(n_{\text{bits}} P_{\text{Noise}})$ . Thus, for a “conventional”  $M$ -ary-PPM symbol with one pulse per symbol, we get the signal to noise power ratio per bit:

$$\text{SNR}_{\text{bit}} = \frac{P_{\text{sig}}}{P_{\text{Noise}} n_{\text{bits}}} = \frac{1}{\log_2(M)} \text{SNR}_{\text{sym}} \quad (4.1)$$

Inserting now more pulses  $M_p < M$  into one symbol, the number of bits per symbol is increased but in addition also the signal power as well, when it is assumed that the pulse power  $P_{\text{pulse}}$  is constant. Thus, we get  $P_{\text{sig}} = M_p P_{\text{pulse}}$  and define the signal to noise power ratio of a “conventional” PPM symbol  $\text{SNR}_{\text{cPPM}} = P_{\text{pulse}}/P_{\text{Noise}}$ . Eq. (4.1) then becomes

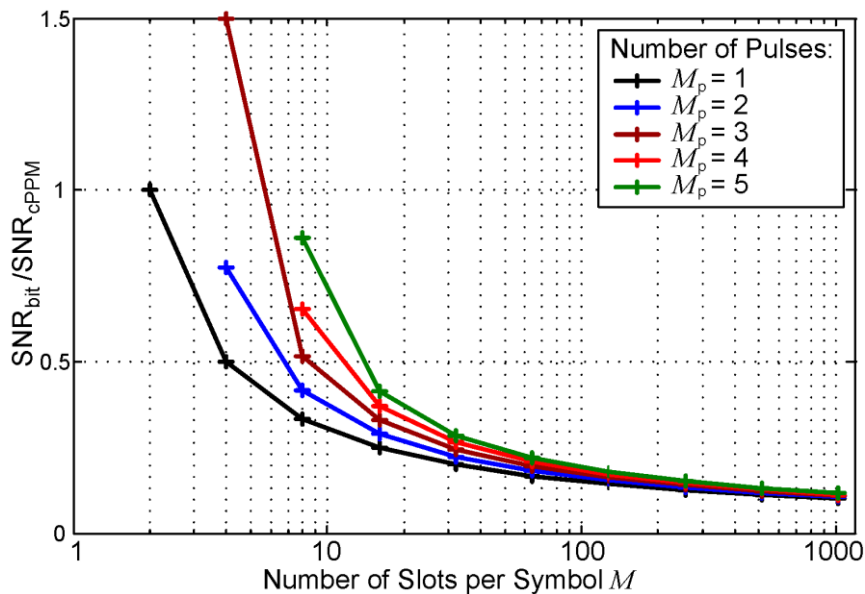


Fig. 4.2 Receiver sensitivities for 1-dimensional multipulse PPM for different values of  $M$  and  $M_p$ . The ratio of signal to noise ratio per bit over signal to noise ratio per symbol of “conventional” PPM is depicted as a function of number of slots per symbol  $M$  for different number of pulses  $M_p$  encoded in one symbol.

$$\text{SNR}_{\text{bit,1D-MP}} = \frac{P_{\text{sig}}}{P_{\text{Noise}} n_{\text{bits}}} = \frac{M_p}{\log_2 \binom{M}{M_p}} \frac{P_{\text{pulse}}}{P_{\text{Noise}}} = \frac{M_p}{\log_2 \binom{M}{M_p}} \text{SNR}_{\text{cPPM}}. \quad (4.2)$$

$M_p$  is the total number of pulses in one symbol. The time-domain representation of such a symbol with  $M=4$  and  $M_p=2$  is exemplarily shown in Fig. 4.1.

The result of Eq. (4.2) is plotted for  $M_p=1\dots 5$  in Fig. 4.2 for a normalized signal to noise power ratio per bit over signal to noise power ratio per “conventional” PPM. It can be seen that the ratio of signal power and bits per symbol decreases with the number of slots, but the minimum ratio is obtained for the one pulse per symbol encoding.

Thus it can be said that by inserting more pulses into one PPM symbol, the total number of bits encoded in one symbol is indeed increased, but since the overall signal power must be increased as well the required energy per bit does not decrease. Thus, if a very low  $\text{SNR}_{\text{bit}}$  is supposed to be achieved, the “conventional” PPM with one pulse per symbol should be favored.

However, inserting more pulses into one PPM symbol does not increase the sensitivity, but since it is possible to transmit more data per symbol, we are able to increase the spectral efficiency (SE). The spectral efficiency of the

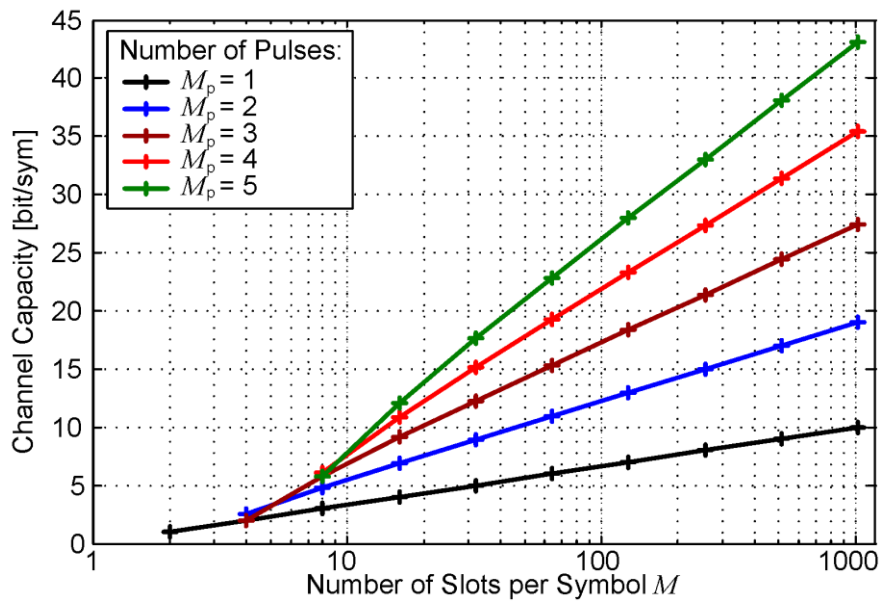


Fig. 4.3 Channel capacity as a function of number of slots per symbol  $M$  for different number of pulses  $M_p$  encoded in one symbol. It is assumed that in one time slot only one pulse can be found.

“conventional” PPM, in which only one pulse per symbol is sent, is defined as [62]:

$$\text{SE}_{\text{PPM}} = \frac{\log_2(M)}{B} = \log_2(M) T_{\text{slot}} \quad (4.3)$$

And indeed, by inserting more pulses into one symbol, the SE can be increased. As shown previously, for a given slot rate, more data can be encoded into one symbol, and thus, the channel capacity  $C_{\text{1D-MP}}$  of multi-pulse PPM increases to [62]:

$$C_{\text{1D-MP}} = \log_2 \left( \frac{M}{M_p} \right) \quad (4.4)$$

The result is depicted in Fig. 4.3. It is clearly visible that the higher  $M$  and  $M_p$ , the larger the channel capacity becomes.

#### 4.1.2 Two Dimensional Multi-Pulse PPM

Up to now, the additional pulses in one multi-pulse PPM symbol were positioned only within empty slots. One could also think of having  $M$  possible positions instead of  $M-1$  to insert additional pulses. In this case, it would be possible that two or more pulses are positioned in the same slot resulting in a pulse that may be  $M_p$  times higher than for “conventional” PPM. But then, the system would gain complexity, because not only the pulse position, but also the pulse height must be determined for proper symbol demodulation. In addition, the system does not increase its sensitivity, since the maximum noise power allowed in one slot to demodulate the symbol correctly does not change. Thus, the signal to noise power ratio per bit does not differ from Eq. (4.1)

$$\begin{aligned} \text{SNR}_{\text{bit,2D-MP}} &= \frac{P_{\text{sig}}}{P_{\text{Noise}} n_{\text{bits}}} \\ &= \frac{M_p}{\log_2(M^{M_p})} \frac{P_{\text{pulse}}}{P_{\text{Noise}}} \\ &= \frac{1}{\log_2(M)} \text{SNR}_{\text{cPPM}} \end{aligned} \quad (4.5)$$

The result of Eq.(4.5) thus equals the black line in Fig. 4.2, i.e. “conventional” PPM with one pulse per symbol.

Thus, this idea is not suitable to improve the receiver sensitivity. But how about the spectral efficiency? As just presented, the number of bit that can be encoded increases the more pulses are added to the symbol. By keeping the required bandwidth constant, the channel capacity increases with the number of pulses and thus becomes:

$$C_{2D-MP} = \log_2(M^{M_p}) = M_p \log_2(M) = M_p C_{PPM} \quad (4.6)$$

with  $C_{PPM}$  the channel capacity of “conventional” PPM.

Thus, it can be said that by means of receiver sensitivity improvement, the application of any version of multi-pulse PPM is not a good choice. However, if the spectral efficiency is of interest, multi-pulse PPM can show some improvement.

## 4.2 FSK versus 2ASK-OSDM

When thinking of modifying the alphabet of PPM or FSK modulation format, the following idea might come up: Let us assume 2PPM. In 2PPM either the first half or the second half of a symbol is filled with optical power. Let us assume that there are more combinations possible. In Fig. 4.4(a) the “conventional” 2PPM alphabet is depicted. The pulse is found either in the first or second half of the symbol. In (b) the new alphabet, called 2amplitude shift keying orthogonal slot-division multiplexing (2ASK-OSDM) is shown. It contains four symbols, where each slot can be filled with optical power, independent from the other slot. Its advantage lies in the ratio between average signal power and bits per symbol: Assuming the power of a pulse being  $P_{\text{pulse}}$ , the average symbol power of 2PPM equals the slot power, since only one slot per symbol is transmitted. However in case (b) the average signal power equals  $P_{\text{sig}} = P_{\text{pulse}}(1 + 1 + 2 + 0)/4 = P_{\text{pulse}}$ . But in

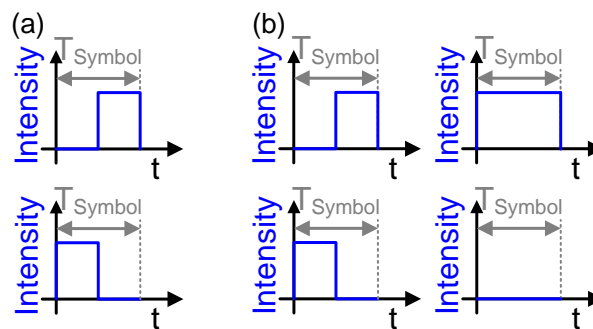


Fig. 4.4 “Conventional” PPM versus 2D-Multipulse PPM (a) “Conventional” 2PPM (Manchester coding) alphabet. There is the pulse either in the first or second half of the symbol. (b) New alphabet, called 2amplitude shift keying orthogonal slot-division multiplexing (2ASK-OSDM), with four symbols.

case (b) two bit per symbol are encoded, where in case (a) only one bit per symbol is encoded. Thus, in this case, the 2ASK-OSDM version should be favored over the 2PPM case.

More generally spoken, our symbol consists of  $M$  slots. Thus, there are  $2^M$  possible combinations that represent now our symbol alphabet. Thus, our alphabet can encode  $M$  bits per symbol. Assuming equiprobable symbols, the average signal power becomes  $P_{\text{sig}} = (M 2^{M-1}) / 2^M = M/2$ . Thus the ratio between signal power and bits per symbol is constant

$$\text{SNR}_{\text{bit}} = \frac{P_{\text{sig}}}{P_{\text{Noise}} n_{\text{bits}}} = \frac{M}{2} \frac{P_{\text{sig}}}{P_{\text{Noise}}} = \frac{1}{2} \frac{P_{\text{sig}}}{P_{\text{Noise}}} \quad (4.7)$$

This makes sense, since multiplexing without the usage of stacking modulation formats does not improve the sensitivity. However, in the binary case, the multiplexed version shows better performance than conventional PPM/FSK, since the higher bandwidth request of PPM/FSK is used in a more clever way. This result already becomes clear, when comparing 2PPM to OOK (without any multiplexing). Both modulation formats contain 1 bit per symbol, but 2PPM requires double the bandwidth than OOK to transmit the same amount of data. And since doubling the required bandwidth always comes along with doubling the noise power, the SNR must be decreased by 3 dB.

However, as soon as the number of frequencies or time-slots is increased beyond the number of 2, the sensitivity improvement is gone, see Fig. 1.1.

### 4.3 Conclusion

In this chapter, some ideas, how to further increase the receiver sensitivity of PPM and FSK have been introduced and discussed. However, it became obvious that for the increase of sensitivity, multi-pulse PPM is not a good choice. Orthogonal slot-division multiplexing only makes sense for  $M = 2$ , for higher  $M$  there is a disadvantage compared to conventional PPM.

## 5 Sensitivity Measurements of 64PPM-PS-QPSK

In this section, the receiver sensitivity of 64PPM-PS-QPSK is discussed, as already mentioned in Fig. 1.1. The following section has been published in Ref. [10]. It has been adapted for fit the layout and nomenclature of this work.

*[Begin of Paper C2]*

### Stacking PS-QPSK and 64PPM for Long-Range Free-Space Transmission

**A. Ludwig<sup>1</sup>, M. L. Schulz<sup>1</sup>, P. C. Schindler<sup>1</sup>, R. Schmogrow<sup>1</sup>, A. Mustafa<sup>1</sup>, B. Moos<sup>1</sup>, S. Brunsch<sup>1</sup>, T. Dippon<sup>2</sup>, D. Malsam<sup>2</sup>, D. Hillerkuss<sup>3</sup>, F. Roos<sup>1</sup>, W. Freude<sup>1</sup>, C. Koos<sup>1</sup>, J. Leuthold<sup>3</sup>**

*<sup>1</sup>Institute of Photonics and Quantum Electronics, Karlsruhe Institute of Technology (KIT), Karlsruhe, Germany*

*<sup>2</sup>Agilent Technologies, Boeblingen, Germany*

*<sup>3</sup>Now with Electromagnetic Fields and Microwave Electronics Laboratory, Swiss Federal Institute of Technology Zürich (ETH), Switzerland*

**Abstract:** In this paper a new sensitivity record for uncoded transmission with 2.6 photons per bit (4.15 dB) is presented. This is achieved using four dimensional (4-D) stacked orthogonal modulation formats i.e. PS-QPSK-64PPM.

### 5.1 Introduction

In optical free-space transmission systems losses are high and transmission links therefore need to operate at the sensitivity limit. An option to optimize free-space transmission links is in a proper choice of modulation formats [64].

Karlsson and Agrell showed in Ref. [12] that a four dimensional (4-D) modulation format such as polarization switched quadrature phase-shift keying (PS-QPSK) is the most power-efficient modulation format among all QAM signals. On the other hand, the sensitivity can be further enhanced by combining the scheme with pulse-position modulation (PPM). In the past PPM has mostly been used in direct detection schemes where it shows unbeaten sensitivity when used with a high number of slots [8]. Yet to achieve high sensitivity using PPM, high bandwidth is required from the hardware, or low data rates have to be taken into account. Thus stacking

QPSK and PPM modulation formats to achieve an even more sensitive system utilizing the same amount of bandwidth makes sense. And indeed, using 16-PPM in combination with DP-QPSK sensitivity of 3.5 photons per bit have been demonstrated at 2.5 Gbit/s [5].

In this paper we show that the sensitivity for uncoded transmission can be increased and demonstrate operation with as little as 2.6 photons per bit by means of the PS-QPSK-64PPM modulation format. A line-rate of 0.56 Gbit/s is demonstrated.

## 5.2 Measurement Principle

The transmitter to encode PS-QPSK-64PPM is shown in Fig. 5.1(a). The transmitter consists of an external cavity laser (ECL) providing 0 dBm output power signal with a 100 kHz linewidth at a wavelength of 1549 nm. Part of the signal is split off for the local oscillator. A dual polarization IQ-modulator is used for coding the information. It is fed by an Arbitrary Waveform Generator (AWG) M8190A from Agilent Technologies with four individually programmable output ports with a 3dB bandwidth of 3.7 GHz. Each output can deliver 12 GSamples/s with a voltage of  $0.7 V_{p-p}$ .

A pseudo-random bit sequence (PRBS) of length of  $2^{15}-1$  has been generated in Matlab and the data have been grouped in blocks of 9 bits. The first 3 bits are mapped to the PS-QPSK and the last 6 bits are encoded onto the 64-PPM symbol. The three bits of the PS-QPSK symbol are mapped onto the four driving signals using a logical XOR operations as suggested in Ref. [3]. The slots of the PPM-symbols have been coded using Gray mapping rules. The PS-QPSK symbols have been stacked onto the PPM symbols which led to the four driving signals with three levels. To find the beginning of the first PPM symbol properly, one BPSK modulated Barker 13 sequence is used as a preamble followed by 51 zeros to fill up one symbol. Each symbol has been sampled 3 times per slot (sps). The 12 GSamples/s thus were used for oversampling and result in a slot rate of 4.0 GHz. With this scheme we generated a symbol rate of 62.5 Mbaud with 9 bit/symbol thus leading to a line-rate of 562.5Mbit/s.

The free-space channel is mimicked by a variable optical attenuator followed by an optical splitter that allows measuring the optical input power into the preamplified receiver. In our simplified channel any other distortions except for optical losses such as scintillation and turbulence have been neglected. The input power of the receiver is measured by means of a

calibrated photodiode at the monitoring port so that the number of photons per bit could be deduced after subtracting the imbalance of the optical coupler and connector losses.

The receiver consists of two erbium doped fiber amplifiers (EDFAs) with optical bandpass filters of a 0.6 nm bandwidth. The first EDFA has a noise figure of 3.1 dB at  $\lambda = 1549\text{nm}$  and provides 35 dB gain. The signal is fed into a dual polarization coherent receiver (DP-coh. Rx) consisting of a dual polarization  $90^\circ$  hybrid followed by four balanced detectors. Two synchronized real-time oscilloscopes with sampling rates of 80 GSamples/s and bandwidths of 32GHz store the signals for offline processing.

The offline processing is performed in Matlab. First, the output signals  $R_x = I_x + jQ_x$  and  $R_y = I_y + jQ_y$  are low-pass filtered with a 3dB bandwidth equal to 60% of the slot rate to reject amplifier noise and thus improve the signal-to-noise ratio (SNR). Then the position of the preamble

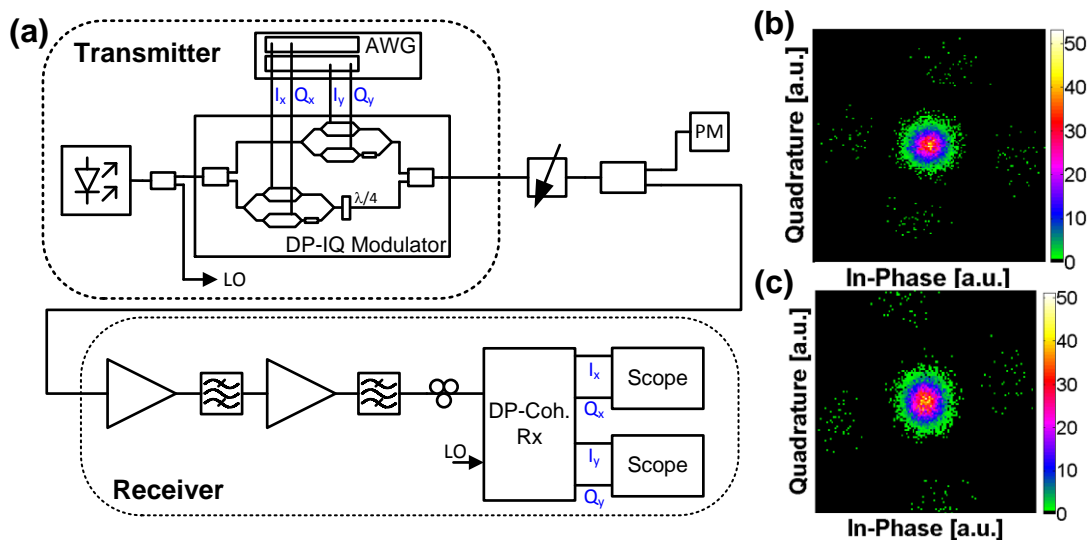


Fig. 5.1(a) Setup scheme with transmitter and preamplified coherent receiver to mimic a free space communication system. The transmitter consists of an external cavity laser (ECL) providing 0 dBm output power at 1549 nm. The laser provides both the cw signal to be encoded with information as well as the local oscillator for reception. The signal is modulated by a dual-polarization IQ-modulator driven by an Arbitrary Waveform Generator (AWG) with four output ports and 12 GHz sampling rate. The effect of the free-space optical channel is reduced to a variable optical attenuator followed by an optical splitter that allows monitoring the optical input power into the preamplified receiver that is used to receive the signal. The signal is detected by a dual polarization  $90^\circ$  hybrid followed by four balanced detectors. Two synchronized real-time oscilloscopes with a sampling rate of 80 GSamples/s store the signals for later offline processing. (b,c) the IQ diagram with color-coded histogram of the first 10000 PS-QPSK-64PPM encoded slots are depicted for x and y polarization. The plots have been taken for a receiver input power of 8.7 photons per bit.

is determined by applying cross correlation with the Barker 13 sequence. Subsequently, down sampling is performed to obtain 64 samples per symbol, i.e. 1 sample per slot. Afterwards, the slot with the highest energy is identified and the PPM symbol is decoded by means of a look-up table. Further, the samples corresponding to the in-phase and quadrature information of both polarizations of the respective peak pulse are stored for later PS-QPSK demodulation. Prior to the demodulation a phase correction is performed using a Kalman filter based estimation algorithm [65]. In the following, the demodulated logical data is compared with the original data for determination of the BER. This procedure is performed for each frame separately. One frame has the length of 32760 bit.

In Fig. 5.1(b) and (c) the IQ diagram with color-coded histograms of the first 10000 PS-QPSK-64PPM encoded symbol slots are depicted for the  $x$ - and  $y$ -polarizations respectively. It can be clearly seen that the center point, i.e. the empty PPM slots, happen more often than the four outer points representing the PS-QPSK signal.

For verification of the experimental results, the setup in Fig. 5.1(a) has been simulated with the help of OptSim and parameters of the equipment in the simulation have been taken from the experiment. The result of which is shown in Fig. 5.2.

### 5.3 Analytical Analysis of Sensitivity

To further judge the quality of the measurement we compared the experiment with analytical calculations as suggested in [11]. Following this reference one can deduce for our case of a PPM sequence with a stacked PS-QPSK signal the following bit-error ratio (BER):

$$\text{BER}_{\text{PPM,PSQ}} = \frac{\text{SER}_{\text{PPM}} \left( \frac{M}{2(M-1)} \cdot \log_2(M) + \frac{n_{\text{PSQ}}}{2} \right)}{\log_2(M) + n_{\text{PSQ}}} + (1 - \text{SER}_{\text{PPM}}) \frac{\text{BER}_{\text{PSQ}} \times n_{\text{PSQ}}}{\log_2(M) + n_{\text{PSQ}}} \quad (5.1)$$

$n_{\text{PSQ}}$  is the number of bits per symbol encoded in PS-QPSK, it equals 3 and  $\log_2(M)$  is the number of bits per symbol encoded in PPM; which is 6 for our modulation format. The first term of the numerator of the equation describes the case that there is a PPM-symbol detected wrongly with the probability  $\text{SER}_{\text{MPPM}}$ . If the PPM-symbol is detected wrongly, this leads

automatically to a certain number of false bits that were encoded in the PPM-symbol. There are  $M - 1$  possible symbols that can be wrong out of all  $M$  symbols and in the average half of all bits encoded in the PPM-symbol may be wrong. If a PPM symbols is wrongly detected this leads to errors in the PS-QPSK symbol as well and all bits in the PS-QPSK signal will be misjudged with a 50% error probability. The second term in the enumerator describes the case, when the PPM-symbol is detected correctly, but there happen to be bit errors in the PS-QPSK symbol. Both terms are normalized by the total number of bits in a PS-QPSK- $M$ -PPM symbol. The symbol error ratio for PPM  $SE_{MPPM}$  can be analytically obtained following Ref [19] and [40]. The  $BER_{PSQ}$  can be found in [3]. Thus, the BER of PS-QPSK-PPM can be derived analytically. The results are shown in Fig. 5.2.

## 5.4 Results

In Fig. 5.2 the results are depicted as BER vs. photons per bit in dB for measured, simulated and theoretical, i.e. analytical results. We find 2.6 photons per bit (PPB) for a  $BER = 10^{-3}$  that correspond to 4.1 dB. It can be seen that the OptSim simulation matches nicely with the measured curve. The difference between analytical results and measurements of 0.75 dB can be explained by the non-ideal noise figure of the preamplifying EDFA and a non-perfect equalization of the phase of the signal. The power of the preamble is negligible since it represents only 0.36 % of the total power.

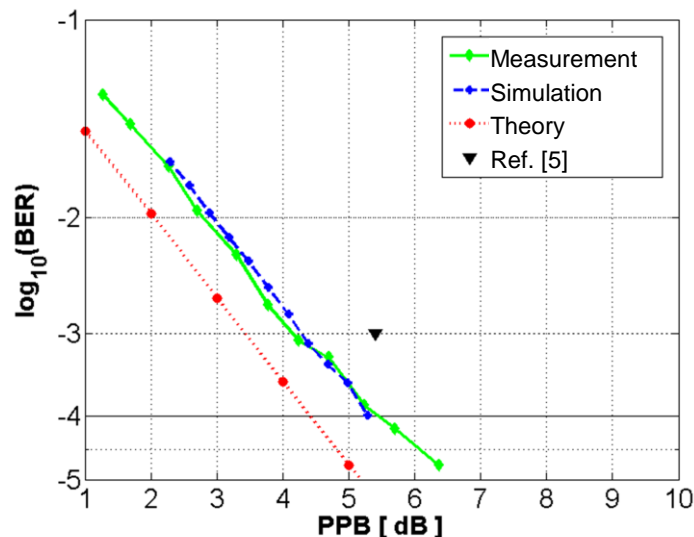


Fig. 5.2 Here the results are shown: BER vs. Photons per Bit in dB for measured, simulated and analytical results. It can be seen that the simulations match very well with the measurement, and there is a slight offset of 0.75 dB to the analytical theory. This offset can be explained by non-ideal noise figure of the preamplifying EDFA and the non-ideal equalization of phase noise.

The total number of evaluated bits for the measurement is  $\sim 229000$ , for the simulation in the same order of magnitude.

## 5.5 Conclusion

We have experimentally demonstrated a receiver sensitivity of 2.6 PPB (4.1 dB) by using stacked 4D modulation format with orthogonal modulation schemes, i.e. PS-QPSK with 64-PPM. This result is only 0.75 dB off the theoretical possible limit. The offset can be explained by the non-ideal preamplifying EDFA and non-perfect equalization of the signal, the preamble used for synchronization can be neglected.

This power-efficient modulation format could be attractive in applications where photon efficiency is of critical importance, such as in space communications.

*[End of Paper C2]*

## 6 Sensitivity Measurements of 64PPM-4FSK-PS-QPSK

In the previous chapter, the high receiver sensitivity of 64PPM-PS-QPSK has been presented and discussed. However, as already mentioned in theory in Chapter 1 and 3, it is possible to increase the sensitivity even further by adding frequency-shift keying (FSK) to the modulation stack. The results of 64PPM-4FSK-PS-QPSK will be discussed in the following more closely. In addition also making multiplexing part of the modulation stack may have some implementation advantages, like 64PPM-2ODFM-PS-QPSK. This hypothesis is investigated more closely in the following.

The following sections are published in [14]. It has been adapted for fit the layout and nomenclature of this work.

*[Begin of Paper J5]*

### **Stacked modulation formats enabling highest-sensitivity optical free-space links**

**Alexandra Ludwig<sup>1,6</sup>, Marc-Lorenzo Schulz<sup>2</sup>, Philipp Schindler<sup>3</sup>, Stefan Wolf<sup>4</sup>, Christian Koos<sup>4</sup>, Wolfgang Freude<sup>4,7</sup> and Juerg Leuthold<sup>5,8</sup>**

<sup>1</sup> *Now with: Rosenberger Hochfrequenztechnik GmbH & Co. KG, 84526 Fridolfing, Germany,*

<sup>2</sup> *Now with: Keysight Technologies, 71034 Böblingen, Germany,*

<sup>3</sup> *Now with: Infinera Corporation, Sunnyvale, USA*

<sup>4</sup> *Karlsruhe Institute of Technology (KIT), Institute IPQ, 76131 Karlsruhe, Germany,*

<sup>5</sup> *ETH Zurich, Institute of Electromagnetic Fields (IEF), 8092 Zurich, Switzerland*

<sup>6</sup>[Alexandra.Ludwig@rosenberger.de](mailto:Alexandra.Ludwig@rosenberger.de)

<sup>7</sup>[W.Freude@kit.edu](mailto:W.Freude@kit.edu)

<sup>8</sup>[JuergLeuthold@ethz.ch](mailto:JuergLeuthold@ethz.ch)

**Abstract:** A new modulation scheme with a sensitivity of 2.3 photons per bit at a bit-error ratio (BER) of  $10^{-3}$  is discussed theoretically and demonstrated experimentally. We achieve a limiting sensitivity of 2.3 photons per bit (3.7 dB photons per bit) by stacking the modulation formats 64PPM, 4FSK and polarization-switched (PS) QPSK. This modulation stack encodes 11 bit per symbol (PPM: 6 bit, FSK: 2 bit, PS-QPSK: 3 bit). We also replaced 4FSK by 2ODFM (2-channel multiplex) for comparison. With

64PPM-2OFDM-PS-QPSK a total of 12 bit are encoded (PPM: 6 bit, 2 OFDM channels with PS-QPSK:  $2 \times 3$  bit). Both modulation stacks show a similar limiting sensitivity and are probably the highest sensitivities so far reported for a BER of  $10^{-3}$ . Our theoretical considerations are supported by simulations and experiments.

©2015 Optical Society of America

(060.1660) Coherent communications; (060.2605) Free-space optical communication; (060.4080) Modulation.

## 6.1 Introduction

Optical free-space transmission systems for long-range applications like optical satellite communication systems need to cope with tremendous losses, because in-line amplification is not possible [4]. Therefore, any receiver has to operate reliably even with a very small number of received photons per bit. For improving the received signal power one could increase the numerical aperture of the transmitter or receiver optics, however, the achievable gain is limited by geometrical size and by pointing accuracy. So for instance, for an inter-satellite link of two geostationary (GEO) satellites a link loss of 55 dB has to be accepted [66]. Such demanding requirements call for a modulation format that offers the highest possible sensitivity.

Whenever high sensitivity is of primary interest while spectral efficiency takes a secondary rank only, pulse-position modulation (PPM) is the best choice [8]. In the past, PPM has mostly been used in direct detection receivers where the format proved to result in unbeaten sensitivity if a large number  $M$  of time slots was employed [4, 16, 17, 56, 67]. For a given data rate, however, an  $M$ -fold bandwidth is required as compared to simple on-off keying (OOK) with the same data rate. Thus, to increase the data rate over that of PPM alone, 16PPM in combination with polarization-multiplexed (PM) quadrature phase shift keying (PM-QPSK) has been used [17], and a limiting sensitivity of 3.5 photons per bit (PPB) at a bit error ratio (BER) of  $10^{-3}$  was demonstrated [11]. This sensitivity can be further enhanced by replacing the PM-QPSK format with polarization-switched QPSK (PS-QPSK) [17], which recently intruded as the most power-efficient modulation format among the common PSK signaling types [3, 12]. And indeed, stacking 64PPM and PS-QPSK results in 2.6 PPB at a BER of  $10^{-3}$  [10].

While all these experiments show remarkable sensitivities, there is still room for improvement by exploiting another degree of freedom, namely frequency-shift keying (FSK) [68]. So far, FSK is rarely found in optical

transmission. This is due to the fact that, similar to PPM, a high number of frequencies and a large receiver bandwidth is required for achieving a better sensitivity. Using FSK, a sensitivity of 3.5 PPB at a BER of  $10^{-3}$  has recently been shown with a single-polarization using 256 frequencies and coherent detection [39].

The sensitivity of all aforementioned schemes can be further improved with the help of strong error detection and correction (FEC) [64], for instance by employing turbo coding. As an example, it has been shown that a sensitivity of 2.1 PPB is possible for BPSK with a 100 % overhead that allows to correct a signal with a BER of  $10^{-1}$  [51].

In this paper we report on improving the sensitivity to 2.3 PPB (3.7 dB) for a raw BER of  $10^{-3}$  by stacking 64PPM with 4FSK and PS-QPSK. A pre-FEC of  $4.45 \times 10^{-3}$  allows the use of a standard FEC with only 7 % overhead for a final BER of  $10^{-15}$  [43]. These are to best of our knowledge the highest sensitivities so far reported for a BER of  $10^{-3}$ .

## 6.2 Stacking Modulation Formats

For a transmission system where a high receiver sensitivity is to be combined with a reasonably large data rate, a modulation format must be chosen where for a given maximum average transmitter power the symbols have a large Euclidean distance while the number of encoded bits per symbol is still acceptably good.

In [3, 12] Karlsson and Agrell have already shown that PS-QPSK is the modulation format with the largest possible Euclidean distance between symbols. PS-QPSK encodes 3 bits per symbol by stacking binary polarization-shift keying with QPSK [2, 11].

The number of encoded bits per symbol can be increased by exploiting other degrees of freedom in the transmitted optical field strength. The previous discussion tacitly assumed that the PS-QPSK symbols occupy consecutive time intervals, the width of which determines the symbol duration (the symbol period). However, if each symbol period is subdivided in  $M$  time slots, and the PS-QPSK symbol is assigned to 1 out of these  $M$  possible time slots, we form a modulation stack of pulse position modulation (PPM) and PS-QPSK. The information content of this new symbol increases by  $\log_2 M$ . Assuming the same symbol duration and the same average power as before, the peak power in the occupied time slot and the required bandwidth increase by  $M$ . The high peak power together with the increased information content per symbol allows to reduce the required number of

photons per bit at the receiver and thus to increase the sensitivity. The spectral efficiency is decreased though. Yet, if it is sensitivity that is most important, this could be worth the price [10]. In addition, the modulation stack can be extended by  $N$ -ary FSK. This increases the information content of the symbol by another factor  $\log_2 N$  and reduces the required number of photons per bit even more – at the price of another reduction of spectral efficiency.

In the quest for the ultimate sensitivity one should also weigh in the options provided by multiplexing techniques. Multiplexing typically comes at the price of increased transmitter power. As an example: In the transition from PS-QPSK to polarization multiplexed (PM) QPSK one wins 1 bit of information per symbol at the price of doubling the average signal power [3, 12]. Another option for multiplexing is applying wavelength division multiplexing (WDM) [8] or orthogonal frequency division multiplexing (OFDM) [20]. While an increase of the OFDM subcarrier number  $N$  increases the spectral efficiency, the SNR per bit remains the same: Compared to one channel, two channels need double the power and transmit double the number of bits. However, channel crosstalk, quantization errors and nonlinearities might further decrease the overall sensitivity of the system. Since our goal is to reach an ultimately low number of received photons per bit, multiplexing as such is not the proper strategy. However, if multiplexing is part of a stacked modulation format, then stacking PM-QPSK and PPM might be a good compromise between increasing the number of bits per symbol and optimizing the Euclidean distance [11].

In view of the prior art as discussed in this section, we conclude that stacking the proper modulation formats reduces the required number of received photons per bit considerably. In this respect a PPM-FSK-PS-QPSK format appears to be the optimum modulation stack regarding modulation complexity and sensitivity. However, a combined modulation/multiplexing stack like PPM-OFDM-PS-QPSK with more bits per symbol but a larger limiting number of received photons per bit seems to be an interesting candidate as well. In the following we verify this statement by showing results of an implementation of a 64PPM-4FSK-PS-QPSK modulation stack with a sensitivity of 2.3 PBB compared to a 64PPM-2OFDM-PS-QPSK modulation/multiplexing stack with 2.4 PBB.

## 6.3 Operation Principle and Measurement Setup

In this section, we explain the experimental setup. We further describe waveform generation and signal demodulation as used in the experiments and for the simulations.

### 6.3.1 Measurement Setup

The measurement setup is depicted in Fig. 6.1. At the transmitter a fiber laser with a linewidth  $< 1$  kHz provides 13 dBm output power at a wavelength of 1549.5 nm ( $f_c = 193.5$  THz). Half of the power is split off and serves as a local oscillator (LO) for coherent reception. A dual-polarization (DP) IQ-modulator encodes the information on the optical carrier. An arbitrary waveform generator (AWG) is programmed to provide four synchronized offline-generated data streams. Each AWG output operates at 12 GSa/s with a voltage-swing of  $0.7 V_{pp}$  and a 3 dB bandwidth of about 3 GHz.

The free-space channel is emulated by a variable optical attenuator (VOA). In our simplified channel model, distortions such as scintillations and turbulences are neglected, and thus our channel represents an inter-satellite link in space, where only path loss due to the divergent beam plays a significant role [69]. In [66] the typical loss for an inter-satellite link between two geostationary satellites is calculated. The authors show that the link loss for bridging a distance of 45.000 km amounts to 55 dB when using two antennas with an aperture of 30 cm (using 850 nm wavelength). Yet, to overcome larger distances such as envisioned in the Mars exploration projects, much larger link loss budgets are involved. With our modulation stack we could provide a link budget of 100 dB. This would be obtained when transmitting a signal with an average power of 26 dBm, and by receiving with a sensitivity of  $-74$  dBm. Under these conditions, our limiting sensitivity of 2.3 received photons per bit would allow to detect a 128 Mbit/s data stream.

Our receiver consists of two cascaded erbium-doped fiber amplifiers (EDFAs) with a 0.6 nm wide optical band-pass filter in-between. The first EDFA has a noise figure of 3.1 dB at 1549 nm and provides 35 dB gain. The second EDFA provides a constant output power. A manually operated polarization controller adjusts the signal such that the field strengths per symbol in both orthogonal  $x$  and  $y$ -directions (as defined by the receiver) are equal. The signal is fed into a polarization diverse coherent receiver (Pol.-Diverse Coh. Rx) consisting of a dual-polarization  $90^\circ$  hybrid and four

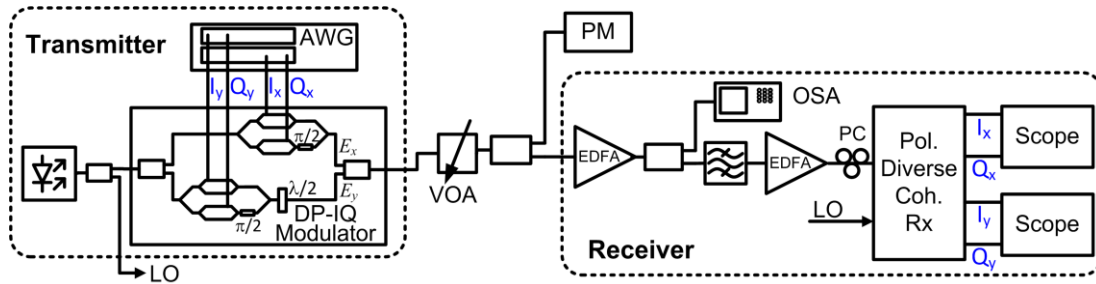


Fig. 6.1 Setup with transmitter and pre-amplified coherent receiver. The signal is modulated by a dual-polarization (DP) IQ-modulator driven by an arbitrary waveform generator (AWG). The free-space optical channel is emulated by a variable optical attenuator (VOA), followed by a coupler that taps the optical input and monitors the power entering the pre-amplified receiver with a power meter (PM). An optical spectrum analyzer (OSA) is used to monitor the OSNR and the polarization controlled (PC) signal is detected by a coherent polarization-diversity receiver. Two real-time oscilloscopes store the signals for offline processing. The laser acts both as a continuous-wave source for the transmitter and as a local oscillator (LO)

balanced detectors. Two synchronized real-time oscilloscopes with sampling rates of 80 GSa/s and analog bandwidths of 32 GHz record the signals for offline processing.

The average number of photons per bit at the receiver is deduced from a calibrated power meter (PM) connected to a 50 % tap coupler right in front of the receiver.

Alternatively, the optical signal-to-noise power ratio (OSNR) is measured using a high-resolution optical spectrum analyzer (OSA) that is connected to a 10 % tap coupler after the first optical pre-amplifier. Average power and OSNR measurement lead to comparable results for the received number of photons per bit as will be discussed in section 6.7.

### 6.3.2 Signal Generation

The waveforms with the 64PPM-4FSK-PS-QPSK symbols are generated using a Matlab program. The computed waveforms are stored in the AWG memory. The data are organized in a very long frame consisting of 2047 symbols. Each symbol comprises of 64 PPM slots with a slot width  $T_{\text{slot}}=1.33$  ns (slot rate  $R_{\text{slot}} = 1 / T_{\text{slot}} = 750$  MHz). Each PPM symbol is sampled  $64 \times 16$  times. A preamble is added for PPM frame synchronization. This preamble occupies one PPM symbol and consists of a single BPSK-modulated Barker13 sequence [70]. The stored data frame is then repeated periodically to yield an uninterrupted data stream.

The 64PPM-4FSK-PS-QPSK format encodes 11 bits in one symbol. The 11 bits/symbol are derived from 11 independent pseudo-random bit sequences (PRBS), six of which are encoded in the PPM, two are encoded as FSK, and three are assigned to encode PS-QPSK.

First, the 64PPM symbols are generated. Gray coding maps 6 bit to one PPM symbol. In Fig. 6.2(a) the PPM symbols are displayed in the time-domain (top row), in a complex IQ constellation plane (middle row), and in the frequency domain (bottom row). A PPM symbol comprises of one pulse and many empty PPM slots.

Fig. 6.2(b) depicts 4FSK with an orthogonal frequency spacing corresponding to the PPM slot rate  $R_{\text{slot}} = 750 \text{ MHz}$   $f_{\pm 1} - f_c = \pm R_{\text{slot}}$ ,  $f_{\pm 2} - f_c = \pm 2 \times R_{\text{slot}}$ . These four tones are created by single-sideband modulation (SSB) [19].

The PS-QPSK symbols are generated by encoding 3 bits onto the 4 input signal streams  $I_{x,y}$  and  $Q_{x,y}$  of a dual-polarization IQ-modulator by adding an even-parity bit, i. e., the fourth bit is assigned a “0” if the sum of the three bits is even, and it is assigned a “1” if the sum is odd [3]. As a result we obtain 8 optical symbols as a subset of 16 possible optical states of a regular PM-QPSK. The 8 symbols of the subset are linearly polarized at an angle of  $\pm 45^\circ$  with respect to the  $x$ -polarization as defined by the receiver, and are chosen for a maximum Euclidean distance. Although the information content has decreased by one bit when going from PM-QPSK to PS-QPSK,

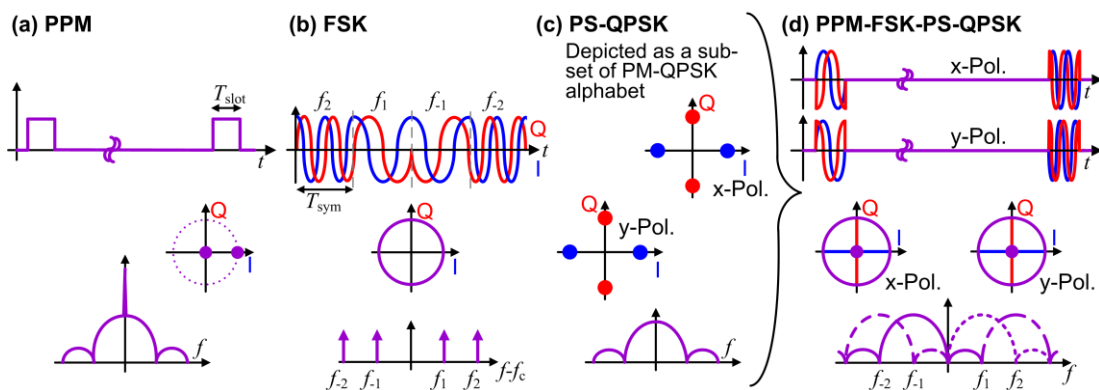


Fig. 6.2 Schematic display of stacking PPM with FSK and PS-QPSK symbols represented in time domain (top row), in constellation space (middle row), and in frequency domain (bottom row). The columns show typical (a) PPM, (b) FSK and (c) PS-QPSK symbols. The PS-QPSK symbols are depicted as a subset of the PM-QPSK symbols. The right-most column (d) displays the PPM-FSK-PS-QPSK stack. Each PPM pulse comprises optical sine and cosine-shaped optical fields that contain the information on the frequencies, phases and polarization.

the required number of received photons per bit has decreased, since the increase of the Euclidean distance over-compensates the loss of information content. The PS-QPSK symbols are depicted in Fig. 6.2(c) in the complex plane for  $x$ -polarization and  $y$ -polarization, respectively. The two QPSK constellation diagrams depicted in Fig. 6.2(c) look like PM-QPSK constellations. However, the polarization switching becomes obvious, if a polarization beam splitter is inserted into the signal path with its polarization eigenstates rotated by  $45^\circ$  with respect to the  $x$ -polarization. At the bottom of Fig. 6.2(c) a typical NRZ spectrum for PS-QPSK is shown.

In the following, the generation of the stack is described in more detail: First, four FSK tones at  $f_{\pm 1} - f_c = \pm 750 \text{ MHz}$  and  $f_{\pm 2} - f_c = \pm 2 \times 750 \text{ MHz}$  are generated by single-sideband modulation [19]. Each tone is separated from its neighbor by an integer multiple of the PPM slot rate  $R_{\text{slot}} = 1 / T_{\text{slot}} = 750 \text{ MHz} = (12 / 16) \text{ GHz}$ , see Fig. 6.2(b), which corresponds to the OFDM orthogonality condition between slot duration  $T_{\text{slot}}$  and subcarrier frequency spacing. The choice of  $R_{\text{slot}}$  results from an AWG sampling rate of 12 GSa/s and 16-fold oversampling per PPM slot. We encode 2 bit on each FSK symbol and transmit one out of four possible orthogonal frequencies. The PS-QPSK symbols are encoded by appropriately modulating the phase of the  $I_{x,y}$  and  $Q_{x,y}$  signals which define the FSK symbol.

The FSK-PS-QPSK symbols to be generated are interpreted as spectral Fourier coefficients. For 4FSK-PS-QPSK, there is one non-zero complex input coefficient per symbol and per polarization. To find the associated time-discrete  $I_{x,y}$  and  $Q_{x,y}$  drive signals in Fig. 6.1 we perform a 16-point inverse fast Fourier transform (IFFT) per symbol and per polarization. The real parts of each IFFT output represent the time-discrete version of the cosine-shaped  $I_{x,y}$  drive signals, and the imaginary parts define the sine-shaped  $Q_{x,y}$  drive signals. The FSK-PS-QPSK information is encoded as a phasor that rotates with a certain speed and direction with respect to a given starting point.

Besides the advantage that only one laser is required for 4FSK, our technique provides orthogonal signals as in the case of OFDM as we had mentioned before. This similarity can be exploited by transmitting more than one FSK frequency in the same PPM time slot. With two simultaneously transmitted frequencies, we combine modulation stacking and multiplexing. The limiting sensitivity achieved with this 2OFDM-PS-

QPSK modulation/multiplexing stack will be later on compared with the results for a 4FSK-PS-QPSK modulation stack.

Finally, the 4FSK-PS-QPSK signals have to fill the proper non-zero PPM slots of Fig. 6.2(a) for completing the 64PPM-4FSK-PS-QPSK stack, see Fig. 6.2(d). The many empty PPM slots dominate the time-domain representation of the symbol. Each PPM pulse contains a frequency and a phase/polarization information. As shown in Fig. 6.2, the PPM pulse is described by the sine and cosine-shaped temporal signals with different frequencies and phases. The completed procedure explained above generates 4 time-discrete signals  $I_x$ ,  $Q_x$ ,  $I_y$  and  $Q_y$  that are stored in the AWG for driving the DP-QPSK modulator.

If 64PPM-2OFDM-PS-QPSK is generated, a similar procedure is applied. We use  $f_1$  and  $f_2$  as orthogonal subcarrier frequencies, which both are modulated with independent PS-QPSK information. We now have two non-zero complex coefficients per OFDM-PS-QPSK symbol and per polarization. As with FSK-PS-QPSK, we apply a 16-point IFFT for each PPM time slot and each polarization for generating the non-zero  $I_x$ ,  $Q_x$ ,  $I_y$  and  $Q_y$  drive signals for the proper PPM time slot.

### 6.3.3 Signal Demodulation

The demodulation of the received 64PPM-4FSK-PS-QPSK signal is discussed next, followed by the corresponding process for 64PPM-2OFDM-PS-QPSK.

The first steps in the demodulation process are resampling of the signal to generate a waveform with 128 samples per slot, and synchronization of the data by using the Barker13 preamble to detect the starting point of each frame. Resampling and synchronization has to be done for both polarizations, which are available at the outputs of the dual polarization 90° hybrid in Fig. 6.1. Each polarization carries the same PPM and FSK information.

After synchronization, we compute a 128-point fast Fourier transform (FFT) for each slot and each polarization, and evaluate the moduli of the complex output coefficients. Because the demodulation differs in part for 64PPM-4FSK-PS-QPSK and 64PPM-2OFDM-PS-QPSK formats, we describe both cases separately.

**64PPM-4FSK-PS-QPSK:** To extract the PPM and FSK information, the moduli of the complex output coefficients for  $x$  and  $y$ -polarization are added for each of the 64 slots. Since the 4 frequencies of the FSK tones are known,

we only look for the presence of any of the 4 frequencies. The position of the maximum element within the resulting  $4 \times 64$  matrix determines the location of the PPM pulse with the associated FSK information.

Next, the PS-QPSK information has to be extracted from the complex output coefficient from the FFT associated with the proper PPM slot and FSK frequency. For this, the symbols are demodulated using maximum likelihood estimation. Prior to a successful PS-QPSK demodulation we need a precise polarization alignment and phase estimation. For this a nonlinear Kalman-filter estimation algorithm [6] has been implemented. This is necessary since the manually adjusted polarization controller in front of the coherent frontend is not stable enough. For mapping the PS-QPSK data to the correct quadrant of the constellation diagrams in Fig. 6.2(c), the Kalman filter algorithm is modified to operate with a training sequence. To do so, an additional training sequence has been added after the synchronization preamble. This sequence consists of 25 PPM-FSK-PS-QPSK symbols with known pulse positions, frequencies, phases and polarizations has been added. The Kalman-filter algorithm then optimizes phase and polarization alignment for each FSK frequency separately.

For a successful demodulation one should also make sure that the  $I$  and  $Q$  arms of the nested MZM in Fig. 6.1 are out of phase by  $90^\circ$ . Any phase deviation (quadrature error) leads to an elliptical IQ-plot in Fig. 6.2. Such a quadrature error can be corrected fairly easily in the receiver by numerically correcting phase shifts on  $I$  or  $Q$  such that the SSB signal is restored and does not have a spurious frequency component at the opposite frequency.

The received and decoded data (not including the training sequence) are compared with the transmitted data for counting the errors of the PPM, FSK and PS-QPSK reception.

**64PPM-2OFDM-PS-QPSK:** For this case the demodulation process is very similar to the case described above. However, the FSK demodulation step is omitted since the two OFDM carriers  $f_1$  and  $f_2$  in Fig. 6.2 are always switched on. For PPM-OFDM demodulation, the  $4 \times 64$  matrix for the PPM-FSK demodulation now reduces to a vector of length 64, which contains in each of its elements the sum of the moduli of the two complex FFT values at the OFDM carrier frequencies in two polarizations, i. e., the sum of four moduli. The PPM symbol is detected by finding the maximum value in this vector. The demodulation procedure of the PS-QPSK symbols remains the same as described above. The received payload data are compared with the

transmitted data for counting the errors of the PPM sequence and the two multiplexed PS-QPSK signals.

## 6.4 Theoretical Sensitivity Analysis of Stacked Modulation Formats

Before reporting on the experiments we derive theoretical expressions for the sensitivity of the stacked modulation formats PPM-FSK-PS-QPSK and PPM-OFDM-PS-QPSK. Details on the theoretical receiver sensitivities for the individual modulation formats PPM, FSK and PS-QPSK are given in section 6.8.

For stacking PPM, FSK and PS-QPSK we apply and extend the approach in Ref. [11]. For PPM-FSK-PS-QPSK we distinguish three cases:

1. The *M*-ary PPM symbol was detected wrongly with a symbol error probability  $SER_{PPM}$  and an associated bit error probability  $BER_{PPM} = SER_{PPM} M / (2(M-1))$  according to Eq. (6.16). In this case the detected *N*-ary FSK and PS-QPSK information is random so that on average half of their bits are wrong, i. e., the average number of erroneous bits is  $\frac{1}{2} \log_2(N)$  and  $\frac{1}{2} \times 3$ , respectively.
2. The PPM symbol was correctly detected with a probability equal to  $1 - SER_{PPM}$ , but the *N*-ary FSK symbol was detected wrongly with a symbol error probability  $SER_{FSK}$  and an associated bit error probability  $BER_{FSK} = SER_{FSK} N / (2(N-1))$  according to Eq. (6.16) with (6.19) and (6.20). In this case the detected PS-QPSK bits are random so on average half of them are wrong leading to an average number of  $\frac{1}{2} \times 3$  erroneous bits.
3. The PPM and the FSK symbols were correctly detected with a probability  $(1 - SER_{PPM})(1 - SER_{FSK})$ , but the PS-QPSK symbol (PSQ for short) was detected wrongly with a bit error probability  $BER_{PSQ}$  according to Eq. (6.21).

Because not all these cases contribute the same amount of erroneous bits, the respective bit error probabilities have to be calculated by relating the number of erroneous bits to the total number  $\log_2(M)|_{PPM} + \log_2(N)|_{FSK} + 3|_{PS-QPSK}$  of bits which are transmitted by the stacked *M*-PPM-*N*-FSK-PS-QPSK modulation format. As a result we find

$$\begin{aligned}
\text{BER}_{\text{total}}^{(\text{FSK})} = & \frac{\text{SER}_{\text{PPM}} \left( \frac{M}{2(M-1)} \log_2(M) + \frac{1}{2} \log_2(N) + \frac{1}{2} \times 3 \right)}{\log_2(M) + \log_2(N) + 3} \\
& + (1 - \text{SER}_{\text{PPM}}) \frac{\text{SER}_{\text{FSK}} \left( \frac{N}{2(N-1)} \log_2(N) + \frac{1}{2} \times 3 \right)}{\log_2(M) + \log_2(N) + 3} \\
& + (1 - \text{SER}_{\text{PPM}})(1 - \text{SER}_{\text{FSK}}) \frac{\text{BER}_{\text{PSQ}} \times 3}{\log_2(M) + \log_2(N) + 3}.
\end{aligned} \tag{6.1}$$

If less than 3 modulation formats are stacked, the number of transmitted bits has to be adjusted properly: Without PPM, we have  $\text{SER}_{\text{PPM}} = 0$  and  $M = 0$ , without FSK  $\text{SER}_{\text{FSK}} = 0$  and  $N = 0$  hold, and without PS-QPSK we substitute 3 bit by 0 bit, i. e., we replace all occurrences of the number 3 in Eq. (6.1) by zero.

For 64PPM-2OFDM-PS-QPSK, the FSK-related terms in Eq. (6.1) do not exist, but a PS-QPSK signal is transmitted in both OFDM channels. This doubles the number of PS-QPSK bits and results in a total BER of

$$\begin{aligned}
\text{BER}_{\text{total}}^{(\text{OFDM})} = & \frac{\text{SER}_{\text{PPM}} \left( \frac{M}{2(M-1)} \cdot \log_2(M) + \frac{1}{2} \times 2 \times 3 \right)}{\log_2(M) + 2 \times 3} \\
& + (1 - \text{SER}_{\text{PPM}}) \frac{\text{BER}_{\text{PSQ}} \times 2 \times 3}{\log_2(M) + 2 \times 3}
\end{aligned} \tag{6.2}$$

Fig. 6.3 depicts the total calculated BER for the various stacked modulation /multiplexing formats. Fig. 6.3(a) shows the BER versus the number of photons per bit while Fig. 6.3(b) displays the BER as a function of the number of photons per symbol.

In Fig. 6.3(a) it can be seen that the stacked modulation formats 64PPM-4FSK-PSQPSK and 64PPM-OFDM-PSQPSK behave similarly and require as little as 1.9 photons per bit (i.e. 2.7 dB per bit). The high sensitivity can be understood by the fact that as many as 11 and 12 bit have been encoded in one symbol of the stacked modulation formats. It is now instructive to plot the BER from Eq. (6.1) and (6.2) as a function of photons per symbol, see Fig. 6.3(b). This plot shows that the error probability for a PS-QPSK symbol is lower than the error probability for a 4FSK format, and that the 4FSK error probability is lower than the probability for an error in the 64PPM format. The error probability for a stacked modulation format then

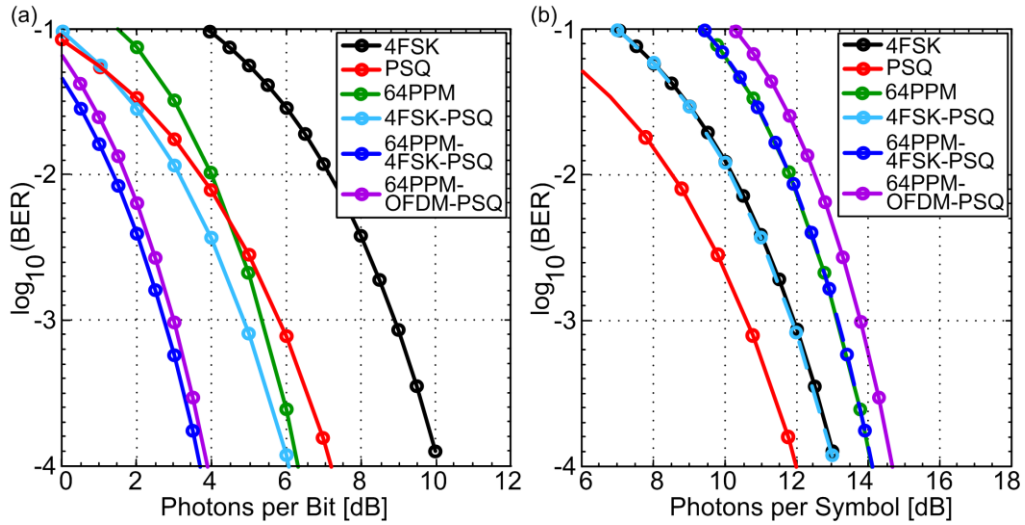


Fig. 6.3 Calculated bit error ratios (BER) for different modulation/multiplexing stacks. (a) BER as a function of the number of photons per bit (b) BER as a function of the number of *photons per symbol*.

cannot be lower than the probability of its worst constituent. Thus, the error probability per symbol for a 64PPM-4FSK-PSQPSK stack is indeed identical to the error probability of the 64PPM format, i. e., the reception is limited by the error probability of the 64PPM format. Once the PPM coding has been correctly detected, the FSK and PSQ signals are usually correctly detected as well. This becomes evident from the fact that PS-QPSK requires fewer photons per symbol. Thus, one can transmit almost two PS-QPSK symbols with the same number of photons that are required for detecting a PPM symbol. This is exactly what is done when transmitting 64PPM-2OFDM-PSQ. With 2OFDM we simultaneously transmit 2 FSK subcarriers with a PS-QPSK symbol on each subcarrier. This way we encode 6 bit in 2 OFDM carriers rather than 5 bit with the FSK-PS-QPSK stack. Because 2OFDM requires only half the optical bandwidth compared to 4FSK, the OFDM scheme is to be favored whenever the spectral efficiency in optical free-space transmission systems becomes important.

## 6.5 Experiment and Simulation

To verify the theoretical prediction that PPM-FSK-PS-QPSK is among the most sensitive modulation formats, we perform simulations and experiments with the setup described in Fig. 6.1. For a realistic performance prediction by simulation, we match all important parameters to the experiment, namely laser power and linewidth, sampling rate and RF power of the AWG,  $\pi$ -voltage of the modulator, and the gain and noise figure of the EDFAs. However, the low-pass characteristics of the electrical devices at transmitter

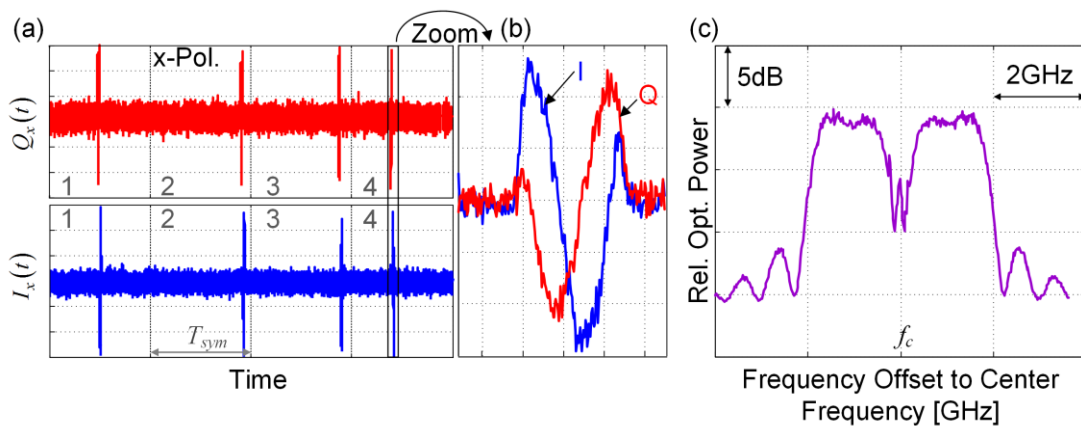


Fig. 6.4 Measured 64PPM-4FSK-PS-QPSK receiver signal. (a) In-phase (blue) and quadrature (red) components of a baseband signal as a function of time. The plots show the x-polarization components of 4 random symbols with symbol duration  $T_{sym}$ . (b) Zoom into the non-zero slot of the 4th symbol. (c) Optical spectrum. Four peaks at  $\pm 750$  MHz and  $\pm 1.5$  GHz are to be seen. The carrier  $f_c$  in the center of the spectrum is (not perfectly) suppressed.

and receiver were neglected. For the simulations we used the RSoft OptSim program package.

A measurement of the received 64PPM-4FSK-PS-QPSK signal is depicted in Fig. 6.4. For clarity, a receiver input power of  $-46.5$  dBm was chosen ( $>1000$  PPB), much more than what actually would be needed for a reliable reception. In Fig. 6.4(a) we show four PPM symbols with duration  $T_{sym}$ . One PPM pulse per symbol can be seen. A close-up of the fourth PPM symbol is shown in Fig. 6.4 (b). Each pulse consists of sine and cosine oscillations for  $I$  and  $Q$ , respectively. Since we see only one oscillation period in Fig. 6.4 (b), it must be frequency  $f_{-1}$  or  $f_1$ , see Fig. 6.2(b). Frequencies  $f_{-2}$  or  $f_2$  would show 2 oscillation periods within one PPM time slot. From the phase relation between  $I$  and  $Q$  we conclude that the associated phasor rotates clockwise with a frequency  $f_{-1}$ . The phases of  $I$  and  $Q$  together describe the QPSK information of the symbol. The information in the IQ components has to be retrieved by subsequent phase-estimation algorithm.

In Fig. 6.4(c) the spectrum of the optical signal has been depicted. Four peaks at  $\pm 750$  MHz and  $\pm 1.5$  GHz indicate the frequencies of the FSK symbols with their modulation sidebands. The carrier frequency  $f_c$  in the center of the spectrum is only partially suppressed, due to a finite extinction ratio of the Mach-Zehnder interferometer and due to an imperfect modulator bias.

The results of sensitivity measurements together with simulations and theoretical calculations are shown in Fig. 6.5. The curves display the bit error ratio (BER) as a function of the number of photons per bit for our measurements (dashed lines with diamonds, ---◆---), for simulations (dotted lines with +-markers, ···+···), and for theoretical calculations (solid lines with circular markers, —○—), respectively.

First, in Fig. 6.5(a), the BER for 4FSK (black) and PS-QPSK (PSQ, red) are plotted along with the BER for 64PPM (green). We then stacked two modulation formats and characterized the BER for 4FSK-PS-QPSK (light blue), see Fig. 6.5(b). Finally, 64PPM is added for a 64PPM-4FSK-PS-QPSK stack (blue). In this plot we also show 64PPM-2OFDM-PS-QPSK (purple). The latter modulation/multiplexing stack transports the largest information content with 12 bit/symbol, i. e., 6 bit by 64PPM and 3 bit via each of the 2 OFDM subcarriers.

For 4FSK we measure a minimum number of 9 dB photons per bit at a BER of  $10^{-3}$  which is very close to what one would expect for orthogonal 4FSK [11]. Theoretical results given in [11] for orthogonal 4FSK are outperformed

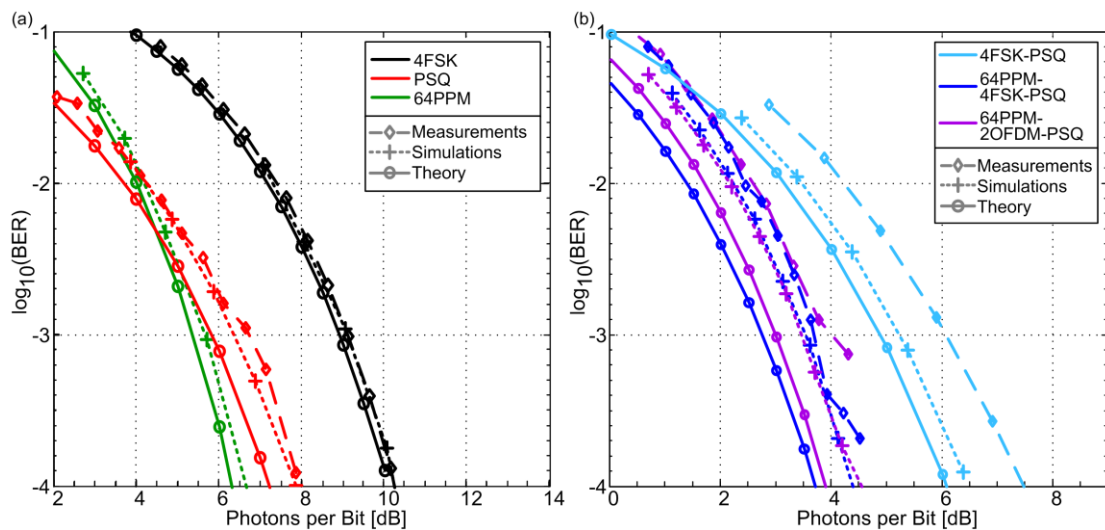


Fig. 6.5 Bit error ratio (BER) as a function of the number of photons per bit for different modulation formats. PSQ abbreviates the format PS-QPSK. (a) Individual modulation formats 4FSK, PS-QPSK, and 64PPM with sensitivities per bit of 9 dB, 7 dB, and 5 dB, respectively, at a target BER =  $10^{-3}$ . (b) Stacked modulation formats 4FSK-PS-QPSK, 64PPM-4FSK-PS-QPSK, and 64PPM-2OFDM-PS-QPSK. The limiting number of photons per bit reduces when stacking more modulation formats. The stacked format 64PPM-4FSK-PS-QPSK shows a limiting photon number per bit of 3.7 dB, slightly better than 64PPM-2OFDM-PSQ. Theoretically calculated BER for various modulation format stacks comprising 64PPM, 4FSK, PS-QPSK and including 2OFDM are shown for comparison.

by 0.1 dB, since we aligned the polarization of the signal in the detector for reception of an equal power per symbol in the  $x$  and  $y$ - polarization, see Section 6.8.

For PS-QPSK (PSQ) we find values that are reasonably close to what one would expect from theory [3, 12]. PS-QPSK is predicted to have a minimum number of 5.9 dB photons per bit at a BER of  $10^{-3}$ . In the present experiments we found a minimum number of 6.8 dB photons per bit, which is only 0.9 dB off from the theoretical limit. This offset can be explained by the non-ideal preamplifier and a non-perfect matched low-pass filter used for demodulation. Simulations and measurements differ slightly, but lie within the expected uncertainties with numerical simulations.

Fig. 6.5(b) shows the BER for a number of modulation stacks, all measured at symbol rates of  $R_{\text{sym}} = (1/64) \times R_{\text{slot}} = (1/64) \times 750 \text{ MHz} \approx 11.7 \text{ MHz}$ . We start with 4FSK-PS-QPSK having 5 bit per symbol. In our measurements, we determine a limiting number of 6 dB photons per bit for a BER of  $10^{-3}$ . It can be seen that the limiting number of photons per bit for 4FSK-PS-QPSK is by 1 dB better than for PS-QPSK. The simulations predict 5 dB photons per bit. The discrepancy stems from electronic hardware's bandwidth limitations, which could not be determined with sufficient accuracy and was left out for the simulations.

The next result shown in Fig. 6.5(b) refers to a 64PPM-4FSK-PS-QPSK stack with 11 bits per symbol. We achieved a record-low number of 2.3 PPB (3.7 dB) at a BER of  $10^{-3}$ . Thus, stacking 4FSK-PS-QPSK with 64PPM results in an improvement of more than 2 dB compared to 4FSK-PS-QPSK.

Finally, we compare the 64PPM-4FSK-PS-QPSK stack with the frequency-division multiplexed 64PPM-2OFDM-PS-QPSK scheme. In this case, the 4FSK coding is replaced by a coding onto 2 OFDM subcarriers. This multiplexing technique leads to 12 bit per symbol instead of only 11 bit per symbol for the 4FSK case. Again, a sensitivity of about 2.4 PPB is found at a BER of  $10^{-3}$ .

The analytical results discussed in the previous Section compare well with measurement and simulations. We find for both PPM-FSK-PS-QPSK and 64PPM-2OFDM-PS-QPSK a small penalty of about 1 dB at  $\text{BER} = 10^{-3}$  against the analytical predictions. This penalty is most likely due to a non-ideal representation of continuous sine and cosine waves by the time-discrete and quantized outputs of our AWG. Additional impairments come through phase distortions due to the low-pass characteristic of the electrical devices, and through a non-ideal phase-estimation in the receiver.

The finding that the modulation stack 64PPM-4FSK-PS-QPSK and the modulation/multiplexing scheme 64PPM-2OFDM-PS-QPSK behave very similar, has already been explained above with the help of Fig. 6.3(b). Thus we will not discuss it here again.

Finally, we should comment on the effect of using the same laser as a sender in the transmitter and as a local oscillator at the receiver. Under the assumption that the QPSK symbol duration (i. e., the PPM time slot) is short, an independent high-quality local oscillator would not significantly influence the systems performance, and no penalty could be measured. This is true for our local oscillator laser with a 1 kHz linewidth where a phase drift from one symbol to the next is very small. In future, such a system would probably be operated at larger symbol rates such that drifts from one symbol to the next would even be smaller.

## 6.6 Conclusion

In this paper, we demonstrate stacking of PPM with FSK and PS-QPSK. We demonstrated experimentally a record-high receiver sensitivity of 2.3 photons per bit (3.7 dB) at  $\text{BER} = 10^{-3}$  by using 64PPM in combination with 4FSK and PS-QPSK. In stacking these modulation formats we were able to encode 11 bit in one 64PPM-4FSK-PS-QPSK symbol. It was further shown that a similar sensitivity is obtained when encoding 12 bit in a 64PPM-2OFDM-PS-QPSK symbol. Theoretical analysis and numerical simulations verified the experimental results. Stacking modulation formats is highly attractive for applications where best receiver sensitivity is required and spectral efficiency is of lesser importance, such as in free-space communication systems

## 6.7 Appendix 1: Number of Photons per Bit

To determine the number of photons per bit that are required for reception with a target BER of  $10^{-3}$ , two different measurement techniques are used.

First, the numbers of photons per bit are calculated from the average received signal power  $P_{\text{Sig}}$  as measured with a power meter.

With the center frequency  $f_c$ , Planck's constant  $h$ , the 64PPM symbol rate  $R_{\text{sym}} = (1/64) \times R_{\text{slot}} = (1/64) \times 750 \text{ MHz} \approx 11.7 \text{ MHz}$  and the number of bits  $n_{\text{bit/sym}}$  per symbol, we find the number of photons per bit (PPB) as

$$\text{PPB} = \frac{P_{\text{Sig}}}{hf_c R_{\text{bit}}} = \frac{P_{\text{Sig}}}{hf_c R_{\text{sym}} n_{\text{bits/sym}}} \quad (6.3)$$

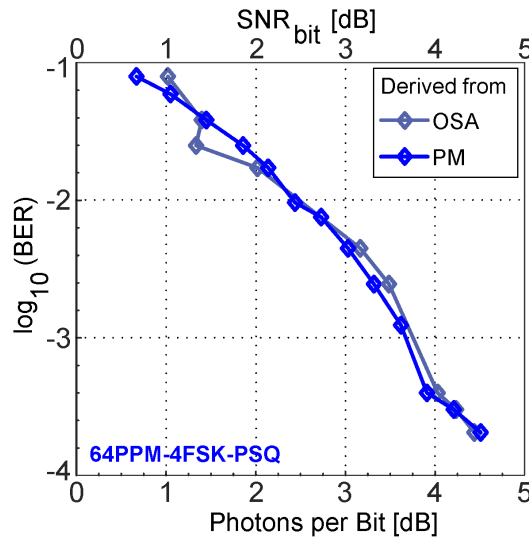


Fig. 6.6 Comparison of the results derived from the power meter (PM) and the optical spectrum analyzer (OSA) for 64PPM-4FSK-PS-QPSK.

Here, for a 64PPM-4FSK-PSQPSK symbol  $n_{\text{bits/sym}} = 11$ .

The second way to determine the number of photons per bit is by measuring the OSNR. In this experiment, the OSNR is measured with the help of a high-resolution optical spectrum analyzer with 20 MHz resolution to verify the results shown previously that are derived from the power meter. It is the same device from which the spectrum shown in Fig. 6.4(c) is derived. The  $\text{SNR}_{\text{bit}}$  can directly be derived from an OSNR measurement [2] and equals the number of photons per bit [29],

$$\text{SNR}_{\text{bit}} = \frac{2B_{\text{O}}}{R_{\text{sym}} n_{\text{bits/sym}}} \text{OSNR} \quad (6.4)$$

According to the spectrum Fig. 6.4(c), the optical signal bandwidth is  $B_{\text{O}} = 6R_{\text{slot}} = 6 \times 750 \text{ MHz} = 4.5 \text{ GHz}$ . Note that for our definition of the OSNR the noise power is not measured in a 0.1 nm wide reference bandwidth, but rather measured in the actual signal bandwidth  $B_{\text{O}}$ . Therefore our values for OSNR describe the signal to noise power ratios of 4.5 GHz bandwidth.

The measured OSNR values are in good agreement with the photons per bit derived by the received signal power as shown Fig. 6.6.

## 6.8 Appendix 2: Sensitivity of PPM, FSK and PS-QPSK formats

We assume a polarization-diversity receiver with an optical pre-amplifier, and we concentrate on coherent reception. We describe the received

baseband signal in  $x$  and  $y$ -polarizations by the vector  $\mathbf{p}(t) = r_x(t)\vec{e}_x + r_y(t)\vec{e}_y$  (orthogonal unit vectors  $\vec{e}_{x,y}$ ), which comprises the signal vector  $\mathbf{s}(t)$  and the noise vector  $\mathbf{n}(t)$ ,

$$\mathbf{p}(t) = \mathbf{s}(t) + \mathbf{n}(t),$$

$$\mathbf{s} = \begin{pmatrix} s_x \\ s_y \end{pmatrix} = \begin{pmatrix} I_x + jQ_x \\ I_y + jQ_y \end{pmatrix}, \quad \mathbf{n} = \begin{pmatrix} n_x \\ n_y \end{pmatrix} = \begin{pmatrix} n_{I,x} + jn_{Q,x} \\ n_{I,y} + jn_{Q,y} \end{pmatrix} \quad (6.5)$$

The noise terms of in-phase and quadrature in both polarizations are  $n_{I,x,y}$  and  $n_{Q,x,y}$ , respectively. These noise terms are assumed to be independently Gaussian distributed with zero mean and variance  $\sigma_{x,y}^2 = \sigma_{I,x,y}^2 = \sigma_{Q,x,y}^2 = \sigma^2$ .

In the following, the bit error ratios of the constituents of the stacked modulation formats are considered separately, i.e., PPM, FSK, and PS-QPSK. Alternatively, the primary PPM format can also be followed by an OFDM step which replaces FSK. Because our PPM demodulation is different for FSK and OFDM coding, we have to adapt the calculated bit-error ratios accordingly.

**PPM:** PPM symbols are orthogonal, and the field in each time slot can be interpreted as an ASK signal: The received signal in each slot represents one ASK symbol having either the amplitude  $A$ , if there is a pulse, or the amplitude zero if the slot is empty. We therefore refer to the results from a sensitivity analysis for ASK signals [40] and adapt them for PPM.

In the present experiments, each PPM symbol is simultaneously sent with equal power in  $x$  and  $y$ -polarization. Our demodulation technique adds the amplitudes received in the  $x$ - and  $y$ -polarizations. We define a new amplitude quantity  $r_{\text{FSK}}$  for each time slot

$$r_{\text{FSK}} = |r_x| + |r_y|,$$

$$r_{x,y} = s_{x,y} + n_{x,y} = I_{x,y} + n_{I,x,y} + j(Q_{x,y} + n_{Q,x,y}). \quad (6.6)$$

This received amplitude quantity, which is impaired by noise, must be compared to the pure signal  $A_{\text{FSK}}$  of the amplitude in  $x$  and  $y$ -polarization

$$|s_x| = |s_y| \equiv A_{\text{FSK}}, \text{ where } A_{\text{FSK}}^2 \in \{0, \mathcal{E}_{\text{slot}}/T_{\text{slot}}\}. \quad (6.7)$$

As already mentioned, both polarizations carry the same power. The sum of these powers  $\frac{1}{2}|s_x|^2 + \frac{1}{2}|s_y|^2 = A_{\text{FSK}}^2$  in an occupied PPM slot represents the energy  $\mathcal{E}_{\text{slot}}$  per slot duration  $T_{\text{slot}}$ , and is zero elsewhere. The probability density function (PDF)  $p_r$  of each of the two absolute-value terms  $r = |r_{x,y}|$

in Eq. (6.6) is given by the Rice PDF in an occupied slot with  $A = A_{\text{FSK}} \neq 0$ , and by the Rayleigh PDF for an empty slot with  $A = A_{\text{FSK}} = 0$ , respectively [71] (p. 48, Eq. (2.3-43), (2.3-56))

$$p_r(r, A) = \begin{cases} \frac{r}{\sigma^2} e^{-\frac{r^2+A^2}{2\sigma^2}} I_0\left(\frac{Ar}{\sigma^2}\right) & \text{for } r > 0 \\ 0 & \text{for } r \leq 0. \end{cases} \quad (6.8)$$

The random variables  $|r_x|$  and  $|r_y|$  are statistically independent with respect to their noise contributions  $n_x$  and  $n_y$ , therefore their sum  $r_{\text{FSK}} = |r_x| + |r_y|$  results in a PDF which is a convolution [40]

$$p_{\text{FSK}}(r_{\text{FSK}}, A_{\text{FSK}}) = p_r(|r_x|, A_{\text{FSK}}) * p_r(|r_y|, A_{\text{FSK}}) = (p_r * p_r)(r_{\text{FSK}}, A_{\text{FSK}}) \quad (6.9)$$

We evaluate this convolution numerically.

In the case of 64PPM-2OFDM we transmit per occupied PPM-slot two OFDM subcarriers, which are subscripted with  $\alpha$  and  $\beta$ . We apply an FFT to the signal in each PPM time slot and for each polarization, and look at the  $2 \times 2$  complex Fourier coefficients  $s_{x,y,\alpha}$  and  $s_{x,y,\beta}$  which are associated with the two OFDM subcarrier signals,

$$s_\alpha = \begin{pmatrix} s_{x\alpha} \\ s_{y\alpha} \end{pmatrix} = \begin{pmatrix} I_{x\alpha} + jQ_{x\alpha} \\ I_{y\alpha} + jQ_{y\alpha} \end{pmatrix}, \quad s_\beta = \begin{pmatrix} s_{x\beta} \\ s_{y\beta} \end{pmatrix} = \begin{pmatrix} I_{x\beta} + jQ_{x\beta} \\ I_{y\beta} + jQ_{y\beta} \end{pmatrix} \quad (6.10)$$

We proceed as in Eq. (6.6) and form the sum of the moduli for  $x$  and  $y$ -polarizations  $r_{\text{FSK}\alpha} = |r_{x\alpha}| + |r_{y\alpha}|$  and  $r_{\text{FSK}\beta} = |r_{x\beta}| + |r_{y\beta}|$  for each subcarrier  $\alpha$  and  $\beta$ ,

$$\begin{aligned} r_{\text{OFDM}} &= r_{\text{FSK}\alpha} + r_{\text{FSK}\beta} = |r_{x\alpha}| + |r_{y\alpha}| + |r_{x\beta}| + |r_{y\beta}| \\ &= \left| I_{x\alpha} + n_{I,x\alpha} + j(Q_{x\alpha} + n_{Q,x\alpha}) \right| \\ &\quad + \left| I_{y\alpha} + n_{I,y\alpha} + j(Q_{y\alpha} + n_{Q,y\alpha}) \right| \\ &\quad + \left| I_{x\beta} + n_{I,x\beta} + j(Q_{x\beta} + n_{Q,x\beta}) \right| \\ &\quad + \left| I_{y\beta} + n_{I,y\beta} + j(Q_{y\beta} + n_{Q,y\beta}) \right| \end{aligned} \quad (6.11)$$

with

$$|s_{x\alpha}| = |s_{x\beta}| = |s_{y\alpha}| = |s_{y\beta}| \equiv A_{\text{OFDM}} \quad \text{and} \quad 2A_{\text{OFDM}}^2 \in \{0, \mathcal{E}_{\text{slot}}/T_{\text{slot}}\}. \quad (6.12)$$

Again, the sum of the pure signal powers  $\frac{1}{2}|s_{x\alpha}|^2 + \frac{1}{2}|s_{x\beta}|^2 + \frac{1}{2}|s_{y\alpha}|^2 + \frac{1}{2}|s_{y\beta}|^2 = 2A_{\text{OFDM}}^2$  in an occupied PPM slot represents the energy  $\mathcal{E}_{\text{slot}}$  per slot duration  $T_{\text{slot}}$ , and is zero elsewhere. The random variables  $|r_{x\alpha}|$ ,  $|r_{y\alpha}|$ ,  $|r_{x\beta}|$  and  $|r_{y\beta}|$  are statistically independent with respect to their noise contributions, therefore the PDF of  $r_{\text{OFDM}}$  is computed by the convolution

$$\begin{aligned} p_{\text{OFDM}}(r_{\text{OFDM}}, A_{\text{OFDM}}) &= \\ p_{\text{FSK}}(r_{\text{FSK}\alpha}, A_{\text{OFDM}}) * p_{\text{FSK}}(r_{\text{FSK}\beta}, A_{\text{OFDM}}) & \quad (6.13) \\ = (p_{\text{FSK}} * p_{\text{FSK}})(r_{\text{OFDM}}, A_{\text{OFDM}}) & \end{aligned}$$

Again we evaluate this convolution numerically.

Now that we know the PDFs of the quantities  $r_{\text{FSK}}$  and  $r_{\text{OFDM}}$  which we want to detect, the resulting bit error ratio (BER, bit error probability) can be calculated. The PPM symbol error ratio (SER, symbol error probability) can be expressed according to [56] (Eq. (4.34)) in terms of the probability  $P_{\text{sc}}$  to detect a correct symbol,

$$\text{SER}_{\text{PPM}} = 1 - P_{\text{sc}}. \quad (6.14)$$

Since *M*-ary PPM is an orthogonal signaling scheme with equal energy in each symbol, an optimum detector chooses the signal with the largest cross-correlation between received symbol and any of the  $M$  possible symbols, i. e., the slot with the maximum value  $r_1 = \max(r_{\text{FSK}})$  or  $r_1 = \max(r_{\text{OFDM}})$  within a PPM symbol is regarded to carry the information. Mathematically it is advantageous to calculate first the probability of a correct decision. The probability to correctly detect the information in slot 1 is the joint probability of the  $M - 1$  independent events that the unoccupied slots have amplitudes smaller than  $r_1$ , averaged with the PDF that actually  $r_1$  occurs,

$$\begin{aligned} P_{\text{sc}} &= \int_{-\infty}^{\infty} \left[ \int_{-\infty}^{r_1} p_0(r_0) dr_0 \right]^{M-1} p_1(r_1) dr_1 \\ &= \int_{-\infty}^{\infty} \left[ 1 - \int_{r_1}^{\infty} p_0(r_0) dr_0 \right]^{M-1} p_1(r_1) dr_1 \end{aligned} \quad (6.15)$$

Depending on the use of FSK or OFDM, the function  $p_0(r_0)$  is the probability density function of the signal in an empty PPM slot, namely  $p_{\text{FSK}}(r_0, A_{\text{FSK}})$  or  $p_{\text{OFDM}}(r_0, A_{\text{OFDM}})$  for  $A_{\text{FSK}} = 0$  or  $A_{\text{OFDM}} = 0$ , respectively. For occupied slots the PDF  $p_1(r_1)$  equals  $p_{\text{FSK}}(r_1, A_{\text{FSK}})$  or

$p_{\text{OFDM}}(r_1, A_{\text{OFDM}})$  for  $A_{\text{FSK}} = \sqrt{\mathcal{E}_{\text{slot}}/T_{\text{slot}}}$  or  $A_{\text{OFDM}} = \sqrt{\mathcal{E}_{\text{slot}}/(2T_{\text{slot}})}$ , respectively. The PDFs  $p_{\text{FSK,OFDM}}$  were specified in Eq. (6.9) and Eq. (6.13).

Ultimately, we are interested in the BER rather than the SER. The BER is obtained as follows: For a correct symbol any of the  $M$  possible slots is occupied with equal probability. The alphabet consists of  $M$  symbols. Therefore an erroneous symbol is left to occupy any of  $M - 1$  possible time slots. Because the symbol error probability in Eq. (6.14)-(6.15) relates to all possible statistically independent slots in a PPM symbol, the error probability  $\text{SER}_{\text{PPM}} / (M - 1)$  for a specific symbol at a given slot position is smaller than  $\text{SER}_{\text{PPM}}$  by a factor of  $1 / (M - 1)$ .

The set of  $M$  symbols transports a number of  $k = \log_2(M)$  bits. To find the probability  $\text{BER}_{\text{PPM}}$  for a bit error one needs to determine how many of the  $k$  bits will be corrupted if one symbol is erroneous. Assuming that any one of the bits in a specific symbol is wrong with equal probability, there are half the number of symbols  $M / 2 = 2^{k-1}$  which share this bit and are therefore wrong with equal probability. Thus the bit error ratio increases over the symbol error ratio for a specific symbol by a factor of  $2^{k-1}$ . As a consequence, the probability for detecting a wrong bit in a specific symbol is [19] (Eq. (4.4-12))

$$\text{BER}_{\text{PPM}} = \frac{2^{k-1}}{2^k - 1} \text{SER}_{\text{PPM}} = \frac{M}{2} \frac{1}{M - 1} \text{SER}_{\text{PPM}} \quad (6.16)$$

If the BER as a function of photons per bit is of interest, we need to specify the receiver more closely. Our pre-amplified receiver has a power gain  $G$ , an inversion factor  $n_{\text{sp}}$  and an electrical bandwidth  $B$ . Substituting the PDFs in Eq. (6.15) by Eq. (6.9) or Eq. (6.13), the BER for PPM can be calculated, Eq. (6.16). It depends on the signal energy  $\mathcal{E}_{\text{slot}}$  per slot (which is equivalent to the total signal energy  $\mathcal{E}_s$  for a symbol because only one slot can be occupied), and on the noise spectral density of amplified spontaneous emission  $N_{\text{ASE}} = n_{\text{sp}}(G - 1)hf_c$  per polarization [2, 19, 56], where  $n_{\text{sp}}$  is the inversion factor and  $hf_c$  represents the photon energy. The energy of a symbol in both polarizations is  $\mathcal{E}_s = G \text{ PPS } hf_c$ , if PPS denotes the number of photons per symbol. The signal-to-noise power ratio per polarization is

$$\text{SNR}_x = \frac{\frac{1}{2} A_{\text{FSK}}^2}{\sigma_x^2} = \frac{\mathcal{E}_s}{N_{\text{ASE}}} = \frac{G \text{ PPS } hf_c}{n_{\text{sp}}(G - 1)hf_c} \approx \text{PPS}, \quad (6.17)$$

$$\text{PPB} = \frac{\text{PPS}}{n_{\text{bit/sym}}}$$

The approximation holds for a fully inverted amplifier  $n_{sp} \approx 1$  and a large power gain  $G \gg 1$  [56]. The number of photons per bit results from the number of photons per symbol divided by the number of bits  $n_{\text{bits/sym}}$  encoded in one symbol. The resulting  $\text{BER}_{\text{PPM}}$  for pure 64PPM according to Eq. (6.14)-(6.15) and (6.9), i. e., without subsequent OFDM multiplexing, is depicted in Fig. 6.3(a).

**FSK:** The condition that the  $N$ -ary FSK frequency spacing equals the reciprocal symbol rate establishes orthogonal signaling, and in this respect FSK as employed in our experiments is closely related to PPM [19]. For 4FSK we use four orthogonal frequencies having a frequency spacing of  $nR_{\text{slot}} = n\Delta f$  with  $n \in \{\pm 1, \pm 2\}$  and find the analytical notation:

$$\begin{aligned} s_n(t) &= A \cos(2\pi n \times \Delta f t) + j A \sin(2\pi n \times \Delta f t) \\ &= A \exp(j 2\pi n \times \Delta f t) \end{aligned} \quad (6.18)$$

Thus our FSK alphabet realizes an orthogonal signaling scheme having correlation coefficients of 1 or 0 [19, 59]. In this sense our 4FSK signaling resembles 4PPM.

However, in our experiment we use a demodulation technique in the frequency domain. We do so by applying a Fourier transform to the complex FSK symbols during a PPM time slot, and determine the signal sent by the maximum modulus of the Fourier transform. Thus, in analogy to Eq. (6.5) the received signal in the frequency domain reads

$$\begin{aligned} \tilde{\rho}(f) &= \int_{-\infty}^{+\infty} [s(t) + n(t)] e^{-j2\pi f t} dt, \\ \tilde{r}_x(f) &= \int_{-\infty}^{+\infty} [I_x(t) + n_{I,x}(t) + j(Q_x(t) + n_{Q,x}(t))] e^{-j2\pi f t} dt, \\ \tilde{r}_y(f) &= \int_{-\infty}^{+\infty} [I_y(t) + n_{I,y}(t) + j(Q_y(t) + n_{Q,y}(t))] e^{-j2\pi f t} dt. \end{aligned} \quad (6.19)$$

Only the four discrete frequencies  $f_n$  with  $n \in \{\pm 1, \pm 2\}$  of the FFT are of interest for our signal demodulation. For extracting the FSK information, we define

$$\tilde{r}_F(f_n) = |\tilde{r}_x(f_n)| + |\tilde{r}_y(f_n)|, \quad \tilde{r}_{x,y}(f_n) = \int_{f_n - \frac{1}{2}\Delta f}^{f_n + \frac{1}{2}\Delta f} \tilde{r}_{x,y}(f) df. \quad (6.20)$$

We then find the maximum value of  $\tilde{r}_F(f_n)$  for  $n \in \{\pm 1, \pm 2\}$ . Thus, for the demodulation of the FSK information we apply a similar demodulation scheme as in PPM and therefore expect a similar receiver sensitivity. Thus

for  $N$ -ary FSK, Eq. (6.9) and Eq. (6.14)-(6.17) hold when substituting  $M = N$ . The result is depicted for 4FSK in Fig. 6.3(a) and Fig. 6.7.

**PS-QPSK:** This modulation format comprises a set of bi-orthogonal signals with 8 constellation points and complementary bit encoding (see [59] pp. 198-203). As suggested in [3], for comparison see also [19], eq.4.4-25, p. 208, we use the inverted bit pattern for anti-correlated symbols for bit encoding to achieve a minimum BER for a given SER. As a result, we find the BER [3]:

$$\text{BER}_{\text{PSQ}} = \frac{1}{2\sqrt{\pi}} \int_{-\infty}^{+\infty} \left(3 - 3\text{erfc}(r) + \text{erfc}^2(r)\right) \text{erfc}(r) \exp\left[-\left(r - \sqrt{\frac{\mathcal{E}_s}{N_0}}\right)^2\right] dr \quad (6.21)$$

The quotient  $\text{PPS} = \mathcal{E}_s/N_0$  describes the symbol energy divided by the noise spectral density and equals the number of photons per symbol. The result of this equation is depicted in Fig. 6.3(a) and Fig. 6.4.

## 6.9 Acknowledgements

We acknowledge support from Keysight Technologies (formerly Agilent Technologies' Electronic Measurement Group), NKT Photonics, the Institute of Radio-Frequency and Electronics at Karlsruhe Institute of Technology (KIT), and the Institute of Robust Power Semiconductor Systems of the University of Stuttgart. We further acknowledge support by the Open Access Publishing Fund of KIT.

[End of Paper J5]

## 6.10 Addendum: Discussion of Results

Previously, it has been shown in Section 6.5 that the modulation stack 64PPM-4FSK-PS-QPSK and 64PPM-2OFDM-PS QPSK modulation/multiplexing scheme behave very similarly. This result is discussed in more detail in the following.

Previously, it has been stated in Section 6.4 that for 64PPM-4FSK-PS-QPSK the performance of 64PPM limits the sensitivity performance of the whole stack, whereas with 64PPM-2OFDM-PS-QPSK this is not the case. For the following discussion, Fig. 6.7 is regarded. It shows plots of BER vs. photons *per symbol* for each measured modulation format. It should be kept in mind that the photons per symbol is proportional to the symbol energy.

To find out to what extent the wrongly detected PPM symbols, or the wrongly detected FSK or PSQ symbols contribute to the total BER, we split the total  $\text{BER}_{\text{total}}^{(\text{FSK})}$  from Eq. (6.1) into a simpler form, calculating the ratio of the number of errors detected in each modulation format  $n_{\text{E,xxx}}$  and the total number of detected bits encoded in each modulation format  $n_{\text{xxx}}$ .

$$\begin{aligned} \text{BER}_{\text{total}}^{(\text{FSK})} &= \frac{n_{\text{E,PPM}} + n_{\text{E,FSK}} + n_{\text{E,PSQ}}}{n_{\text{PPM}} + n_{\text{FSK}} + n_{\text{PSQ}}} \\ &= \frac{n_{\text{E,PPM}}}{n_{\text{PPM}}} + \frac{n_{\text{E,FSK}}}{n_{\text{FSK}}} + \frac{n_{\text{E,PSQ}}}{n_{\text{PSQ}}} \end{aligned} \quad (6.22)$$

$$\underbrace{\frac{n_{\text{total}}}{n_{\text{PPM}}}}_{\text{BER}_{\text{PPM}}} + \underbrace{\frac{n_{\text{total}}}{n_{\text{FSK}}}}_{\text{BER}_{\text{FSK}}} + \underbrace{\frac{n_{\text{total}}}{n_{\text{PSQ}}}}_{\text{BER}_{\text{PSQ}}}$$

with  $n_{\text{total}} = n_{\text{PPM}} + n_{\text{FSK}} + n_{\text{PSQ}}$ . The measurement result following Eq. (6.22) is shown in Fig. 6.7 as a function of photons per symbol. It shows the total BER of 64PPM-4FSK-PS-QPSK (blue) as well as the three BERs of each modulation format in green for 64PPM, black for 4FSK and red for PS-QPSK (PSQ). It becomes obvious that all four lines coincide. This indicates that the total BER of 64PPM-4FSK-PS-QPSK is dominated by the 64PPM errors. Once the PPM has been correctly detected the FSK and PSQ are usually correctly detected as well. Or to rephrase the previous sentence: The bit errors found for FSK and PS-QPSK are only caused by the fact that the PPM slot was detected wrongly.

This leads to the conclusion that the PS-QPSK stacked on top of PPM would likely still perform well even with fewer photons per symbol. This is exactly what is done when transmitting 64PPM-2OFDM-PSQ using the same average received power as before. We now simultaneously transmit 2 FSK carriers (2OFDM)  $\alpha$  and  $\beta$  with a PS-QPSK symbol on each subcarrier. We adapt the previous equation having now two times the number of erroneously detected PS-QPSK bit  $n_{\text{E,PSQ}\alpha}$  and  $n_{\text{E,PSQ}\beta}$  as well as the total number of detected bit encoded in each PS-QPSK symbol that are per definition the same  $n_{\text{PSQ}\beta} = n_{\text{PSQ}\alpha}$ . This leads to

$$\begin{aligned} \text{BER}_{\text{total}}^{(\text{OFDM})} &= \frac{n_{\text{E,PPM}} + n_{\text{E,PSQ}\alpha} + n_{\text{E,PSQ}\beta}}{n_{\text{PPM}} + n_{\text{PSQ}\alpha} + n_{\text{PSQ}\beta}} \\ &= \frac{n_{\text{E,PPM}}}{n_{\text{PPM}}} + \frac{n_{\text{E,2OFDM-PSQ}}}{n_{\text{2OFDM-PSQ}}} \end{aligned} \quad (6.23)$$

$$\underbrace{\frac{n_{\text{total}}}{n_{\text{PPM}}}}_{\text{BER}_{\text{PPM}}} + \underbrace{\frac{n_{\text{total}}}{n_{\text{2OFDM-PSQ}}}}_{\text{BER}_{\text{2OFDM-PSQ}}}$$

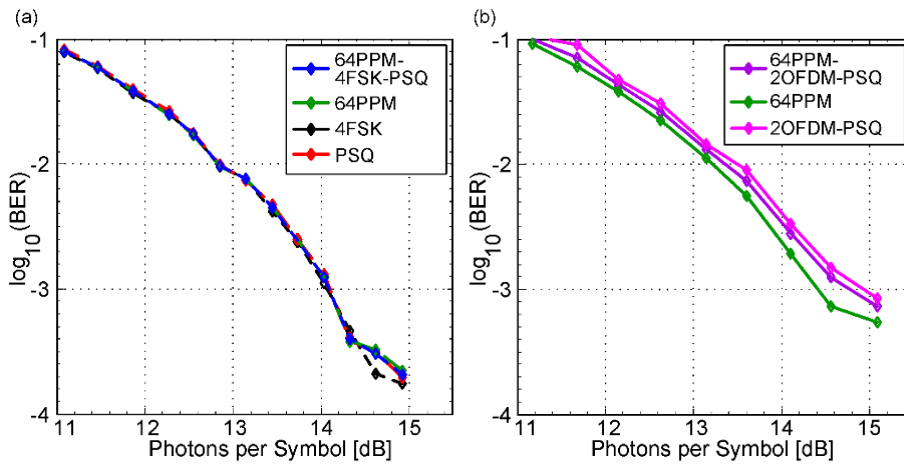


Fig. 6.7 Bit error ratio vs. photons per symbol for (a) 64PPM-4FSK-PS-QPSK and (b) 64PPM-2OFDM-PS-QPSK and its respective BER contributions of 64PPM (green), 4FSK (black), PS-QPSK (red) or 2OFDM-PS-QPSK (magenta). The abbreviation PSQ stands for PS-QPSK. The contributing BER of each modulation format, i.e. each step in the demodulation chain is depicted for clarity. In (a) all modulation formats show the same performance. This leads to the conclusion that 64PPM as the first to be demodulated limits the performance of the consecutive modulation formats. In (b) a different situation is shown: 2OFDM-PS-QPSK shows worse performance than 64PPM. Here, 64PPM does not limit the performance. However, 64PPM shows slightly worse performance, since a higher bandwidth for symbol decision is needed, since now two OFDM subcarriers are looked at with their respective bandwidth. Total BER of the 64PPM-2OFDM-PS-QPSK can be found in the middle of both curves, since it represents an average BER of the 64PPM BER and 2OFDM-PS-QPSK BER.

with  $n_{\text{total}} = n_{\text{PPM}} + n_{\text{PSQ}\alpha} + n_{\text{PSQ}\beta}$ . The result of the measurements for 64PPM-2OFDM-PS-QPSK is shown in experiment in Fig. 6.7(b). In purple, the result for the total stack is shown, whereas in green the BER contribution of 64PPM is depicted as well as the average BER contribution of the two PS-QPSK symbols on the two OFDM subcarriers (2OFDM-PSQ) in magenta. In contradiction to Fig. 6.7(a) the results differ. Here, the total BER is a mean value of 64PPM and 2 times PS-QPSK. This leads to the conclusion that only some errors found in the PS-QPSK symbols result from the fact that the PPM slot was wrongly detected. But there are also some errors, which are caused by the fact that the signal power in each OFDM subcarrier is so little due to the multiplexing that the PS-QPSK has reached its sensitivity limit. The reason, why the total BER is found in the middle is given by the fact that both, 64PPM as well as 2OFDM-PS-QPSK, each have encoded 6 bit.

Comparing Fig. 6.7(a) and (b) one can observe a small difference in the performance of 64PPM. The number of photons required for 64PPM at a  $\text{BER} = 10^{-3}$  differs slightly by around 0.5 dB. This is given by the fact that for the demodulation of 64PPM-4FSK-PS-QPSK the absolute values of the signals in  $x$  and  $y$ - polarization are summed, whereas for 64PPM-2OFDM-PS-QPSK the sum of four absolute values are required: the absolute values of both subcarriers in both polarization. With other words: for 2OFDM double the filter bandwidth is required compared to 4FSK leading to a slightly worse performance. For more detail, please follow the discussion in Section 6.8 concerning Eq. (6.6)-(6.13).

Thus, all in all it can be said that both, 64PPM-4FSK-PS-QPSK and 64PPM-2OFDM-PS-QPSK perform similar due to different sensitivity limiting contributing modulation formats. The first, i.e. 64PPM-4FSK-PS-QPSK is limited by PPM, the latter is limited by the power hungry multiplexing. However, both modulation schemes show very good performances concerning their theoretical sensitivities that are proven in measurements as well.

## 7 Conclusion

In this thesis, a new approach to increase the receiver sensitivity is shown, by stacking modulation formats. Especially in inter-satellite links, the demand for high receiver sensitivity suitable for large link distances is growing, since transmitter power and weight are limited, while measurement devices built on a satellite, like high resolution cameras demand more and more throughput. Since in-line amplification like in terrestrial fiber links is not possible as well as there is a limit to meaningful sizes of receiver antennas, receiver sensitivity is mainly limited by the implemented modulation format.

However, as stated by Shannon, there is a trade-off between receiver sensitivity and spectral efficiency [19]. I.e., if an infinitely good receiver sensitivity should be achieved, the spectral efficiency is infinitely poor, with other words, it would need a system with infinite bandwidth.

There are several ways to deal with this trade-off. On the one hand, it is possible to increase the sensitivity by forward-error-correction (FEC). Hereby, additional information is added to the data to be able to correct erroneous bits. However, to achieve the same net data rate, the gross data rate must be increased by the amount of additional FEC overhead.

A different approach to overcome the trade-off between spectral efficiency and receiver sensitivity is presented in this work. The solution is stacking the correct modulation formats.

For this work, the best mixture of modulation formats has been chosen to be stacking of PPM with FSK and PS-QPSK. Hereby, a sensitivity of 2.3 photons per bit is demonstrated (3.7 dB) at  $\text{BER} = 10^{-3}$ . In stacking these modulation formats we were able to encode 11 bit in one 64PPM-4FSK-PS-QPSK symbol. It is also shown that a similar sensitivity can be obtained when encoding 12 bit in a 64 PPM-2OFDM-PS-QPSK symbol requiring only half of the optical bandwidth. Theoretical analysis and numerical simulations verified the experimental results. This modulation format is highly attractive for all applications where the minimum number of received photons per bit is of paramount importance, such as inter-satellite links.

## Appendix A: Methods

### A.1 Energy Considerations

This section describes the energy considerations of signals in base-band and pass-band. It follows closely Ref. [19] Chapter 2.1-3.

We define a bandpass signal  $x(t) = x_I(t) \cos(2\pi f_c t) - x_Q(t) \sin(2\pi f_c t)$  with  $f_c$  the carrier frequency and  $x_l = x_I(t) + j x_Q(t)$  the analytical low-pass signal with  $x_{I,Q}$  its inphase and quadrature components, respectively.

The energy of the signal  $x(t)$  and its Fourier transform  $X(f)$  is defined by the Rayleigh's (Parseval's) theorem

$$\begin{aligned} \mathcal{E} &= \int_{-\infty}^{\infty} |x(t)|^2 dt \\ &= \int_{-\infty}^{\infty} |X(f)|^2 df \end{aligned} \quad (\text{A.1})$$

We define the positive spectrum  $X_+(f)$  and the negative spectrum  $X_-(f)$ , respectively:

$$X_+(f) = \begin{cases} X(f) & f > 0 \\ \frac{1}{2} X(0) & f = 0 \\ 0 & f < 0 \end{cases} \quad X_-(f) = \begin{cases} X(f) & f < 0 \\ \frac{1}{2} X(0) & f = 0 \\ 0 & f > 0 \end{cases} \quad (\text{A.2})$$

Under the assumption that there is no overlap in frequency domain of  $X_+(f)$  and  $X_-(f)$ ,  $X_+(f) \times X_-(f) = 0$ . Thus, the energy of our signal in frequency domain can be derived to:

$$\begin{aligned} \mathcal{E} &= \int_{-\infty}^{\infty} |X_+(f) + X_-(f)|^2 df \\ &= \int_{-\infty}^{\infty} |X_+(f)|^2 df + \int_{-\infty}^{\infty} |X_-(f)|^2 df \\ &= 2 \int_{-\infty}^{\infty} |X_+(f)|^2 df \\ &= 2\mathcal{E}_+ \end{aligned} \quad (\text{A.3})$$

with  $\mathcal{E}_+$  the energy of the signal having only positive frequencies.

However, for the low-pass signal in frequency domain  $X_l(f)$ , we can rewrite Eq. (A.3) to

$$\begin{aligned}\mathcal{E} &= 2 \int_{-\infty}^{\infty} |X_+(f)|^2 df \\ &= 2 \int_{-\infty}^{\infty} \left| \frac{X_l(f)}{2} \right|^2 df \\ &= \frac{1}{2} \mathcal{E}_l\end{aligned}\tag{A.4}$$

Thus, it can be said that the energy in the low-pass equivalent signal is twice the energy in the passband signal  $\mathcal{E}_l = 2\mathcal{E}$ .

## A.2 Synchronization Preambles for PPM

For the proper demodulation of PPM symbols, it is crucial to know exactly, when the first slot of a symbol starts. In this work here a preamble is chosen and implemented to clearly indicate the beginning of each data frame. Since the system will be operated at very low signal-to-noise ratios (SNRs), the preamble must be unique and easy to be found in the noisy signal. However, it also should occupy only a small portion of the overall signal power to be able to use as much signal power as possible for data transmission. In the following, some common sequences that suit this requirements are discussed.

To find the beginning of the data frame the cross-correlation function between the signal and the preamble is calculated. Therefore the time-discrete signal  $s(t)$  is assumed. Under the assumption of additive noise  $n(t)$ , the received signal  $r(t)$  equals the sum of the transmitted signal  $s(t)$  and noise, i.e.  $r(t) = s(t) + n(t)$ . The following subsection is based on [9].

The correlation defines the similarity measure of two signals. Therefore we assume two time-discrete energy signals  $s_1(t)$  and  $s_2(t)$ . The correlation coefficient depends on relative shift  $m$  of the two signals against each other in time. In a generalized definition the correlation coefficient is also called the cross correlation function (CCF):

$$\varphi_{s_1,2}(m) = \sum_{m=-\infty}^{\infty} s_1^*(t) s_2(t+m) \quad (\text{A.5})$$

with  $*$  denoting the complex conjugate.

For  $s_1(t) = s_2(t)$  Eq. (A.5) becomes the auto-correlation function (ACF)  $\varphi_{ss}(m)$ . Therefore the preamble has to have certain auto-correlation function properties. In the next sections, some commonly used benchmark factors to quantify the performance of a preamble are introduced. Finally different types of preambles are introduced, discussed and the best is chosen to be applied.

### A.2.1 Principal–Secondary Maximum Relation (PSMR) and Merit Factor (MF)

Since in digital signaling, usually binary signals are commonly applied, preambles are investigated, which can be represented by a binary bit sequence. In this application here, the preamble is BPSK modulated, i.e. a logical one is represented by a symbol phase of 0, and a logical zero is represented by a phase value of  $\pi$ . To compare different binary sequences

of length  $N$  and to find the optimum sequence for our specific application we need an appropriate benchmark. In [72] Lüke introduced the Principal-Secondary Maximum Relation (PSMR). It is defined as

$$\text{PSMR} = \frac{\varphi_{ss}(0)}{\max_{m \neq 0 \bmod N} |\varphi_{ss}(m)|}, \quad \forall m \neq 0 \bmod N \quad (\text{A.6})$$

Lindner [1] and Golay [73] have introduced the *Merit Factor* (MF). It is defined for binary sequences of length  $N$  as

$$\text{MF} = \frac{\varphi_{ss}^2(0)}{\sum_{m=1}^{N-1} |\varphi_{ss}(m)|^2} \quad (\text{A.7})$$

In the following these two figure of merits will be used to find a suitable preamble for our PPM-FSK-PS-QPSK modulated data frame.

### A.2.2 Sequences with Good Auto-Correlation Function Properties

For proper determination of the beginning of a data frame, sequences with good auto-correlation functions properties are required. We choose sequences to be of binary nature, since such sequences are easy to generate. In the following three different families are taken into account for finding a suitable preamble.

Table A 1 Lindner sequences up to length 14, according to [1] with principal-secondary maximum relation (PSMR) and Merit Factor.

Length $N$	Bit sequence	PSMR	Merit Factor
6	-1 -1 -1 1 -1 1	2.0	2.57
8	-1 -1 -1 -1 1 1 -1 1	4.0	4.0
9	-1 -1 -1 1 -1 1 -1 -1 1	4.5	3.38
10	-1 -1 -1 -1 -1 1 1 -1 1 -1	5.0	3.85
12	-1 -1 -1 -1 -1 1 1 -1 -1 1 -1 1	6.0	7.21
14	-1 -1 -1 -1 -1 1 1 -1 -1 1 - 1 1 -1 1	7.0	5.17

**A.2.2.1 Linder sequences**

Another type of sequences have been found by Lindner [1, 74]. He derived these sequences by try and error. For all binary sequences of length  $N$ , he calculated the *PSMR* and chose the sequences with the best results. And for these sequences he calculated the *Merit Factor* and again chose the sequences with the best results [1, 74]. The first 14 of these sequences are given in Table A 1 including the Merit Factor and the PSMR.

Comparing the Merit Factor and the PSMR of Lindner and Schroeder sequences one can see that for the same length  $N$  the Lindner sequences perform worse. Thus, they are no longer regarded in this work.

**A.2.2.2 Barker sequences**

Another type of sequences are Barker sequences, that have been first introduced in [75]. Barker code is defined as a sequence  $s(n)$  with binary digits  $s_i = \pm 1$  of length  $N \geq 2$  such that the ACF  $\varphi_{ss}(m) \leq 1$  for all side peaks

$$\varphi_{ss}(m) = \sum_n s^*(n)s(n+m) \leq 1, n \leq N \tag{A.8}$$

There are 13 known Barker sequences which fulfill this condition.

Table A 2 Barker sequences with Merit Factor and MSMR

Length $N$	Bit sequence	PSMR	<i>Merit Factor</i>
2	1 -1	2.0	2.00
3	1 1 -1	3.0	4.50
4	1 1 -1 1/1 1 1 -1	4.0	4.00
5	1 1 1 -1 1	5.0	6.25
7	1 1 1 -1 -1 1 -1	7.0	8.17
11	1 1 1 -1 -1 -1 1 -1 -1 1 -1	11	12.10
13	1 1 1 1 1 -1 -1 1 1 -1 1 -1 1	13	14.08

Barker sequences have two unique properties. Their *PSMR* equals their length thus, the Barker 13 sequence has the highest known *Merit Factor*. This is the reason, why for the experiments presented in this work the Barker 13 sequence is selected due to its high *PSMR* and *Merit Factor*. There are sequences that show a higher *PSMR* or *MF*, than the Barker13, but, they also have more values in their bit sequence. So they contain more power, when modulated onto an optical carrier.

### A.2.3 Conclusion

The Barker13 sequence is chosen to be applied in the experiments presented and discussed in this thesis, due to its very good performance. Since in this work, the Barker13 sequence indicates the beginning of a data frame that consists – consists amongst others – of 64PPM symbols, the Barker13 sequence is slightly adapted: Since each symbol in the data frame consists of 64 time slots, the first 13 time slots of the first symbol are occupied by the Barker13 preamble, whereas the other 51 slots are left empty. Any attempt to make a combination of several sequences leads to a reduction of Merit Factor and the PSMR value and thus should not be applied.

### A.3 Phase- and Polarization Estimation: Kalman Filter

In this chapter one algorithm for digital signal processing is discussed that is able to track phase and polarization of an optical signal. This filter is called Kalman filter. There are other estimation algorithms as well that are also suitable for phase or polarization estimation, like the Viterbi-Viterbi Algorithm or the constant modulus algorithm (CMA), but the performance of these algorithms when applied to a PPM-FSK-PS-QPSK stack was observed to be worse than the performance of the Kalman filter. This is the reason, why it is chosen to be applied in this work. This section follows closely Refs. [6, 76].

The Kalman filter is a state estimator that is based on a set of equations and operates recursively on streams of noisy input data. Its criterion for optimization is the minimization of the quadratic norm of the estimated error. It was first introduced in Ref. [77] and estimates the state of a system based on a system model and filters the result taking into account the measured output signal of the system. The Kalman filter updates the estimation recursively, which allows it to track changes of the system state over time.

According to [76], the Kalman filter is applied to time-discrete, time-variant systems that are either linear or can be approximated to show a linear behavior reasonably good. For tracking the phase and polarization of high-speed optical communication signals the latter is the case, since it can be assumed that the sample time interval is much smaller than the change of phase and polarization over time.

In the following, we will discuss the Kalman filter when applied to PS-QPSK signals. Commonly, the algorithm is blind to the absolute position of the constellation diagram at the output of the filter, so it might happen that the constellation diagram after phase estimation is rotated by integer multiples of  $90^\circ$ . To be able to successfully demodulate the PS-QPSK signal, there are two choices: Either by demodulating all possible rotations, determining their respective BERs and taking minimum one, or using a preamble or pilot sequence that helps the algorithm to find the correct quadrant.

For the experiments about the receiver sensitivity of 64PPM-PS-QPSK presented in Chapter 5, the first approach has been applied.

In Chapter 6 PS-QPSK symbols are stacked with FSK. This will force us to demodulate the PS-QPSK information for each frequency separately. Thus,

the number of possible rotation combinations is increased dramatically and makes a blind demodulation technique (i.e. without pilot sequence) due to calculation time constraints no longer an option. Instead, the Kalman filter is extended by a training sequence.

In addition it should be mentioned that in both experiments discussed in Refs. [10, 14] manual alignment of the polarization was applied such that each PPM pulse had equal powers on  $x$ - and  $y$ -polarization. Thus, as shown in Fig. 3.5, a higher sensitivity can be achieved for PPM. Here, it would have been sufficient to use the Kalman filter only for the correction of the phase error and not the polarization misalignment. This was not the case here, but the polarization re-rotation of the filter was just slightly optimizing the manual alignment.

The Kalman filter as applied in this work is derived from Ref. [6]. The noisy input into the Kalman filter is represented by one complex sample point per PS-QPSK symbol per polarization. All possible states of the output signal are predefined at the beginning of the filtering process, i.e. they describe all eight possible PS-QPSK symbols, see top-right box in Fig. A 1.

The Kalman filter in general always deals with two sets of noise influences that are assumed to be independent showing normal distribution. One is called measurement noise and one is called process noise. These two noise processes are represented by their covariance  $Q$  (process noise) and  $R$  (measurement noise), respectively. It is suggested in [76] to use these two values as “tuning input parameters” to achieve an optimum output result, see Fig. A 1.

Depending on what covariance is defined to be larger than the other, the filter trusts either rather the measured (“real”) values, or its predefined system model, see [76], Chapter 9.1. In the case of the conducted experiments as described in Chapter 6 it was figured out that the best results are achieved, if  $R$  is chosen to be larger than  $Q$ , i.e. the output of the filter strongly depends on the underlying system model, since the measurement data is superimposed by a strong phase noise.

The set of Kalman filter equations as well as the implementation in phase- and polarization sensitive signal processing is discussed in numerous publications [6, 35, 65, 76]. Here, a brief flow-chart diagram is presented, that represents the implementation of the Kalman filter used in Chapter 6 of this thesis.

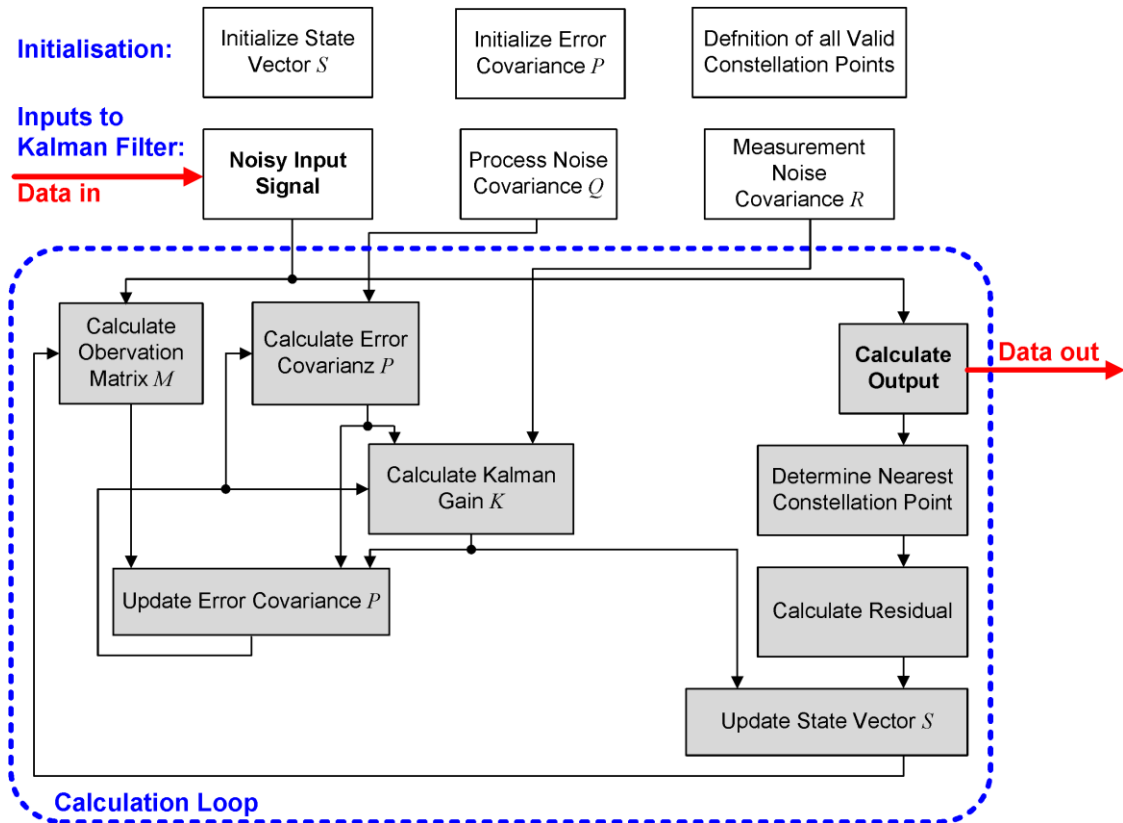


Fig. A 1 Flow-chart diagram of the Kalman filter as applied in this work [6]. First, all important parameters such as the state vector and error covariance matrix are initialized, as well as the definition of valid constellation points. The Kalman filter has three inputs: the noisy input signal as well as two tuning parameters: the process noise covariance as well as the measurement noise covariance. From these three input parameters as well as the definition of the constellation points, the output signal is calculated iteratively.

In the following, the different steps of the filtering process are described with the help of the flow-chart diagram depicted in Fig. A 1. As already mentioned, the input parameters given in the second row of the figure are the noisy input signals in two polarizations, and  $R$  and  $Q$ .

As with all common digital signal processing, we first must initialize all required parameters by suitable starting values that will be recursively updated during each iteration step later on. For initialization, we predefine the state vector  $S$ , the error covariance  $P$  and the allowed system states, i.e. all valid PS-QPSK symbols. This is the overall first step, whenever the Kalman filter is applied and thus is represented in Fig. A 1 by the first row.

After that, the calculation of the output signals is performed: The first two steps in the Kalman filter - as depicted in Fig. A 1 - are the calculation of the error covariance matrix  $P$  and the observation matrix  $M$  by Eq. (2) and (10) from Ref. [6], respectively. From these two measures as well as the

predefined tuning parameter of the measurement noise covariance  $R$  the Kalman gain  $K$  is calculated according to Eq. (3) from Ref. [6]. Once  $K$ ,  $P$  and  $M$  are calculated, the error covariance matrix is updated according to Eq. (5) from Ref. [6].

The output signal of the Kalman filter is derived from the input signal - normalized by mean value and standard deviation - and the state vector, see Eq. (9) from Ref. [6]. The state vector is a key-parameter of the whole filter. As mentioned previously, it had been pre-defined before the filtering process, and will be updated during every filter step by the following procedure: After the output signal has been calculated, one determines the closest and thus most probably the correct PS-QPSK symbol, see Fig. A 1. Consecutively the square of the difference between output signal and closest PS-QPSK symbol is calculated, called "residual". In the last step of the Kalman filter according to Fig. A 1 state vector is updated by weighting the residual with the Kalman gain factor  $K$  and adding to the previous state vector, see Eq. (4) from Ref. [6].

Now, one loop-iteration is finished, and the next sample of the input value is used to calculate the next output sample as in the previous step, but with updated values for  $S$  and  $P$ . Thus, the filter minimizes the residual, i.e. the output error, recursively, that requires some values until it converges.

If the filter is used with a training sequence, the determination of the closest constellation point is skipped, and the residual is calculated directly from the difference between the predefined symbol and the output signal. Thus, the step of determining the nearest constellation point is substituted by the predefined symbol representing the training sequence value which is most probably no longer the nearest point. At the end of the training sequence, one assumes that  $S$  and  $P$  are already set correctly, such that when the filter is applied to real data the orientation of the output symbols in the complex plane is correct. From now on, the filter must only follow the phase noise and polarization rotation.

## Appendix B:References

1. J. Lindner, "Binary sequences up to length 40 with best possible autocorrelation function," *Electronics Letters* **11**, 507-507 (1975).
2. R. J. Essiambre, G. Kramer, P. Winzer, G. Foschini, and B. Goebel, "Capacity limits of optical fiber networks," *J. Lightwave Technol.* **28**, 662-701 (2010).
3. E. Agrell and M. Karlsson, "Power-Efficient Modulation Formats in Coherent Transmission Systems," *J. Lightwave Technol.* **27**, 5115-5126 (2009).
4. D. O. Caplan, "Laser communication transmitter and receiver design," in *Free-Space Laser Communications: Principles and Advances*, J. C. R. Arun K. Majumdar, ed. (Springer New York, 2005), pp. 109-246.
5. X. Liu, T. H. Wood, R. Tkach, and S. Chandrasekhar, "Demonstration of record sensitivity in an optically pre-amplified receiver by combining PDM-QPSK and 16-PPM with pilot-assisted digital coherent detection," in *Optical Fiber Communication Conference*, OSA Technical Digest (CD) (Optical Society of America, 2011), paper PDPB1.
6. T. Marshall, B. Szafraniec, and B. Nebendahl, "Kalman filter carrier and polarization-state tracking," *Opt. Letters* **35**, 2203-2205 (2010).
7. H. Hemmati, *Deep space optical communications*, JPL Deep space communications and navigation series (John Wiley & Sons, Inc., Hoboken, New Jersey, 2006).
8. P. J. Winzer, "Modulation and multiplexing in optical communications," in *Conference on Lasers and Electro-Optics/International Quantum Electronics Conference*, Technical Digest (CD) (Optical Society of America, 2009), paper CTuL3.
9. H. D. Lüke, *Korrelationssignale: Korrelationsfolgen und Korrelationsarrays in Nachrichten- Informationstechnik, Messtechnik und Optik* (Springer-Verlag, Berlin, 1992).
10. A. Ludwig, M.-L. Schulz, P. Schindler, R. Schmogrow, A. Mustafa, B. Moos, S. Brunsch, T. Dippon, D. Malsam, D. Hillerkuss, F. Roos, W. Freude, C. G. Koos, and J. Leuthold, "Stacking PS-QPSK and 64PPM for long-range free-space transmission," in *Photonic Networks and Devices 2013*, OSA Technical Digest (online) (Optical Society of America, 2013), paper NW2C.2.
11. X. Liu, S. Chandrasekhar, T. H. Wood, R. W. Tkach, P. J. Winzer, E. C. Burrows, and A. R. Chraplyvy, "M-ary pulse-position modulation and frequency-shift keying with additional polarization/phase modulation for

- high-sensitivity optical transmission," *Opt. Express* **19**, B868-B881 (2011).
12. M. Karlsson and E. Agrell, "Which is the most power-efficient modulation format in optical links?," *Opt. Express* **17**, 10814-10819 (2009).
  13. A. Ludwig, M.-L. Schulz, P. C. Schindler, K. Kuder, S. Wolf, C. Koos, W. Freude, and J. Leuthold, "Stacking modulation formats for highest sensitivity," in *Integrated Photonics Research, Silicon and Nanophotonics 2014*, OSA Technical Digest (online) (Optical Society of America, 2014), Paper JM2B.2.
  14. A. Ludwig, M.-L. Schulz, P. Schindler, S. Wolf, C. Koos, W. Freude, and J. Leuthold, "Stacked modulation formats enabling highest-sensitivity optical free-space links," *Opt. Express* **23**, 21942-21957 (2015).
  15. F. David, "Neue Verfahren zur Phasensynchronisation in kohärent-optischen PSK-Homodynsystemen," Dissertation (Christian-Albrechts-University of Kiel, Kiel, 2004).
  16. D. Caplan, "High-Performance Free-Space Laser Communications and Future Trends," in *Optical Amplifiers and Their Applications*, Technical Digest (CD) (Optical Society of America, 2005), paper TuB1.
  17. M. Karlsson and E. Agrell, "Multilevel pulse-position modulation for optical power-efficient communication," *Opt. Express* **19**, B799-B804 (2011).
  18. T. A. Eriksson, P. Johannisson, B. J. Puttnam, E. Agrell, P. A. Andrekson, and M. Karlsson, "*K*-Over-*L* multidimensional position modulation," *J. Lightwave Technol.* **32**, 2254-2262 (2014).
  19. J. G. Proakis and M. Salehi, *Digital communications*, 5. ed., McGraw-Hill higher education (McGraw-Hill, Boston [u.a.], 2008).
  20. W. Shieh, H. Bao, and Y. Tang, "Coherent optical OFDM: theory and design," *Opt. Express* **16**, 841-859 (2008).
  21. G. P. Agrawal, *Lightwave technology: Components and devices*, 1st Edition (Wiley-Interscience, 2004), Vol. 1.
  22. G. P. Agrawal, *Fiber-Optic Communication Systems*, 3 ed. (John Wiley & Sons, Inc., New York, NY, 2002).
  23. A. H. Gnauck, G. Raybon, S. Chandrasekhar, J. Leuthold, C. Doerr, L. Stulz, A. Agarwal, S. Banerjee, D. Grosz, S. Hunsche, A. Kung, A. Marhelyuk, D. Maywar, M. Movassaghi, X. Liu, C. Xu, X. Wei, and D. M. E. D. S. A. Gill, "2.5 Tb/s (64x42.7 Gb/s) Transmission Over 40x100 km NZDSF Using RZ-DPSK Format and All-Raman-Amplified Spans," in *Optical Fiber Communications Conference*, OSA Trends in Optics and Photonics (Optical Society of America, 2002), Paper FC2.

24. I. Fatadin, S. J. Savory, and D. Ives, "Compensation of quadrature imbalance in an optical QPSK coherent receiver," *Photonics Technology Letters, IEEE* **20**, 1733-1735 (2008).
25. U. Koc, A. Leven, Y. Chen, and N. Kaneda, "Digital coherent quadrature phase-shift-keying (QPSK)," in *Optical Fiber Communication Conference, 2006 and the 2006 National Fiber Optic Engineers Conference. OFC 2006*, OSA Technical Digest (CD) (Optical Society of America, 2006), paper OThI1.
26. C. S. Petrou, A. Vgenis, A. Kiourti, I. Roudas, J. Hurley, M. Sauer, J. Downie, Y. Mauro, and S. Raghavan, "Impact of transmitter and receiver imperfections on the performance of coherent optical QPSK communication systems," in *21st Annual Meeting of the IEEE Lasers and Electro-Optics Society, 2008.*, (EEE 2008), paper TuFF3.
27. C. S. Petrou, A. Vgenis, I. Roudas, and L. Raptis, "Quadrature imbalance compensation for PDM QPSK coherent optical systems," *Photonics Technology Letters, IEEE* **21**, 1876-1878 (2009).
28. C. Sun Hyok, C. Hwan Seok, and K. Kwangjoon, "Impact of quadrature imbalance in optical coherent QPSK receiver," *Photonics Technology Letters, IEEE* **21**, 709-711 (2009).
29. K. P. Ho, *Phase-modulated optical communication systems* (Springer Science+Business Media, Inc., New York, 2005).
30. X. Tang, Z. Ghassemlooy, S. Rajbhandari, W. O. Popoola, C. G. Lee, E. Leitgeb, and V. Ahmadi, "Free-space optical communication employing polarization shift keying coherent modulation in atmospheric turbulence channel," in *Communication Systems Networks and Digital Signal Processing (CSNDSP), 2010 7th International Symposium on*, (IEEE 2010), 615-620.
31. Z. Xinhui, Y. Yong, S. Yunxu, and L. Chao, "Circle polarization shift keying with direct detection for free-space optical communication," *J. Optical Communications and Networking* **1**, 307-312 (2009).
32. S. Benedetto and P. Poggiolini, "Theory of polarization shift keying modulation," *Communications, IEEE Transactions on* **40**, 708-721 (1992).
33. P. Johannisson, M. Sjödin, M. Karlsson, H. Wymeersch, E. Agrell, and P. A. Andrekson, "Modified constant modulus algorithm for polarization-switched QPSK," *Opt. Express* **19**, 7734-7741 (2011).
34. S. Benedetto and E. Biglieri, *Principles of Digital Transmission: With Wireless Applications* (Kluwer Academic Publishers, 1999).
35. B. Szafraniec, B. Nebendahl, and T. Marshall, "Polarization demultiplexing in Stokes space," *Opt. Express* **18**, 17928-17939 (2010).

36. Z. Yu, X. Yi, Q. Yang, M. Luo, J. Zhang, L. Chen, and K. Qiu, "Polarization demultiplexing in stokes space for coherent optical PDM-OFDM," *Opt. Express* **21**, 3885-3890 (2013).
37. P. Poggiolini, G. Bosco, A. Carena, V. Curri, and F. Forghieri, "Performance evaluation of coherent WDM PS-QPSK (HEXA) accounting for non-linear fiber propagation effects," *Opt. Express* **18**, 11360-11371 (2010).
38. W. Shieh and I. Djordjevic, *Orthogonal frequency division multiplexing for optical communications* (ELSEVIER Inc., 2010).
39. K. Kikuchi and M. Osaki, "Highly-sensitive coherent optical detection of M-ary frequency-shift keying signal," *Opt. Express* **19**, B32-B39 (2011).
40. G. Jacobsen, *Noise in digital optical transmission systems* (Artech House, Inc., 1994).
41. I. P. Kaminow, T. Li, and A. Willner, *Optical fiber telecommunications VI* (Academic Press; 6 edition (May 27, 2013), 2013), p. 1148.
42. P. J. Winzer and R. J. Essiambre, "Advanced optical modulation formats," *Proceedings of the IEEE* **94**, 952-985 (2006).
43. I. T. U. Telecommunication Standardization Sector, "Forward error correction for high bit rate DWDM submarine systems, G. 975.1," (Feb. 2004).
44. M. Seimetz, "Performance of Coherent Optical Square-16-QAM-Systems Based on IQ-Transmitters and Homodyne Receivers with Digital Phase Estimation," in *Optical Fiber Communication Conference and Exposition and The National Fiber Optic Engineers Conference*, Technical Digest (CD) (Optical Society of America, 2006), NWA4.
45. B. Koch, R. Noe, V. Mirvoda, and D. Sandel, "First endless optical polarization and phase tracker," in *Optical Fiber Communication Conference/National Fiber Optic Engineers Conference 2013*, OSA Technical Digest (online) (Optical Society of America, 2013), paper OTh3B.7.
46. J. M. Senior, *Optical fiber communications principles and practice* (Prentice Hall, 2008).
47. F. Derr, "Coherent optical QPSK intradyne system: concept and digital receiver realization," *J. Lightwave Technol.* **10**, 1290-1296 (1992).
48. R. Schmogrow, D. Hillerkuss, M. Dreschmann, M. Huebner, M. Winter, J. Meyer, B. Nebendahl, C. Koos, J. Becker, W. Freude, and J. Leuthold, "Real-time software-defined multiformat transmitter generating 64QAM at 28 GBd," *Photonics Technology Letters, IEEE* **22**, 1601-1603 (2010).

49. "Unmanned Aircraft Systems Roadmap 2005-2030," (Office of the Secretary of Defense, , 2005).
50. T. L. Ivan P. Kaminov, Alan E. Willner, *Optical fiber telecommunications, B: Systems and networks V* (San Diego, 2008).
51. D. J. Geisler, T. M. Yarnall, W. E. Keicher, M. L. Stevens, A. M. Fletcher, R. R. Parenti, D. O. Caplan, and S. A. Hamilton, "Demonstration of 2.1 photon-per-bit sensitivity for BPSK at 9.94-Gb/s with Rate- $\frac{1}{2}$  FEC," in *Optical Fiber Communication Conference/National Fiber Optic Engineers Conference 2013*, OSA Technical Digest (online) (Optical Society of America, 2013), OM2C.6.
52. P. J. Winzer, "Modulation and Multiplexing in Optical Communications," in *Conference on Lasers and Electro-Optics*, (Baltimore, Maryland, 2009).
53. J. Li, *Optical delay interferometers and their application for self-coherent detection*, Karlsruhe Series in Photonics and Communications (KIT Scientific Publishing, Karlsruhe, 2013), Vol. 11.
54. R. Schmogrow, B. Nebendahl, M. Winter, A. Josten, D. Hillerkuss, S. Koenig, J. Meyer, M. Dreschmann, M. Huebner, C. Koos, J. Becker, W. Freude, and J. Leuthold, "Error vector magnitude as a performance measure for advanced modulation formats," *Photonics Technology Letters*, IEEE **24**, 61-63 (2012).
55. W. Freude, R. Schmogrow, B. Nebendahl, M. Winter, A. Josten, D. Hillerkuss, S. Koenig, J. Meyer, M. Dreschmann, M. Huebner, C. Koos, J. Becker, and J. Leuthold, "Quality metrics for optical signals: Eye diagram, Q-factor, OSNR, EVM and BER," in *14th International Conference on Transparent Optical Networks (ICTON)*, (IEEE, 2012), Mo.B1.5.
56. B. S. Robinson, "Semiconductor-based all-optical switching for optical time-division multiplexed networks," (Massachusetts Institute of Technology, 2003).
57. G. Jacobsen, *Noise in digital optical transmission systems* (Artech Bouse (Boston), 1994), p. 387.
58. J. G. Proakis, *Digital communications*, McGraw-Hill series in electrical engineering. Communications and information theory (1983), p. 608.
59. M. K. Simon, S. M. Hinedi, and W. C. Lindsey, *Digital communication techniques, signal design and detection* (Prentice-Hall, Englewood Cliffs, New Jersey, 1994).
60. M. Sjödín, P. Johannisson, H. Wymeersch, P. A. Andrekson, and M. Karlsson, "Comparison of polarization-switched QPSK and polarization-multiplexed QPSK at 30 Gbit/s," *Opt. Express* **19**, 7839-7846 (2011).

61. K.-D. Kammeyer, *Nachrichtenübertragung* (Vieweg+Teubner Verlag, Wiesbaden, 2011), Vol. 5.
62. H. Sugiyama and K. Nosu, "MPPM: a method for improving the band-utilization efficiency in optical PPM," *J. Lightwave Technology* **7**, 465-472 (1989).
63. L. Jing, A. Hylton, J. Budinger, J. Nappier, J. Downey, and D. Raible, "Dual-pulse pulse position modulation (DPPM) for deep-space optical communications: Performance and practicality analysis," in *International Conference on Wireless Communications & Signal Processing (WCSP)*, (IEEE, 2012), 1-7.
64. M. L. Stevens, D. O. Caplan, B. S. Robinson, D. M. Boroson, and A. L. Kachelmyer, "Optical homodyne PSK demonstration of 1.5 photons per bit at 156 Mbps with rate- $\frac{1}{2}$  turbo coding," *Opt. Express* **16**, 10412-10420 (2008).
65. T. Marshall, B. Szafraniec, and B. Nebendahl, "Kalman Filter Based Estimation and Demodulation of Complex Signals," White Paper (2010).
66. M. Pfennigbauer, W. R. Leeb, M. Aspelmeyer, T. Jennewein, and A. Zeilinger, "Free-Space Optical Quantum Key Distribution Using Intersatellite Links," in *Intersatellite Link Workshop*, (Proceedings of the CNES, 2003),
67. D. O. Caplan, J. J. Carney, and S. Constantine, "Parallel direct modulation laser transmitters for high-speed high-sensitivity laser communications," in *Conference on Lasers and Electro-Optics (CLEO)*, OSA Technical Digest (CD) 2011), paper PDPB12.
68. T. A. Eriksson, P. Johannisson, M. Sjodin, E. Agrell, P. A. Andrekson, and M. Karlsson, "Frequency and polarization switched QPSK," in *39th European Conference and Exhibition on Optical Communication (ECOC 2013)*, 2013), paper Th.2.D.4.
69. L. C. Andrews and R. L. Phillips, *Laser Beam Propagation through Random Media* (SPIE-The international Society for Optical Engineering, 2005).
70. R. H. Barker, "Group synchronizing of binary digital systems," in *Communication Theory*, W. Jackson, ed. (London : Butterworth, 1953), pp. 273–287.
71. C. Walck, *Hand-book on statistical distributions for experimentalists*, Internal Report (Universitet Stockholms, Stockholm, 1996).
72. H. D. Lüke, *Korrelationssignale : Korrelationsfolgen und Korrelationsarrays in Nachrichten- und Informationstechnik*,

- Messtechnik und Optik* (Springer-Verlag, Berlin [etc.], 1992), pp. XV, 308 S.
73. M. Golay, "Hybrid low autocorrelation sequences (Corresp.)," *Information Theory, IEEE Transactions on* **21**, 460-462 (1975).
  74. J. Lindner, "Synthese zeitdiskreter Binärsignale mit speziellen Auto- und Kreuzkorrelationsfunktionen," (RWTH Aachen, 1977).
  75. Barker, "Group synchronizing of binary digital systems," in *Communication Theory* W. Jackson, ed. (Butterworths, London, 1953).
  76. U. Kiencke, M. Schwarz, and T. Weickert, *Signalverarbeitung Zeit-Frequenz-Analyse und Schätzverfahren* (Oldenbourg Wissenschaftsverlag GmbH, München, 2008).
  77. R. E. Kalman, "A New Approach to Linear Filtering and Prediction Problems," *Transactions of the ASME – Journal of Basic Engineering*, 35-45 (1960).

## Appendix C: Glossary

### C.1 List of Abbreviations

1D-MP	One dimensional multi-pulse (PPM)
2D-MP	Two dimensional multi-pulse (PPM)
4-D	Four dimensional
ASE	Amplified spontaneous emission
ASK	Amplitude shift keying
AWG	Arbitrary waveform generator
AWGN	Additive white Gaussian noise
BER	bit error ratio
BPS	bit per symbol
BPSK	Binary phase shift keying
CF	Characteristic function
DD	Direct detection
DP	Dual polarization (modulator)
DP-coh. Rx	Dual polarization coherent receiver
DSP	Digital signal processing
EDFFA	Erbium doped fiber amplifier
EVM	Error vector magnitude
FEC	Forward error correction
FFT	Fast Fourier transform
FSK	Frequency shift keying
GEO	Geostationary (satellite)
I	In-phase
IFFT	Inverse fast Fourier transform
LCT	Laser communication terminal
LEO	Low earth orbit (satellite)
LO	Local oscillator
MF	Merit Factor
MGF	Moment generating function
ML	Modulation loss
MZM	Mach-Zehnder modulator
OFDM	Orthogonal frequency division multiplexing
OOK	On-off keying
OPLL	Optical phase locked loop
OSA	Optical spectrum analyzer
OSNR	Optical signal to noise ratio
PBS	Polarization beam splitter

PC	Polarization controlled
PDF	Probability density function
PLL	Phase locked loop
PM	Polarization multiplexed, power meter
PMQ	Polarization multiplexed quadrature phase shift keying
PolSK	Polarization shift keying
PPB	Photons per bit
PPM	Pulse position modulation
PPS	Photons per symbol
PS	Polarization switched
PSMR	Principal-Secondary Maximum Relation
PSQ	Polarization switched quadrature phase shift keying
Q	Quadrature
QPSK	Quadrature phase shift keying
Quad. Point	Quadrature point
RF	Radio frequency
Rx	Receiver
SE	Spectral efficiency
SER	Symbol error ratio
SNR	Signal to noise ratio
sps	Samples per slot
SSB	Single side band
Tx	Transmitter
VOA	Variable optical attenuator
WDM	Wavelength division multiplexing

## C.2 List of Symbols

### C.2.1 Calligraphic Symbols

$\mathcal{E}_b$	Energy per bit
$\mathcal{E}_s$	Energy per symbol
$\mathcal{E}_{\text{slot}}$	Energy per PPM slot
$\Re$	Real part

### C.2.2 Greek Symbols

$\alpha, \beta$	Indices for ODFM subcarrier
$\alpha_p$	Polarization power splitting ratio
$\varphi$	Phase of the of the optical carrier
$\lambda_c$	Carrier wavelength

$\mu$	Mean value
$\rho$	Received signal in time domain
$\hat{\rho}$	Received signal in frequency domain
$\rho_{\xi}$	Correlation coefficient
$\sigma^2$	Variance of Gaussian distributed variables
$\omega$	Angular frequency of the of the optical carrier
$\omega_{IF}$	Angular intermediate frequency

### C.2.3 Latin Symbols

$A$	Amplitude of the optical carrier
$a_n$	Data sequence
$B$	Bandwidth of a signal or receiver
$B_e$	Electrical bandwidth of receiver
$B_O$	Optical signal bandwidth
$B_{ref}$	Reference bandwidth in which the noise power is measured
$C$	Channel capacity
$c$	Speed of light
$d_{min}$	Euclidean distance
$E(t)$	Electrical field of the optical carrier
$E_{in}$	Electrical field of the optical carrier into the modulator
$E_{out}$	Electrical field of the optical carrier at the output of a modulator
$E_{sig}$	Electrical field of the signal
$\bar{e}_{x,y}$	Orthogonal unit vectors
$F_s$	Symbol rate
$f$	Frequency
$f_c$	Carrier frequency
$f_{shift}$	Frequency shift, generated to encode FSK
$f_n$	Frequencies (also with $n = 1, 2, 3$ ) to encode FSK
$G$	Gain of an amplifier
$g(t)$	Pulse shape function
$h$	Planck constant
$I(t)$	In-phase part of an analytical signal
$I_{BR}$	Photo-current of balanced receiver
$K$	Number of degrees of freedom of Marcum Q-function, or number of subcarriers in OFDM
$k$	Number of bits per (PPM) symbol
$M$	Number of constellation points in a modulation Format (e.g. MPPM or M-PSK)
$M_S$	Number of additional occupied PPM slots

$N$	Number of FSK carriers
$N_0$	Noise power spectral density
$N_{\text{ASE}}$	Noise power spectral density of amplified spontaneous emission
$n_{\text{bits/sym}}$	Number of bits encoded in one symbol
$n_E$	Number of erroneous bit
$n_{I,Q,x,y}$	Noise terms of in-phase and quadrature in $x$ - and $y$ -polarization
$n_{\text{FSK}}$	Number of bits per symbol encoded in FSK
$n_{\text{PPM}}$	Number of bits per symbol encoded in PPM
$n_{\text{PSQ}}$	Number of bits per symbol encoded in PS-QPSK
$n_{\text{sp}}$	Inversion factor of an amplifier
$n_{\text{Tx}}$	Number of transmitted bit
$P\{ \}$	Probability
$P_{\text{SC}}$	Probability of a correct symbol
$P_{\text{sig}}$	Signal power
$P_{\text{pulse}}$	Power of one PPM pulse
$P_{\text{Noise}}$	Noise power
$p(r)$	Probability density function
$Q(t)$	Quadrature of an analytical signal
$R_b$	Bitrate
$R_{\text{sym}}$	Symbol rate
$R_{\text{slot}}$	Slotrate of PPM slots
$r(t)$	Received signal in time domain
$\bar{r}(f)$	Received signal in frequency domain
$r_{\text{th}}$	Threshold for symbol decision
$\mathbf{s}(t)$	Signal vector
$s_l(t)$	Low-pass signal
$\text{SNR}_{\text{bit}}$	Signal to noise power ratio per bit
$\text{SNR}_{\text{cPPM}}$	Signal to noise power ratio of “conventional” PPM
$\text{SNR}_{\text{sym}}$	Signal to noise power ratio per symbol
$T_{\text{sym}}$	Symbol duration
$T_{\text{slot}}$	Duration of a PPM-slot
$t$	Time
$V(t)$	Voltage
$V_I(t)$	Driver signal at I-input of nested MZM
$V_Q(t)$	Driver signal at Q-input of nested MZM
$V_{\pi}$	$\pi$ -voltage of a modulator
$x$	$x$ - polarization
$y$	$y$ - polarization

## Appendix D: Acknowledgements (German)

Die vorliegende Dissertation entstand während meiner Tätigkeit am Institut für Photonik und Quantenelektronik am Karlsruher Institut für Technologie (KIT).

Zum Abschluss bleibt mir die angenehme Aufgabe mich bei allen Personen bedanken zu dürfen, die mich beim Gelingen dieser Aufgabe unterstützt haben.

An erster Stelle bedanke ich mich ganz herzlich bei meinem Doktorvater und langjährigen Institutsleiter Herrn Prof. Dr. Leuthold für die Inspiration, die Organisation, das Vertrauen und die Bereitstellung eines Rahmens, der diese Arbeit ermöglichte. Sein Wunsch und seine Bestrebungen wissenschaftliche Erkenntnisse in einer Art und Weise zu publizieren und präsentieren, die es auch dem Laien erlaubt das Wesentliche zu erfassen, ist vorbildlich.

Ebenso möchte ich mich bei Herrn Prof. Freude bedanken, der sich sehr viel Zeit genommen hat meine Arbeiten ausführlich zu diskutieren und kritisch durchzusehen. Sowohl sein großes und wertvolles fachliches als auch linguistisches Wissen haben diese Arbeit stark geformt.

Herr Prof. Koos, dem derzeitigen Institutsleiter, danke ich für seine Motivation, Unterstützung und fachlichen Diskussionen.

Ich möchte auch externen Partnern herzlich danken, die durch das entgeltlose Bereitstellen von diverser Hardware den Erfolg der hier präsentierten experimentellen Erfolge erst möglich gemacht haben. Hier sei das Institut für Hochfrequenztechnik und Elektronik (IHE) des Karlsruher Instituts für Technologie (KIT) unter der Leitung von Prof. Zwick dankend erwähnt für das mehrmalige Ausleihen ihres 2-kanaligen AWGs.

Die anderen beiden Kanäle des AWGs haben mir u.a. netterweise die Kollegen des Instituts für Robuste Leistungshalbleitersysteme der Universität Stuttgart unter der Leitung von Prof. Ingmar Kallfass zur Verfügung gestellt, der sich damals noch im „nahezu-OVP“ Zustand befand. Vielen Dank hierfür.

Des Weiteren bekam ich auch zeitweise grandiose Hardware-Unterstützung aus nicht-universitärem Umfeld. Dankend sei hier die Firma Keysight Technologies (früher Agilent Technologies' Electronic Measurement Group) und Herr Dimitri Malsam genannt, dessen Großzügigkeit bemerkenswert hervorzuheben ist.

Ebenso möchte ich der Firma NKT Photonics danken, deren kurzfristige und unkomplizierte Bereitstellung eines schmalbandigen Lasers die Experimente in letzter Minute gerettet haben.

Ein sehr, sehr herzlicher Dank gilt meinem Bachelor- und Masterstudenten Marc Lorenzo Schulz, dem ich nach momentanem Stand der Dinge mindestens einen Tanklastzug Apfelsaft schulde. Er hat mit seinem einzigartigem Eifer und seiner Neugierde den Einfluss neuer Algorithmen zu simulieren ganz wesentlich zum Erfolg dieser Arbeit beigetragen. Vielen herzlichen Dank!

Danken möchte ich auch meinen ehemaligen Bürokollegen René Bonk und Nicole Lindemann danken, die für mich durch ihre eigene Zielstrebigkeit und Durchhaltevermögen zu sehr großen Vorbildern wurden.

Ebenfalls ein herzliches Dankeschön geht an Robert Palmer, der stets mit Rat und Tat bei Fragen zur Verfügung stand und seit unserem gemeinsamen Bayernaufenthalt durch gemeinsame Freizeitaktivitäten nur unwesentlich zur zeitlichen Verzögerung dieser Arbeit beigetragen hat.

Ebenfalls explizit „Danke“ sagen möchte ich Stefan Wolf, Djorn Karnick, Philipp Schindler und unserem einzigartigen Premium-Postdoc Sebastian Köber für die vielen gemeinsamen Stunden zum Abschalten. Unvergessen sind die unzähligen Diskussionsrunden auf der „Brandlast“, das Actimel-Kickern oder auch die gemeinsamen Ausflüge auf den Watterkopf und dem obligatorischen anschließenden kühlen Getränk in Ettlingen.

Meinen ehemaligen Kollegen Dr. René Schmogrow, Dr. Swen König, Dr. Sean O’Duill, Dr. Jingshi Li, Dr. Arishti Melikyan, Dr. David Hillerkuß, Sascha Mühlbrandt, Jörg Pfeifle, Simon Schneider, Mathias Laueremann und Claudius Weimann danke ich ebenfalls für die angenehme kollegiale Atmosphäre, gemeinsame Kaffee- und Kickerpausen, sowie für gesellige Grillabende auf dem Institutsdach.

Außerdem danke ich all meinen weiteren Studenten, die wesentlich zum Erfolg dieser Arbeit beigetragen haben. Mein Dank geht an Kevin Kuder, Benjamin Moos, Ahmad Mustafa, Fabian Roos und Sebastian Brunsch.

Ein besonderer Dank geht auch an die (teilweise inzwischen ehemaligen) Techniker des IPQs. Ihre schnelle und unkomplizierte Unterstützung sucht ihresgleichen. Ebenso möchte ich auch dem IPQ-Sekretariat, vor allem Frau Lehmann, danken, die als gute Seele immer zur Stelle war und auch mal die eine oder andere Träne zu trockenen wusste.

Zuletzt gilt mein herzlicher Dank meinen Eltern, meiner Schwester und meinem Freund, ebenso wie den zahlreichen weiteren Verwandten unserer (Groß-) Familie. Egal durch welche Täler, Tiefen oder Höhen ich im Laufe dieser Dissertation ging, ihre unbedingte Liebe und Unterstützung war mir sicher.

## Appendix E: List of Publications

### E.1 Journal Publications

- [J1] D. Hillerkuss, R. Schmogrow, T. Schellinger, M. Jordan, M. Winter, G. Huber, T. Vallaitis, R. Bonk, P. Kleinow, F. Frey, M. Roeger, S. Koenig, **A. Ludwig**, A. Marculescu, J. Li, M. Hoh, M. Dreschmann, J. Meyer, S. Ben Ezra, N. Narkiss, B. Nebendahl, F. Parmigiani, P. Petropoulos, B. Resan, A. Oehler, K. Weingarten, T. Ellermeyer, J. Lutz, M. Moeller, M. Huebner, J. Becker, C. Koos, W. Freude, and J. Leuthold, "26 Tbit s<sup>-1</sup> line-rate super-channel transmission utilizing all-optical fast Fourier transform processing," *Nat. Photon* 5, 364-371 (2011).
- [J2] R. Schmogrow, M. Winter, M. Meyer, D. Hillerkuss, S. Wolf, B. Baeuerle, **A. Ludwig**, B. Nebendahl, S. Ben-Ezra, J. Meyer, M. Dreschmann, M. Huebner, J. Becker, C. Koos, W. Freude, and J. Leuthold, "Real-time Nyquist pulse generation beyond 100 Gbit/s and its relation to OFDM," *Opt. Express* 20, 317-337 (2012).
- [J3] P. C. Schindler, R. Schmogrow, M. Dreschmann, J. Meyer, I. Tomkos, J. Prat, H. G. Krimmel, T. Pfeiffer, P. Kourtessis, **A. Ludwig**, D. Karnick, D. Hillerkuss, J. Becker, C. Koos, W. Freude, and J. Leuthold, "Colorless FDMA-PON With Flexible Bandwidth Allocation and Colorless, Low-Speed ONUs [Invited]," *J. Opt. Commun. Netw.* 5, A204-A212 (2013).
- [J4] P. C. Schindler, A. Agmon, S. Wolf, R. Bonk, L. Meder, M. Meltsin, **A. Ludwig**, R. Schmogrow, M. Dreschmann, J. Meyer, J. Becker, M. Nazarathy, S. Ben-Ezra, T. Pfeiffer, W. Freude, J. Leuthold, and C. Koos, "Ultra-dense, wingle-wavelength DFT-spread OFDMA PON with laserless 1.2 Gb/s ONU ready for silicon photonics integration," *J. Lightwave Technol.* 33, 1650-1659 (2015).
- [J5] **A. Ludwig**, M.-L. Schulz, P. Schindler, S. Wolf, C. Koos, W. Freude, and J. Leuthold, "Stacked modulation formats enabling highest-sensitivity optical free-space links," *Opt. Express* 23, 21942-21957 (2015).

## E.2 Conference Proceedings

- [C1] J. Li, K. Worms, P. Vorreau, D. Hillerkuss, **A. Ludwig**, R. Maestle, S. Schule, U. Hollenbach, J. Mohr, W. Freude, and J. Leuthold, "Optical vector signal analyzer based on differential direct detection," in LEOS Annual Meeting Conference Proceedings, 2009), Paper TuA4.
- [C2] **A. Ludwig**, M.-L. Schulz, P. Schindler, R. Schmogrow, A. Mustafa, B. Moos, S. Brunsch, T. Dippon, D. Malsam, D. Hillerkuss, F. Roos, W. Freude, C. G. Koos, and J. Leuthold, "Stacking PS-QPSK and 64PPM for long-range free-space transmission," in Photonic Networks and Devices 2013, OSA Technical Digest (online) (Optical Society of America, 2013), Paper NW2C.2.
- [C3] C. Weimann, S. Wolf, D. Korn, R. Palmer, S. Koeber, R. Schmogrow, P. C. Schindler, L. Alloatti, **A. Ludwig**, W. Heni, D. Bekele, D. L. Elder, H. Yu, W. Bogaerts, L. R. Dalton, W. Freude, J. Leuthold, and C. Koos, "Silicon-organic hybrid (SOH) frequency comb source for data transmission at 784 Gbit/s," in 39th Optical Communication (ECOC 2013), 2013, Paper Th.2.B.1.
- [C4] **A. Ludwig**, M.-L. Schulz, P. C. Schindler, K. Kuder, S. Wolf, C. Koos, W. Freude, and J. Leuthold, "Stacking modulation formats for highest sensitivity," in Integrated Photonics Research, Silicon and Nanophotonics 2014, OSA Technical Digest (online) (Optical Society of America, 2014), Paper JM2B.2.
- [C5] P. C. Schindler, M. Laueremann, S. Wolf, D. Korn, R. Palmer, S. Koeber, W. Heni, **A. Ludwig**, R. Schmogrow, D. L. Elder, L. R. Dalton, W. Bogaerts, H. Yu, W. Freude, J. Leuthold, and C. Koos, "Ultra-short silicon-organic hybrid (SOH) modulator for bidirectional polarization-independent operation," in European Conference on Optical Communication (ECOC), 2014, Paper Mo.4.5.5.
- [C6] P. C. Schindler, A. Agmon, S. Wolf, R. Bonk, L. Meder, M. Meltsin, **A. Ludwig**, J. Becker, M. Nazarathy, S. Ben-Ezra, T. Pfeiffer, W. Freude, J. Leuthold, and C. Koos, "Ultra-dense, single-wavelength DFT-spread OFDM PON with laserless 1 Gb/s ONU at only 300 MBd per spectral group," in European Conference on Optical Communication (ECOC), 2014, Paper We.1.6.5.